Metals Encapsulated in Microporous Organic Polymers (MOPs) with Magnetic Carbon-Coated Cobalt Nanoparticles as a Versatile Support and their Applications in Catalysis

Dissertation

Zur Erlangung des Doktorgrades der Naturwissenschaften

Dr. rer. nat.

der Fakultät für Chemie und Pharmazie

der Universität Regensburg

vorgelegt von
Maryam Homafar
Aus dem Iran

Regensburg 2022

Die Arbeit wurde angeleitet von: Prof. Dr. Oliver Reiser

Promotionsgesuch eingereicht am: 01.08.2022

Promotionskolloquium am: 12.10.2022

Prüfungsauschuss: Vorsitz: API. Prof. Dr. Rainer Müller

                                   1. Gutachter: Prof. Dr. Oliver Reiser

                                   2. Gutachter: Prof. Dr. Arno Pfitzner

                                   3. Prüferin: Prof. Dr. Ruth M. Gschwind

Für Meiner Familie

تقدیم به خانواده ام

"Science progresses best when observations
force us to alter our preconceptions."

Vera C. Rubin (1928-2016)

Table of contents

Abbreviations

)))	ultrasound	Cs_2CO_3	cesium carbonate
atm	atmosphere	D	dimensional
AAS	atomic absorption spectrometry	DCX	dichloroxylene
BCMA	bis (chloromethyl) antracene	emu	electromagnetic unit
BCMPB	4,4'-bis(chloromethyl)biphenyl	FDA	formaldehyde dimethyl acetal
BET	Brunauer-Emmett-Teller	GC	gas chromatography
BJH	Barrett-Joyner-Halenda	h	hour(s)
BODIPY	boron-dipyrromethene	hcc	highly conjugated and crystalline
conc	concentrated	HCPs	Hypercrosslinked polymers
Co/C	carbon-coated cobalt nanoparticle	HAADF-STEM	high-angle annular dark-field scanning transmission electron microscopy
CMPNs	conjugated microporous polymer nanosheets	HK	Horvath-Kawazoe
CMPs	conjugated microporous polymers	IR	infrared
CNTs	carbon nanotubes	^{i}Pr	iso-propyl
CuAAC	copper-catalyzed azide-alkyne cycloaddition	ILs	Ionic liquids
C-(KTB-Pd)	KAPs-1,3,5-triphenylbenzene	ICP-OES	inductively coupled plasma-optical emission spectrometry
C-(KB-Pd)	KAPs-benzene	KPS	knitting aryl network polymers
C-(CPR-Pd)	chloromethyl polystyrene Resin	Me	methyl
CMBP	chloromethylbiphenyl	MC	mechanochemical method
COFs	covalent organic frameworks	Ms	mass spectrometry
CTFs	covalent triazine-based frameworks	MCDE	monochlorodimethylether
CCl_4	tetra chloromethane	MNPs	magnetic nanoparticles

MPs	microporous materials	PLGA	poly (lactide-co-glycolide)
MSI	metal-support interaction	PAMAM	polyaminoamido
MCDE	monochlorodimethylether	PIPS	polymerization-induced phase separation
MOFs	metal-organic frameworks	Ph	phenyl
MOPs	microporous organic polymers	Phh$_3$	triphenylphosphine
MW	microwave	PS	Polystyrene network
n.d.	not determined	r.t	room temprecure
nm	nanometer(s)	S	surface area
NMR	nuclear magnetic resonance	s	second(s)
NPs	nanoparticles	SESE	spontaneous emulsification solvent evaporation
NHC	N-heterocyclic carbene	SPIONs	superparamagnetic iron oxide NPs
Pd/C	carbon-coated palladium nanoparticle	SEM	scanning electron microscopy
p-	para-	t	time
ppm	parts per million	T	temperature
ppv	polyvinyl alcohol	TEM	transmission electron microscopy
PPNs	porous polymer networks	TEOS	tetraethyl orthosilicate
PIMs	polymers of intrinsic microporosity	TOF	turn over frequency
PVA	polyvinyl alcohol	TON	turn over number
POPs	porous organic polymers	TGA	thermo-gravimetric analysis
P$_2$O$_5$	phosphorus pentoxide	THF	tetrahydrofuran
polyST-DVB	polystyrene-co-divinylbenzene	TLC	thin-layer chromatography
PEG	poly (ethyleneglycol)	TBAB	borane-*tert*-butylamine
PCL	poly (caprolactone)	TPP	triphenyphosphine
PLA	poly (lactic acid)	V$_{0.1/tot}$	ratio of micropore volume over the total pore volume

VBC   vinylbenzene chloride

wt%   weight present

XPS   X-ray photorlectron spectroscopy

A. Introduction

Heterogeneous catalysis has been widely used in various industrial scientific approaches in the production of pharmaceuticals, agrochemicals, fine chemicals, flavors, fragrances, and dietary supplements. The key factor of this utilizing emanates from their high selectivity and readily retrievable and reusability properties [1]. Although homogeneous catalysts have important advantages in catalytic activity and selectivity, their arduous separation is a huge obstacle in industrial applications. Conversely, heterogeneous catalysis offers significant support to optimal utilizing time, energy, and chemicals. Hence, heterogeneous catalysts are more desirable for industrial applications owing to the convenience of their recovering and recycling. Heterogeneous catalysis is divided into two certain classes: supported and unsupported methods. In unsupported catalysts, the metal is dissolving chemically whereas the metal in the supported method is immobilized on the platform of carbon, graphite, alumina, or inorganic salts. In supported catalysis, metals are deposited on the surface by which the interaction between the metal and support increases, causing efficient transformation of metal [2, 3].

It should be stated that aggregation and leaching are the main issues of metal nanoparticles in catalysis applications. This problem can be restrained easily by immobilizing nanoparticles on the desired support. To do so, metal nanoparticles have been immobilized on zeolites [4], ordered mesoporous silica (OMSs) [5], metal-organic frameworks (MOFs) [6], carbon nanotubes [7], ionic liquids (ILs) [8], the ionic polymer [9], carbon [10] and carbon-coated nanoparticles [11].

1. Microporous materials (MPs)

Microporous polymers MPs (pore width <2 nm) with extraordinarily high surface area materials have attracted considerable attention in scientific applications over the years. Indeed, the special structural and functional features of MPs cause them to be used in catalysis/synthesis considerably. MPs are designed in two forms, contain metal atoms *e.g.* Metal-organic framework (MOFs) or metal-free organic polymers [12]. Among microporous solids such as zeolites [13], silica [14], carbon materials [15], porous organic cages [16] and polysisesquioxanes [17], microporous organic polymers (MOPs) have attracted extensive interest in catalysis applications due to their favorable properties. They exhibit high surface area, tunable pore size, low skeletal

density, and high chemical stability. Moreover, light elements such as H, C, N, O and B can be coupled in MOPs structure *via* relatively strong covalent bonds. As a result, these metal-free materials have lesser mass densities and higher stabilities towards MOFs [18].

Numerous MOPs, metal-free organic polymers, have been developed such as hypercrosslinked polymers (HCPs) [19], polymers of intrinsic microporosity (PIMs) [20], covalent organic frameworks (COFs) [21], conjugated microporous polymers (CMPs) [22], covalent triazine-based frameworks (CTFs) [23], porous aromatic frameworks (PAFs) [24], porous polymer networks (PPNs) [25].

The first examples of HCPs were developed *via* Friedel-Crafts alkylation of polystyrene-type precursors with external bifunctional crosslinking electrophiles agents by Tsyurupa and Davankov in the early 1970s (Scheme 1). The chloromethyl group is introduced to the phenyl rings to form the methylene bridges. On the other hand, the unavailability of the adjacent phenyl rings to the chloromethyl groups decrees this conversion. Furthermore, removing hydrogen halide as a by-product in this MPs being an inconvenience. Another limitation of these MPs is swelling in many solvents which leads to being not processed into membranes [26, 27, 28].
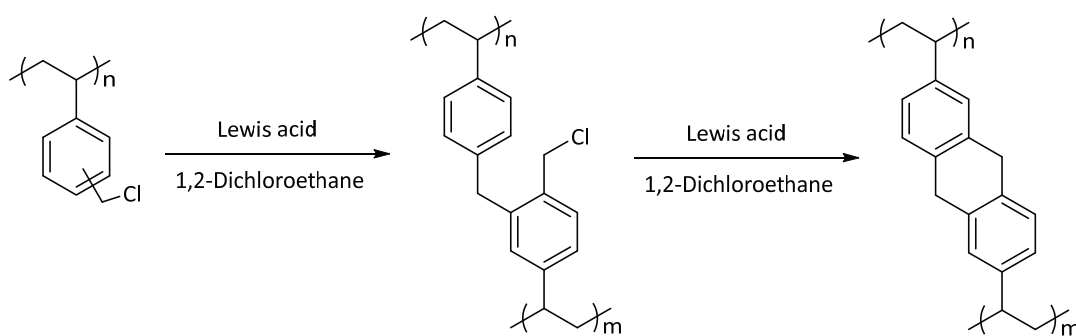
Scheme 1. Friedel-Crafts catalyzed hypercrosslinked reaction of DVB-VBC precursor resins.

Since the discovery of Davankov resins, various well-defined porous polymer networks with customized micromorphology and functionalities were designed and performed in diverse applications such as catalysis, drug delivery, separation, gas storage, and chemical sensing [29].

MOPs have demonstrated excellent potential in catalyst synthesis. Their porous structure as appropriate support not only can control the metal nanoparticle sizes through spatial restriction but also is capable to disperse particles homogeneously and avoid them from agglomeration [30]. A new synthetic strategy for microporous polymers is "knitting" rigid building blocks with an external cross-linker that developed by Tan and coworkers. Varies monomers were used with the aim of formaldehyde dimethyl acetal (FDA) as a low-cost and commercially available external cross-linker in a one-step Friedel-Crafts reaction. Their research exhibited the highest surface area of 1391 $m^2.g^{-1}$ using a small monomer together with a high cross-linker ratio [31]. Sherringtun and co-worker investigated the effect of various Lewis acid catalysis ($AlCl_3$, $FeCl_3$, $SnCl_4$), solvents, and monomer ratios. They found that $FeCl_3$ in dichloroethane shows the best catalytic activity based on the resulted surface areas. They mentioned this can be attributed to the compromise between solubility and the molecular size which can directly influence the pore properties [26]. Moreover, a crucial parameter in MOPs is Brunauer–Emmett–Teller (BET) specific surface area which is not only affected by the nature of monomer but also can be changed by the Lewis acid catalysis and external cross-linker ratio in the reaction.

On the other side, magnetic nanoparticles (MNPs) are found as non-toxic and readily accessible support with high recyclability. Their activity and selectivity can be manipulated by surface modification. The unique properties of this support make them a promising heterogeneous catalyst in life science. In other words, MOPs can evolve magnetic nanoparticles to achieve the desired catalyst [32].

2. Magnetic nanoparticles supported catalysts

Magnetic NPs have attracted attention as catalyst supports due to their enormous influence on minimizing catalyst loss, time and energy consumed, and high capacity of heating. The bottom-up methods are commonly used to obtain these materials. This approach provides fine control of the size and shape of the particles as well as high yields and a convenient scale-up. Magnetic NPs not only enable to be well dispersed in the reactions but also provide a large surface area to have more interactions with the substrates. Ultimately, they can be efficiently separated from the product almost without losing catalyst mass by a simple external magnet. In this regard, various magnetic nanoparticles such as elemental metals (*e.g.* Fe, Ni, Co, Cr, Mn, Gd, Cd) and

their oxides like magnetite FeO, Fe_2O_3 and Fe_3O_4, their alloys (*e.g.* FePt, CoPt), and ferrites MFe_2O_4 (M= Co, Mn, Cu, Zn) were used in catalysis applications. For example, superparamagnetic iron oxide NPs (SPIONs) attracted huge interest in various applications such as biomedical applications and catalysis [33]. Although the naked metal nanoparticles itself can act as the catalyst, the agglomeration phenomenon and oxidation limit their catalytic activity. These obstacles could be overcome by the core-shell approach [31].
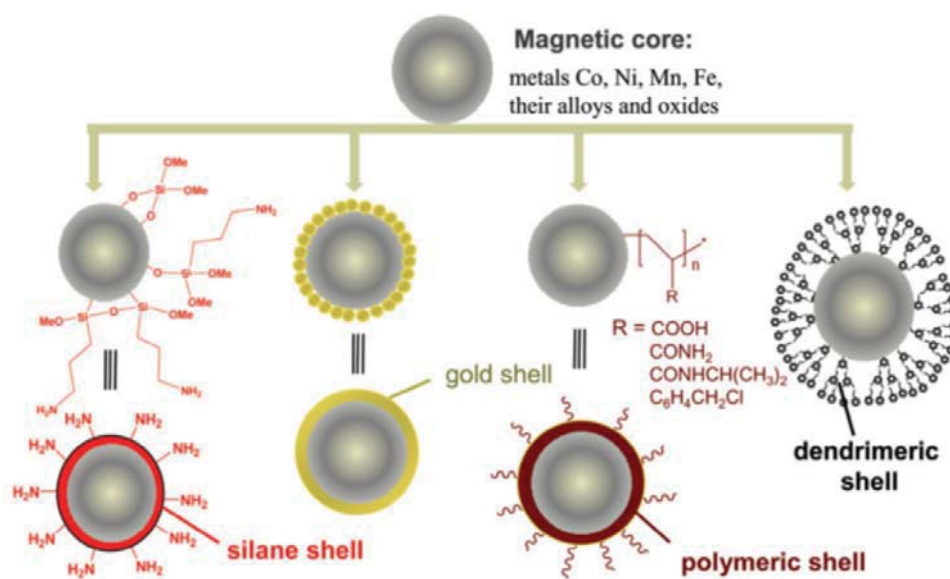

Figure 1. Various surrounded shells. Reproduced with permission from reference [34]. Copyright 2012, Institute of Pharmacology Polish Academy of Science.

The magnetic core can increase the recycability performance of the catalyst. In addition, the surface offers the possibility of covalent functionalization along with higher stability in solutions. The surrounded shell not only provides opportunities to bind different groups but also protects the core from degradation which ultimately leads to boosting catalytic activity. Hence, Magnetic NPs are coated with nanoshell/nanoparticles to improve reactivity. Various surface coatings were applied for magnetic NPs based on the envisaged applications (Figure 1) [34].

2.1. Silica coating magnetic NPs

Silica-coated was developed as the desired platform in various catalytic and biomedical applications by the pioneering research of Liz-Marzan, Mulvaney, and co-workers in 1996 [35].

Their outstanding properties such as nontoxic, rich surface chemistry, controllable porosity, high thermal stability, and optical transparent received a huge research interest as a promising core-shell. Silica-coated magnetic nanoparticles are prepared mostly by Stöber [36] or reverse microemulsion [37] methods. In the Stöber method, silica shell is produced by the hydrolysis and subsequent condensation of tetraethyl orthosilicate (TEOS) in an aqueous solution. The silica thickness can be obtained between 2 and 100 nm [33]. Xia et al. used combining commercial ferrofluids and Stöber methods to produce monodisperse silica colloids-coated iron oxide nanoparticles with larger silica colloids (100-700 nm in diameter)(Figure 2). The new strategy was based on organophilic behavior of iron oxide nanoparticles that causes emulsion drops in an alcoholic medium.They showed that the size of silica can be controlled by the concentration of iron oxide and type of consumed solutions. The saturated magnetization of 700 nm silica magnetite particles was obtained 0.37 emu.g^{-1} [38]. Notably, the presence of excess amorphous silica in individual silica-coated magnetic NPs leads to decreasing the magnetic property of resulted materials.
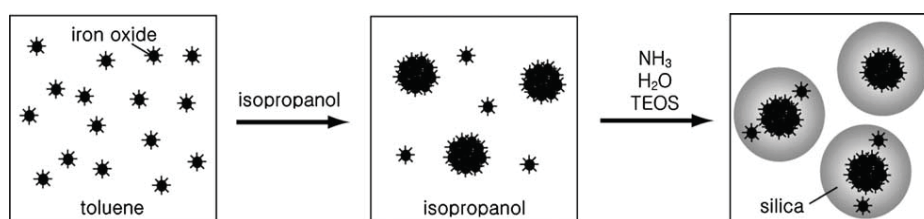

Figure 2. Synthesis of silica colloids loaded with iron oxide NPs. Reproduced with permission from reference [38]. Copyright 2004, Elsevier.

Afterward, Connor and co-workers developed ultra-thin silica-coated magnetic nanoparticles with a silica shell 2 nm and better-saturated magnetization of 15 emu.g^{-1} through the microemulsion method [37]. In this method, Igepal CO-520 was used in the formation of micelles. The micelles can control the extent of silica shell around the particles through hydrolysis and condensation of TEOS. Hence, the thickness of the silica shell can be tunable by the concentration of TEOS or nanoparticles. Further approaches were achieved by immobilization of an organocatalyst on magnetite-silica NPs. 4-N, N-dialkylaminopyrdine (DMAP) catalyst was employed on $Fe_3O_4@SiO_2$ to produce the first magnetic nanoparticle-supported DMAP analog for

heterogeneous nucleophilic catalyst (Scheme 2). The resulted catalyst demonstrated promising activity in the acetylation of phenylethanol. The catalyst was decanted from reaction with an external magnet and used 30 cycles without physical or chemical degradation. It is noteworthy that the reaction could proceed at a low loading of catalyst (0.2 mmol.g^{-1}) [39].
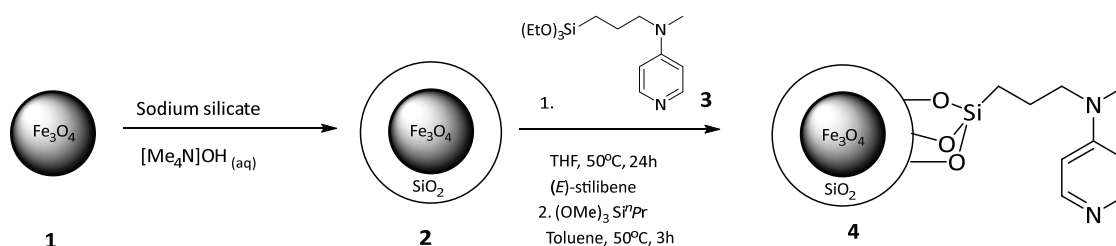
Scheme 2. Synthesis of first organocatalyst **4** on silica-coated magnetic nanoparticles **2**.

To enhance the possibility of metal nanoparticle capturing, the silica surface is modified with various groups such as glycerol, amine, azide, imidazolidine, chlorodiphenylphosphine, etc.. Reiser et al. employed two strategies for azide functionalization on Fe_3O_4@silica NPs to graft copper(II)azabis(oxazoline) complexes.
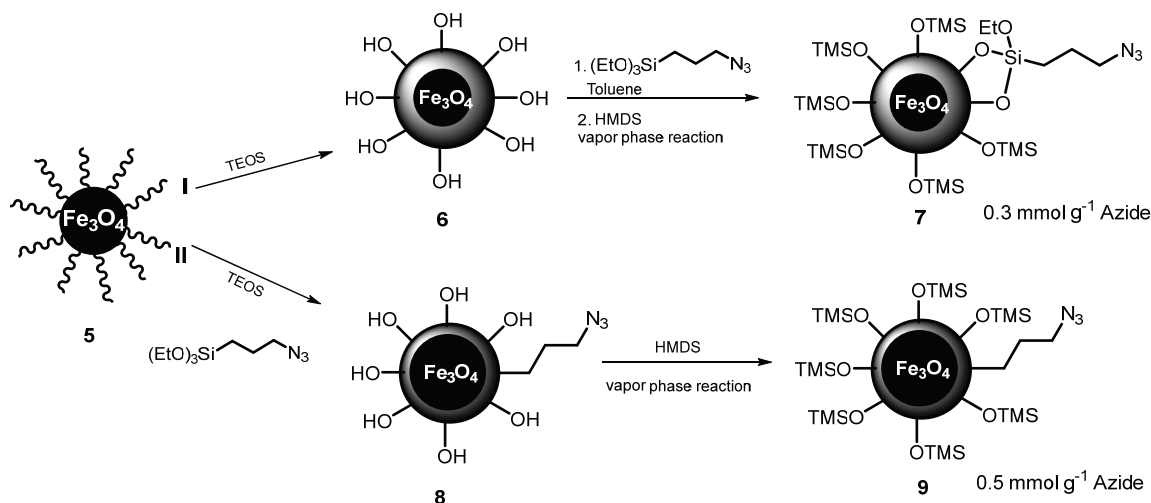

Scheme 3. Synthesis of azide-functionlized F_3O_4@SiO_2 nanoparticles out of reverse micelles **5**.

The core-shell structures **6**, **8** were synthesized by coating a SiO_2 shell around a reverse micelles **5** through a post-grafting and a single-step method (Scheme 3). Two different thicknesses of the silica shell with different amounts of azide moieties were obtained **7**, **9**. Following azide functionalization, azabis(oxazolines) was used as a chiral ligand on the support *via* copper(I)

catalyzed azide/alkyne cycloaddition (CuAAC) reaction. The ligand loading was estimated to be 0.1 mmol.g^{-1} and 0.3 mmol.g^{-1} on **7** and **9** supports, respectively . The catalytic performance was investigated in the asymmetric benzoylations of hydrobenzion (±)-16. The catalysts demonstrated excellent activity, yield, recyclability, and selectivity. At the end of the reactions, the catalysts could be easily recovered through magnetic decantation with no metal leaching. The results showed that azide-functionalized magnetic@silics nanoparticles act as a promising surface to catch important ligands such as azabis (oxazolines) *via* ''click'' reaction [40].

Du and co-worker reported the modified Fe$_3$O$_4$/SiO$_2$ using chlorodiphenylphosphine and glycerol to support palladium nanoparticles (Scheme 4). A high glycerol loading up to 1.01 mmol.g^{-1} was obtained on the magnetic support. The resulted catalyst was employed in Suzuki cross-coupling and Heck coupling reactions. The catalyst exhibited excellent catalytic performance even at loadings as low as 0.76 mol % for Suzuki coupling and 0.95 mol % for Heck coupling, respectively [41].
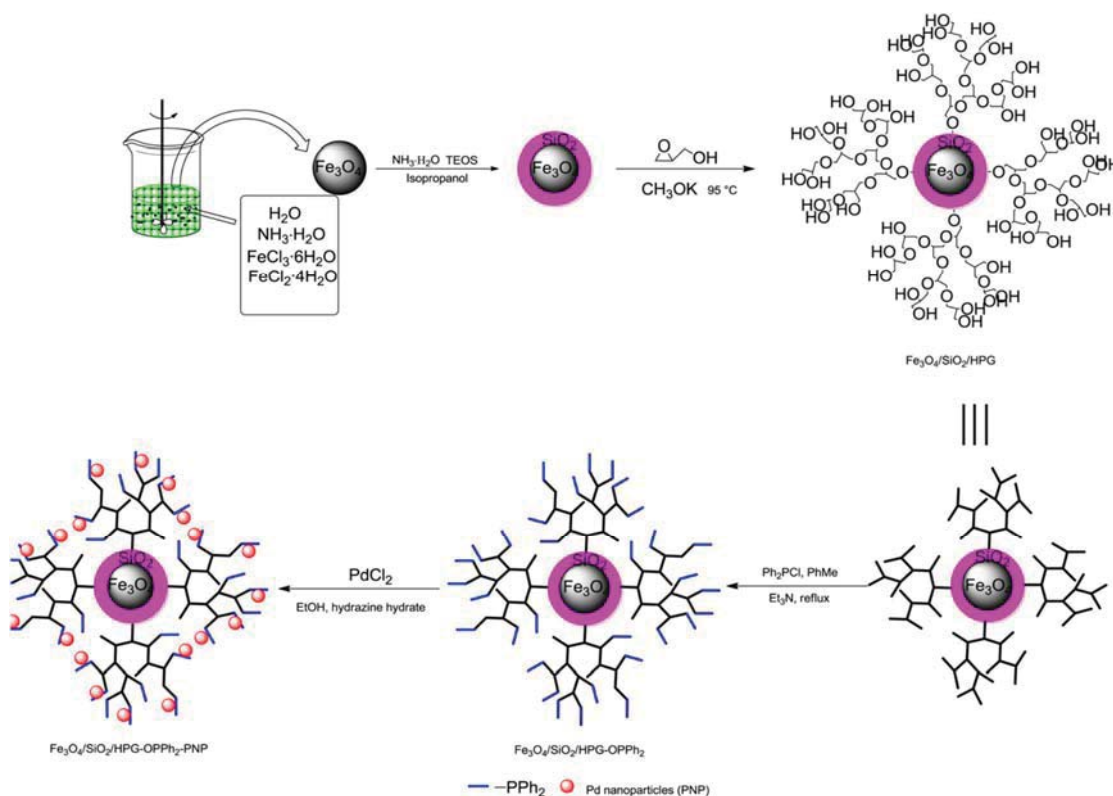
Scheme 4. Fe$_3$O$_4$/SiO$_2$ core/shell treated by chlorodiphenylphosphine and glycerol. Reproduced with permission from reference [41]. Copyright 2012, Elsevier.

2.2. Gold-decorated magnetic NPs

Another core-shell nanostructure which gained interest in analytical chemistry and nanomedicine is gold-coated magnetic NPs. Gooding et al. immobilized gold on magnetic NPs through direct and indirect methods (Figure 3). In this methodology, the thickness of the shell can be adjusted by employing different gold precursors. Moreover, the optical and magnetic properties of Au@MNPs can be controlled by changing their size, shell thickness, shape, charge, and surface modification [42]. Gold shell surface trends to bind with amine and thiol terminal groups which are more efficient in organic molecules applications [43].
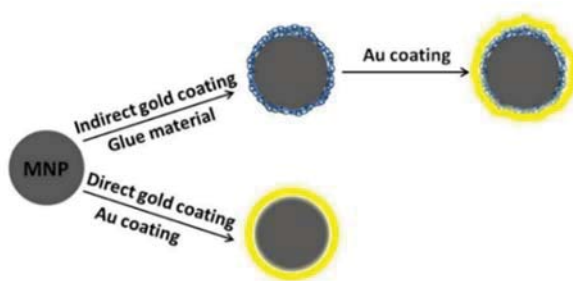

Figure 3. Gold coating methods.

Zhong et al. developed Fe-oxide@Au NPs using different methods such as thermal processing of Fe-oxide (e.g, Fe_2O_3, Fe_3O_4) NPs and Au NPs or sequential formation of Fe-oxide core and Au shell to obtain highly-monodisperse Fe-oxide@Au [44]. Even though the gold shell possesses high chemical stability and biocompatibility, the synthesis and characterization of the desired size of gold shell nanostructures and their coating methods are still challenging.

2.3. Polymer coating magnetic NPs

Natural proteins or polysaccharides such as chitosan [45], alginate [46] as well as synthetic polymers like poly (pyrrole) [47], poly(aniline) [48], poly (ethyleneglycol)(PEG) [49], poly (vinyl alcohol) (PVA) [50] , polyesters such as poly (lactic acid) [51] and poly (glycolic acid) [52] can be used for core-shell NPs in order to increase the possibility of functional groups loading.

In this regard, poly(caprolactone)(PCL), poly (lactic acid) (PLA), and Poly(lactide-co-glycolide) (PLGA) were employed for polymeric core-shell NPs using the spontaneous emulsification solvent evaporation (SESE) method. Average size ranging of polymeric core-shell NPs was obtained from

100-200 nm. The resulting platforms could be a great candidate for drug delivery, theranostics, or bioimaging applications [53]. Moreover, polysaccharide, chitosan was used as promising support due to the presence of hydroxyl and amine functional groups on its surface. Zhang et al. immobilized chitosan on the Fe_3O_4-SiO_2 surface using the covalent binding method (Figure 4). They investigated the productivity of enzymes in high reaction temperatures. The immobilized MNPs@chitosanase exhibited high stability compared to free chitosanase (with the residual activity of 19.4% and 8.4%, respectively). However, the catalytic efficiency of MNPs@chitosanase decreased after the second run which was attributed to the dropping of chitosanases from the carrier [54].
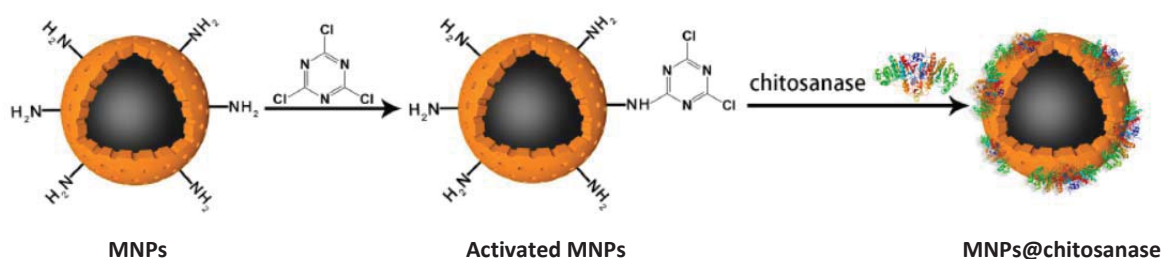

MNPs   **Activated MNPs**   **MNPs@chitosanase**

Figure 4. The immobilization of chitosan onto the Fe_3O_4-SiO_2.

Kamrul 's group was the first to synthesis chitosan immobilized on Fe_3O_4 as a heterogeneous catalyst for the reduction of 4-nitrophenol. To get this purpose, magnetic chitosan was modified with methyl salicylate (MS) and silver (Ag) NPs. The catalytic performance of Fe_3O_4@CS@MS@Ag showed good activity and recyclability for five iterative cycles without significant change in activity (with an efficiency of 90%) [45].

Gao et al. grew oleate polymer on the surface of the γ-Fe_2O_3 core *via* an emulsion polymerization method. 1,4-divinylbenzene (DVB) was used as across-link for the shell polymers along with 4-vinylbenzene chloride (VBC) as a linkage substrate for embedding Pd-NHC complexes. The efficiency of the catalyst was examined in the Suzuki-Miyaura reaction and exhibited good activity even at low catalyst loadings (0.015 mol%). The recyclability of the catalyst was investigated for five consecutive runs and no significant loss of the catalyst activity observed [55].

2.4. Dendrimers Coating magnetic NPs

Dendrimers or starburst polymers were developed by the pioneering research of Tomalia [56] and Newkome [57]. In 1998, the first dendrimer encapsulated metal NPs was developed as an efficient homogenous catalyst [58]. However, it is obvious that homogeneous catalysts cannot show to some extent catalytic efficiency comparable with heterogeneous catalysts.

Dendrimer polymer possesses numerous functional end groups compared to linear polymers. Moreover, by using polymeric shell the solubility of the support would enhance in an organic solvent. Alper 's group was the first to develop the polyaminoamido (PAMAM) dendrimers on the surface of $Fe_3O_4@SiO_2$ and used it as a noble metal nanocatalyst support. The resulted support was immobilized with Rh complexes and employed in hydroformylations reactions. The catalytic performance of the catalyst demonstrated high activity and selectivity for five runs [59].

Then, $Fe_3O_4@PS@PAMAM$-Ag nanocomposites were prepared by Yan et al. as an efficient catalyst with polystyrene (PS) for the reduction of 4-nitrophenol. The catalytic activity was studied in six successive reaction cycles (1.64 wt% Ag loading). However, slight decrease was observed after the seventh recycling and the silver loading was obtained 0.66 wt% at the tenth cycle which showed a partial decomposition of the dendrimer together with Ag NPs [60]. On the other hand, from a practical point of view, the preparation of PAMAM dendrons on the $Fe_3O_4@SiO_2$ surface needed a long time.

In this regard, Reiser et al. introduced various synthetic methods for the synthesis of dendrimers and polymers on the magnetic supports with a high capability of loading reagents, scavengers, and chelators [61].

There are some limiting factors for the aforementioned-coated shells in catalytic applications. For example, the coating of silica is not always easy when OH-groups on the metal nanoparticle surface not being sufficient or hydrolysis has been carried out on the silica surface because of the presence of covalent bonds or other metal oxides. Fully deposition of the gold shell along with controlling their thickness and smoothness are also great challenges in gold coating [42]. Moreover, gold cannot be a promising material for coating due to its cost. The limiting factors of dendrimer and polymer shells can be attributed to the long preparation times, complicated synthesis, and low capability in recyclability.

2.5. Carbon coating magnetic NPs

As mentioned already, the efficient approach to protect pure metal nanoparticles (Co, Fe) from oxidation is encapsulation of the core metal with a carbon shell. The productive carbon shell not only protects the core from oxidation but also make a homogeneous platform for further functionalization. Moreover, carbon materials are considered excellent candidates for catalyst support, since these materials can stabilize catalysts through π-interactions with sp^2 carbon atoms and consequently increase the catalytic ability [33]. Notably, the magnetization of metal core is not decreased by the carbon shell [62]. Cobalt core with high saturation magnetization ($M_{S, bulk} \leq 163$ emu.g^{-1}) was coated with carbon by Stark et al. and showed excellent properties with a saturation magnetization of 158 emu.g^{-1} together with a large surface area. In this methodology, covalent functionalization of the carbon surface is carried out with various groups like chloro, nitro, and amino. The one to three carbon layers with an average diameter of about 50 nm were deposited on the cobalt core *via* reducing flame spray pyrolysis [63]. These outstanding properties led them to be utilized in catalysis applications. Reiser et al. proposed two functionalization methods for the carbon surface of the Co/C beads *via* covalent and/or noncovalent bonds [64]. Multifunctional carbon nanomaterials were immobilized on Co/C NPs through a combination of covalent and noncovalent reactions in this group. π-π stacking interactions and diazonium/"click" reactions proceeded coating of pyrene-tagged boradizaindacene (BODIPY) and dendrimers on the surface (Figure 5).
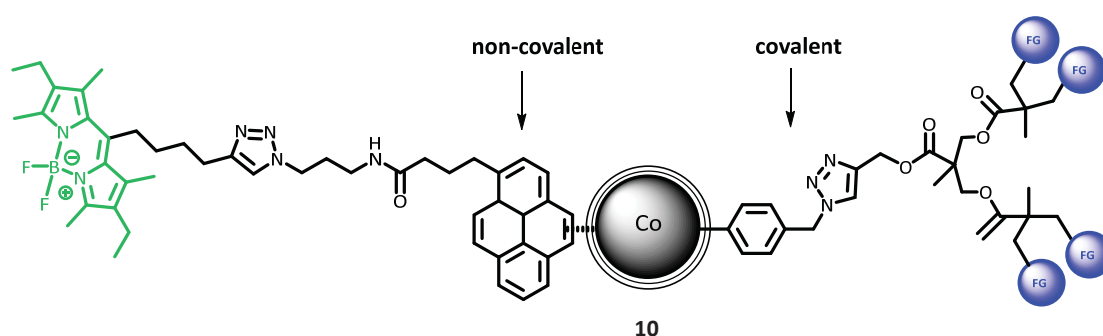

Figure 5. Covalent and non-covalent functionalization of nanomagmetic carbon surface.

Reiser's group also employed a non-covalent functionalization strategy to disperse palladium NPs on the graphene surface of Co/C nanobeads (Scheme 5). The resulting catalyst using the

microwave irradiation synthesis method indicated high dispersion compared to conventional methods. The so obtained catalyst was used in the hydrogenation of various alkenes. The catalytic performance of the catalyst showed high activity and recyclability for six consecutive cycles with almost no loss in activity [11].
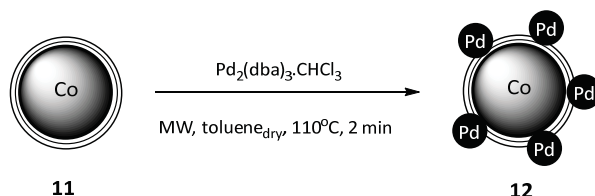
Scheme 5. The immobilization of Pd onto the Co/C nanobeads *via* microwave irradiation method.

Based on this previous investigation, palladium NPs were incorporated into the microporous organic polymer encapsulated with Co/C nanobeads. To do so, Co/C nanobeads were covalently functionalized *via* diazonium chemistry by dispersing them with aniline groups in hydrochloric acid, water, and a pre-cooled solution of sodium nitrite. The polymeric networks were produced by "knitting" rigid aromatic building blocks by the external cross-linker formaldehyde dimethyl acetal (FDA) and iron chloride as a catalyst (Scheme 6). In the following chapters, the catalytic ability of our synthesized catalysts along with their recycling and the significant separable feature will be highlighted.
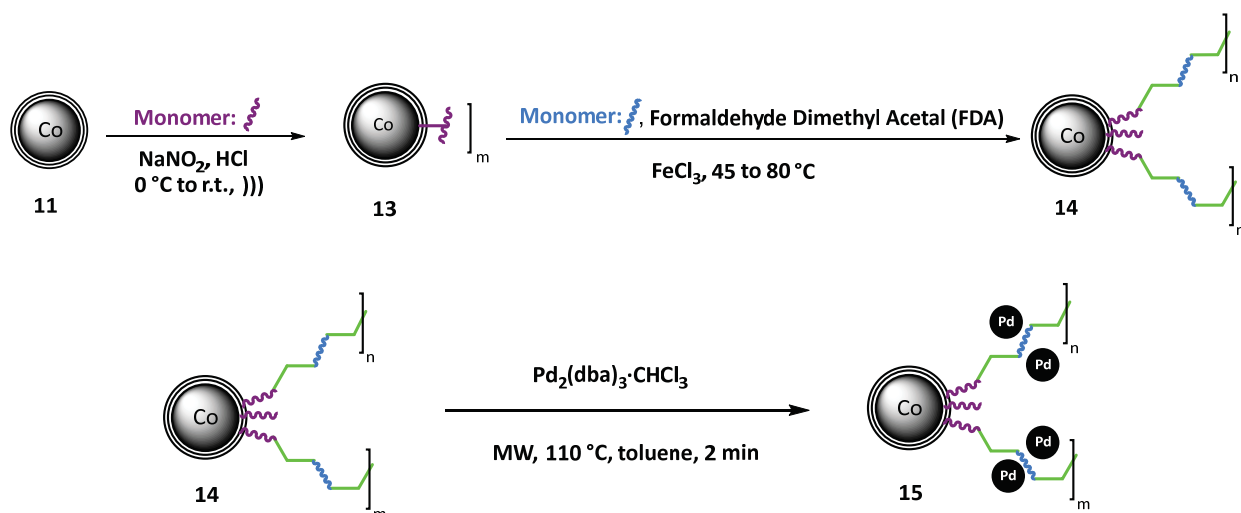
Scheme 6. Synthesis of Pd@MOPs@Co/C **15**.

3. The rationale behind using Pd nanoparticles

A wide range of chemical reductions has been performed by supported metals such as palladium [11], platinum [65], and ruthenium [66]. Based on the catalytic application, the metal would select. For example, carbon-carbon multiple bonds, multiple bond isomerization, aromatic bonds, and carbon-heteroatom single bonds are reduced by supported palladium catalyst. Owing to the inherent advantages of retrieving and reusing, a heterogeneous palladium catalyst has been exploited either for C-C coupling reactions in most organic synthesis and pharmaceutical fields [67], or electrochemical devices such as fuel cells [68].

In the last decades, cross-coupling reactions have been noticed as a significant and convenient reaction for constructing complex organic molecules in the industry. The most common coupling reactions consist of Suzuki-Miyaura [69], Mizoroki Heck [70], Sonogashira [71], and Stille [72] which have emerged as impressive practical methods, can also be promoted with Pd NPs. Indeed, Pd NPs possess attractive features which cause them to be widely used as an efficient catalyst. As the Wacker process [73] showed, one form of Pd can be switched to the other form by oxidant or reductant easily. The versatility of palladium catalysts can be attributed to the lack of single electron transfer and radical process which causes them widely used in chemoselective reactions. Palladium as a late transition metal can form d^8 Pd (II) and d^{10} Pd (0) complexes. Hence, this metal tends to coordinate at the same time with unsaturated species like π-compounds and σ bands compounds. Based on the Pauling scale the electronegativity of palladium is 2.20, so the Pd–C bonds are nonpolar and more stable [74]. Besides, their high activity and high surface-to-volume ratio lead to achieving high turnover frequency (TOF) in reactions. Accordingly, the catalyst can be used in the reaction without further preparation and ligand addition. Last but not least, pd nanoparticles are considered as an environmentally benign catalyst [11].

4. References

[1] O. Deutschmann, H. Knözinger, K. Kochloeftl , T. Turek, Heterogeneous Catalysis and Solid Catalysts, Wiley **2009**.

[2] F.Nerozzi, *Platinum Metals Rev*. **2012**, 56, 236-241.

[3] D.J.Cole-Hamilton, *Science*. **2003**, 299, 1702-1706.

[4] D.G. Blackmond, R.Oukaci, B. Blanc. and P.Gallezot, *J. catal*. **1991**, 131, 401-411.

[5] N. Ng, S. Law, R. Mukti and F. Adam, *J. Taiwan Inst. Chem. Eng*. **2014**, 45, 1435–1442.

[6] K. Brown, S.Zolezzi, P. Aguirre, D.Venegas-Yazigi, V.Paredes-Garc´ıa, R. Baggio, M. A. Novak, E. Spodine, *RSC*. **2009**, 1422–1427.

[7] M. Zhu, L. Xu, L.Du, Y. An, C. Wan, *Catal*. **2018**, 638.

[8] D. Zhao, Z. Fei, W. Ang, P. Dyson, *small*. **2006**, 2, 879–883.

[9] X. Yang, Z. Fei, D. Zhao, W. Ang, Y. Li, P. Dyson, *Inorg. Chem*. **2008**, 47, 3292–3297.

[10] F. Ronaiouliz-Rlilnoso, *Carbon*. **1998**, 36, 159-175.

[11] Q. Kainz, R. Linhardt, R. Grass, G. Vilé, J. Pérez-Ramírez, W. Stark, O. Reiser, *Adv. Funct. Mater*. **2014**, 24, 2020–2027.

[12] M. Snehasish and D. Neeladri, *J. Mater. Chem. A*. **2015**, 3, 23577–23586.

[13] M. Navlani-García, M. Martis, D. Lozano-Castelló, D. Cazorla-Amorós,K. Moribc , H. Yamashita, *Catal. Sci. Technol*. **2015**, 5, 364.

[14] G. Li, H. Yang, W. Lia, G. Zhang, *Green Chem*. **2011**, 13, 2939.

[15] B. Guo , L. Chang , K. Xie , *J. Nat. Gas Chem*. **2006**, 15, 223.

[16] A. I. Cooper, *Angew. Chem. Int. Ed*. **2011**, 50, 996–998.

[17] J. Rathore, Q. Dai, B. Davis, M. Sherwood, R. D. Miller, Q. Lin, A. Nelson, *J. Mater. Chem*. **2011**, 21, 14254.

[18] J. X. Jiang , A. I. Cooper , in Functional Metal-Organic Frameworks: Gas Storage, Separation and Catalysis, (Ed: M. Schroder), Springer-Verlag Berlin , Berlin , **2010** 1–33 .

[19] Sh. Xu, Y.Luo, B.Tan, *Macromol. Rapid Commun*. **2013**, 34, 471–484.

[20] P. M. Budd, B. S. Ghanem, S. Makhseed, N. B. McKeown, K. J. Msayib, C. Tatershall, *Chem commun*. **2004**, 230–231.

[21] X.Feng, X. Dinga and D.Jiang, *Chem. Soc. Rev*. **2012**, 41, 6010–6022.

[22] Y. Xu, Sh. Jin, H. Xu, At. Nagai and D. Jiang, *Chem. Soc. Rev*. **2013**, 42, 8012–8031.

[23] Sh. Ren, M. J. Bojdys, R. Dawson, A. Laybourn, Y.Z. Khimyak, D.J.Adams , A. I Cooper, *Adv. Mater*. **2012**, 24, 2357–2361.

[24] T. Ben, Sh. Qiu, *CrystEngcomm*. **2013**, 15, 17-26.

[25] W. Lu, J. P. Sculley, D.Yuan, R. Krishna, Zh. Wei, H. C. Zhou, *Angew. Chem. Int. Ed*. **2012**, 51,7480-7484.

[26] J. H. Ahn, J. E. Jang, Ch. G. Oh, S. K. Ihm, J. Cortez, D. C. Sherrington, *Macromolecules*. **2006**, 39, 627–632.

[27] M.P. Tsyurupa, V.A. Davankov, *React Funct Polym*. **2002**, 53, 193-203.

[28] J. Huanga, S. R. Turner, *Polymer Rev*. **2018**, 58, 1-41.

[29] N. Chaoui, M.Trunk, R. Dawson, J.Schmidt, A. Thomas, *Chem. Soc. Rev*. **2017**, 46, 3302-3321.

[30] L. Stadler, M. Homafar, A. Hartl, Sh. Najafishirtari, M. Colombo, R. Zboril, M. Petr, M. B. Gawande, J. Zhi, O. Reiser, ACS Sus. Chem. Eng. 2019, 7, 2388-2399.

[31] B. Li, R. Gong, W. Wang, X. Huang, W. Zhang, H. Li, Ch. Hu, B. Tan, *Macromolecules*. **2011**, 44, 2410-2414.

[32] L.M. Rossi, N. J.S. Costa, F.P. Silva, R. V. Gonçalves, *Nanotachnol Rev*. **2013**, 2, 597-614.

[33] Q. M. Kainz, O. Reiser, *Acc. Chem. Res.* **2014**, *47*, 667.

[34] A. Z. Wilczewska, K. Niemirowicz, K. H. Markiewicz, H, Car, *pharmacologial Reports*. **2012**, 64, 1020-1037

[35] L. M. Liz-Marzan, M. Giersig, P. Mulvaney, *Langmuir*. **1996**, 12, 4329-4335.

[36] W. Stöber, A. Fink, E. Bohn, *J COLLOID INTERF SCI*. **1968**, 26, 62-69.

[37] M. Zhang, B.L. Cushing,Ch. J O'Connor, *Nanotechnalogy*. **2008**, 19.

[38] S. H. Im, Th. Herricks, Y. Tack Lee, Y. Xia, *Chem. Phys. Lett*. **2001**, 401, 19-23.

[39] C. Dlaigh, S. A. Corr, Y.Gunko, S. J. Connon, *Angew. Chem. Int. Ed*. **2007**, 46, 4329-4332.

[40] A. Schätz, M. Hager , O. Reiser, *Adv. Funct. Mater*. **2009**, 19, 2109-2115.

[41] Q. Du, W. Zhang, H. Ma, J. Zheng, B. Zhou, Y. Li, *Tetrahedron*. **2012**, 68, 3577-3584.

[42] S. M. Silva, R.Tavallaie, L. Sandiford, R. D. Tilleya, J. Justin. *J.Name*. **2013**, 00, 1-3.

[43] I. Robinson, L. D. Tung, S. Maenosono, C. Wälti, N. T. Thanh, *Nanoscale*. **2010**, 2624.

[44] L. Wang, H. Y. Park, S.Im Lim, M. J. Schadt, D. Mott, J. Luo, X. Wang , Ch. Zhong, *J. Mater. Chem*. **2008**, 18, 2629-2635.

[45] K. Hasan, I. A. Shehadi, N. Dek Al-Bab, A. Elgamouz, *Catalyst*s. **2019**, 9, 839.

[46] M. A . Morales, P. V. Finotelli, J. A. H. Coaquira, M. H. M. Rocha-Leão, C. Diaz-Aguila, E.M. Baggio-Saitovitch, A. M. Rossi, *Mater. Sci. Eng. C*. **2008**, 28. 253-257.

[47] Y. Zhang, Z. Zhang, Sh. Xu, L. Yu, Q. Tang, *J. Name*. **2012**, 00, 1-3.

[48] Sh. Rashid, N. A. Mazlan, J. M. Sapari, M. R. Ramachandran, K. P. Sambasevam, *J. Phys. Conf. Ser*. **2018**, 1123.

[49] S. Mondini, S. Cenedese, G. Marinoni, G. Molteni, N. Santo, C.L. Bianchi, A. Ponti, *J. Colloid. Interface Sci*. **2008**, *322*, 173.

[50] S. Y. Kim, B. Ramaraj, K. R. Yoon, *Surf. Interface Anal*. **2012**, 44, 1238-1242.

[51] F. Chen, Q. Gao, G.Hong, J. Ni, J. Magn. Magn, *Mater.* **2008**, 320, 1921.

[52] N. Tudorachi, A. P. Chiriac, F. Mustata*, Composites*. **2015**,150-159.

[53] Marta Szczęch and Krzysztof Szczepanowicz. *Nanomaterials*, **2020**, 10, 496.

[54] W. Wang, N. Guo, W. Huang, Zh. Zhang, X. Mao. *Catalysts*. **2018**, 8, 401.

[55] P. D. Stevens, J. Fan, H. R. Gardimalla, M. Yen, Y. Gao, *Organic letters*. **2005**, 2085-2088.

[56] D. A. Tomalia, H. Baker, J. Dewald, M. Hall, Kallos, *Polym. J*. **1984**, 17, 117-132.

[57] G. R. Newkome, Z. Yao, G. R. Baker, V. K. M. Gupta, *J. Org. Chem*. **1985**, 2003-2004.

[58] M. Zhao, L. Sun, R. M. Crooks, *J. Am. Chem. Soc*. **1998**, 120, 4877- 4878.

[59] R. Abu-Reziq, H. Alper, D. Wang, M. L. Post, *J. A. Ch. Society*. **2006**, 128, 5279-5282.

[60] D. Gaofei, S. Yan, F. Zhifeng, Y. Wantai, *Chin*. *J.* Catal. **2012,** 33, 651– 658.

[61] Q. M. Kainz, O. Reiser, Acc. Chem. Res. 2014, 47, 667–677

[62] Q. M. Kainz, A. Schätz, A. Zöpfl, W. J. Stark, O. Reiser, *Chem. Mater.* **2011**, *23*, 3606–3613.

[63] R. N. Grass, E. K. Athanassiou, and W. J. Stark, *Angew. Chem. Int. Ed*. **2007**, 46, 4909-4912.

[64] Q. M. Kainz, A. Späth, S. Weiss, Th. D. Michl,A. Schätz, W. J. Stark, B.König, O. Reiser, *ChemistryOpen*. **2012**, 1, 125-129.

[65] F. Zhao, Y. Ikushim, M. Arai, J. *Catal*. **2004**. 224, 479-483.

[66] C. M. Eichenseer, B. Kastl, M. A. Pericàs, P. R. Hansonc, O. Reiser, *ACS Sustain. Chem. Eng*. **2016**, 4, 2698–2705.

[67] Zh. Wang, W.Chen, Z. Han, J. Zhu, N. Lu, Y. Yang, D. Ma, Y. Chen, S. Huang, *Nano Res*. **2014**, 7, 1254-1262.

[68] S. Cheong, J. D. Watt, R. D. Tilley, *Nanoscale*. **2010**, 2, 2045–2053.

[69] J. Hu, Y. Wang, M. Han, Y. Zhou, X. Jiang, P. Sun, *Catal. Sci. Technol*. **2012**, 2, 2332.

[70] Z. Maiyong, D. Guowang, *J. Phys. Chem. C*. **2011**, 115, 24743–24749.

[71] B. Lin, S. Huang, W. Wu, C. Mou, F. Tsai, *Molecules*. **2010**, 15, 9157–9173.

[72] V. Calo`, A. Nacci, A. Monopoli, F. Montingelli, *J. Org.* Chem. **2005**, 70, 6040-6044.

[73] J. Smidt,W. Hafner, R. Jira, J. Sedlmeier,R. Sieber,R. Rüttinger,H. Kojer, *Angew. Chem*. **1956**, 71, 176–182.

[74] R. J. Boyd, G. E. Markus, *J. Chern. Phys*. **1981**, 75, 5385.

B. Main Part

1. Microporous Organic Polymer (MOP) Encapsulated with Palladium Nanoparticles and Co/C Nanobeads for Hydrogenation and C-C Coupling Reactions
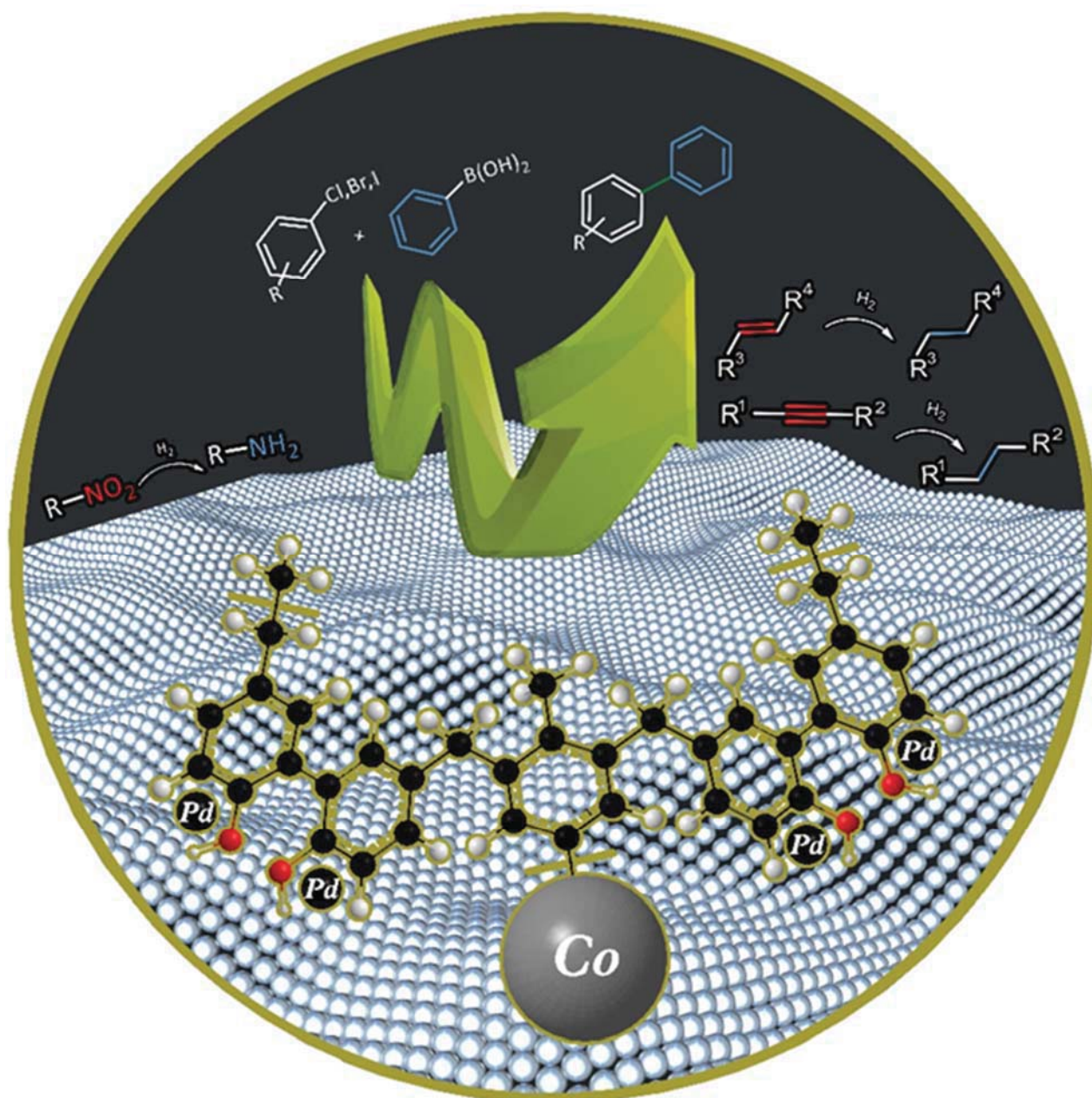
1.1. Hydrogenation

1.1.1. Introduction

Hydrogenation is fundamentally important for producing intermediary products for fine chemistry [1]. The process is performed by activation of molecular hydrogen through transition metals and promotes a great variety of reduction reactions such as alkenes, alkynes and nitro arenes in the chemical industry [2]. Over the last decade, many efforts have been dedicated to improve recyclable catalysts to optimize utilizing time, energy, and chemicals.

One possibility to arrive at recyclable catalyst is the immobilization of transition metals into polymeric matrix. To do so, porous polymers are a promising choice due to their high surface area, tunable pore size, low skeletal density, and high chemical stability. A representative example was reported by Wang et al. with the preparation of two flexible porous organic polymers (POPs) CPP-F1 and CPP-F2 with 1,2,3-triazolyl group based on click reaction. The polymers were constructed with different building units (Scheme 7).
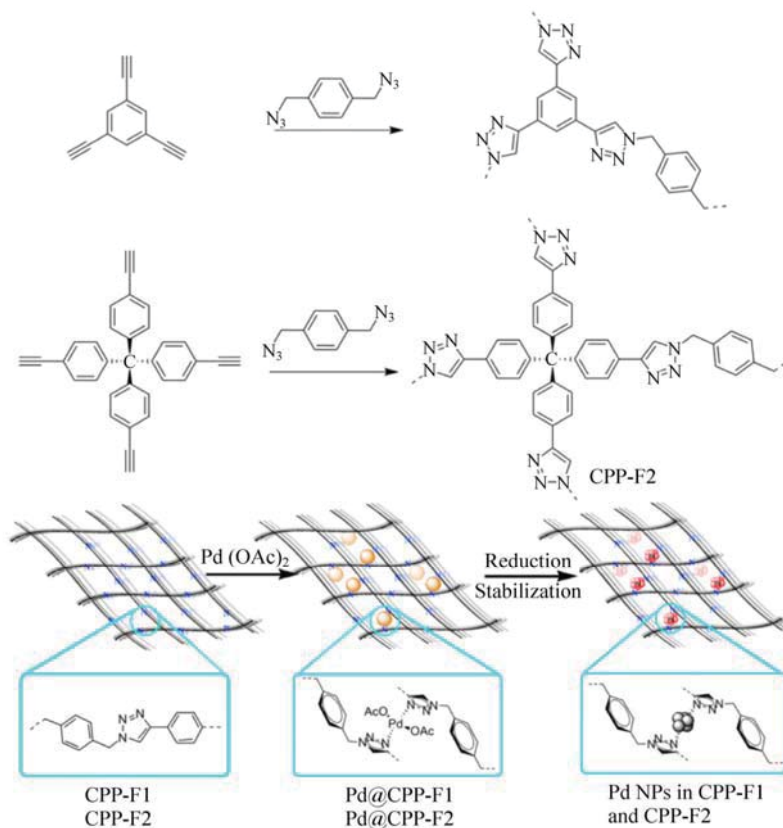
Scheme 7. Synthesis of CPP-F1 and CPP-F2 and Pd nanoparticles formation. Reproduced with permission from reference [3]. Copyright 2014, Springer Nature.

19

Field-emission scanning electron microscopy (SEM) images of these polymers showed a 3D network and a granular morphology for CPP-F1 and CPP-F2, respectively. $Pd(OAc)_2$ was incorporated into the polymers and Pd nanoparticles were obtained after hydrogentation. The resulting catalysts were applied in the hydrogenation of olefins and nitrobenzene. The catalysts showed good activity and recyclability for six runs, albeit CPP-F2 exhibited higher selectivity in the hydrogenation of 1,3-cyclohexadiene to cyclohexane. This selectivity was attributed to the smaller size of CPP-F2 (3.8 nm and 7.1 nm) comparison to CPP-F1 (7.4 nm) which can produce more active sites. Also, Pd nanoparticles were distributed on the external surface of CPP-F1, while in CPP-F2 the interior pores and the external surface were dispersed by Pd nanoparticles. The highest Brunauer-Emmett-Teller (BET) surface areas were reported 12 $m^2 \cdot g^{-1}$ and 28 $m^2 \cdot g^{-1}$ for CPP-F1 and CPP-F2, respectively. The recycled catalysts were obtained by filtration and reused for the next runs. In both catalytic systems, the 1,2,3-triazolyl group had an essential effect on polymer linkages and well dispersion of Pd nanoparticles [3]. In our work, the efficiency of the various functional groups was also investigated in hydrogenation reactions. In contrast to the 1,2,3-triazolyl group in POPs (CPP-F1 and CPP-F2) which made low surface areas and lack of permanent porosities, introducing hydroxyl groups by 2,2'-biphenol as the monomer into the microporous organic polymer (MOP) turned out to be the high surface area (389 $m^2 \cdot g^{-1}$) and main particle sizes of 2 and 3 nm.

In this respect, Ishida et al. introduced three different monomers into conjugated microporous polymers (CMPs) as a support for Pd nanoparticles (Scheme 8). The catalytic performance of three backbones with various functional groups were investigated in hydrogenation and oxidation reactions. The Pd nanoparticles were embedded in the porous network concurrently with the polymerization followed by thermal treatment with N_2 and H_2 in order to prevent aggregation of Pd nanoparticles on the surface. The resulting catalysts were applied in the hydrogenation of N-benzylideneaniline. The results revealed that Pd/CMP-2-H_2 and Pd/CMP-OH-H_2 have the same catalytic activity which has been attributed to a similar size of Pd nanoparticles. On the other hand, for the oxidation reaction of benzyl alcohol, the hydroxyl group in Pd/CMP-OH-H_2 showed significant catalytic activity compared to the other catalysts [4].
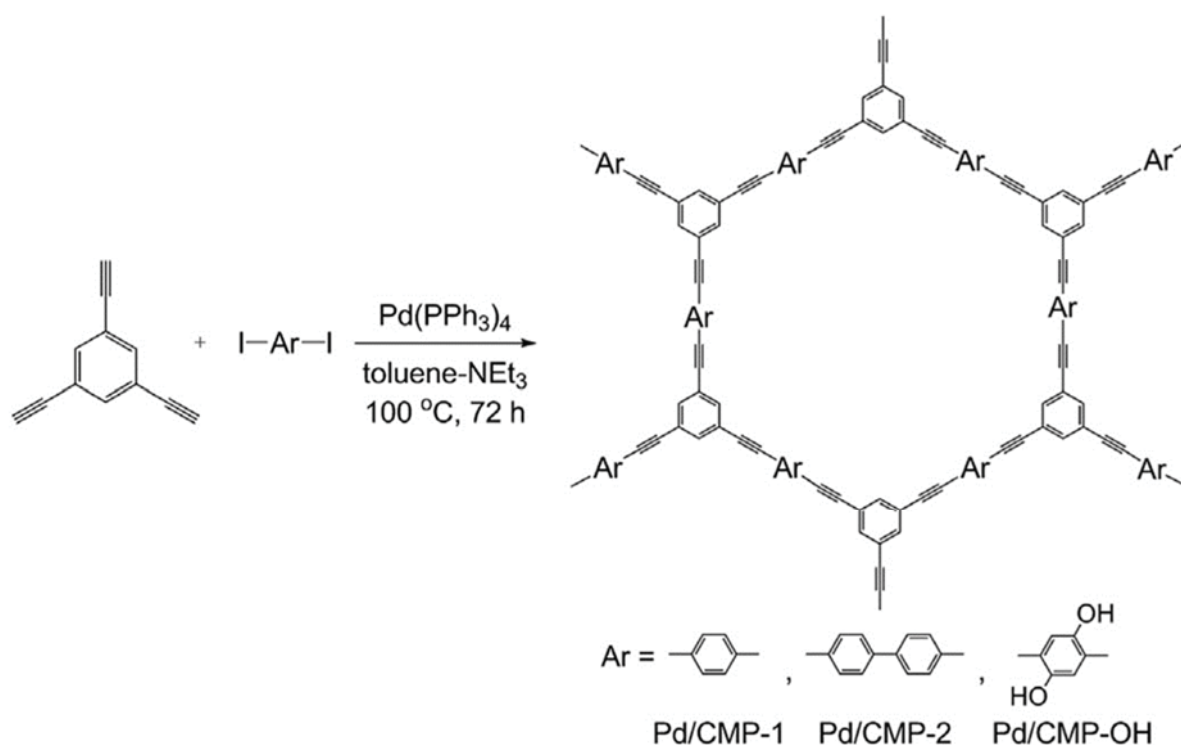
Scheme 8. Synthesis of CMPs.

An appropriate polymeric network not only generates a higher surface area but also leads to a higher metal loading, which enables catalysts to be used for large-scale applications.

In order to synthesis a catalyst with high loading ability up to 3 mmol.g^{-1}, Reiser et al. incorporated Pd nanoparticles on magnetic nanobeads functionalized with imidazolium-based ionoc liquids (ILs) using different polymer shells. Novel hybrid systems were synthesized *via* the three following procedures: the first catalyst was obtained by direct attaching of ILs on the surface of nanobeads (Pd@PS-IL@Co/C), for the second catalyst (Pd@Bz-IL@Co/C), ILs was coated to the surface of the polymer and the third catalyst (Pd@Spacer-IL@Co/C) was attached to the spacer. The catalysts were investigated in terms of various Pd loadings, Pd precursors, hydrogenation reactions, and recycling. The results showed that incorporation of Pd(0) precursor (Pd$_2$(dba)$_3$.CHCl$_3$) using microwave irradiation is more efficient than the reduction of a Pd (II) precursor (Na$_2$PdCl$_4$). Moreover, the catalysts with a flexible ionic liquid modified could stabilize Pd nanoparticles efficiently in a high Pd loading (Scheme 9) [5].
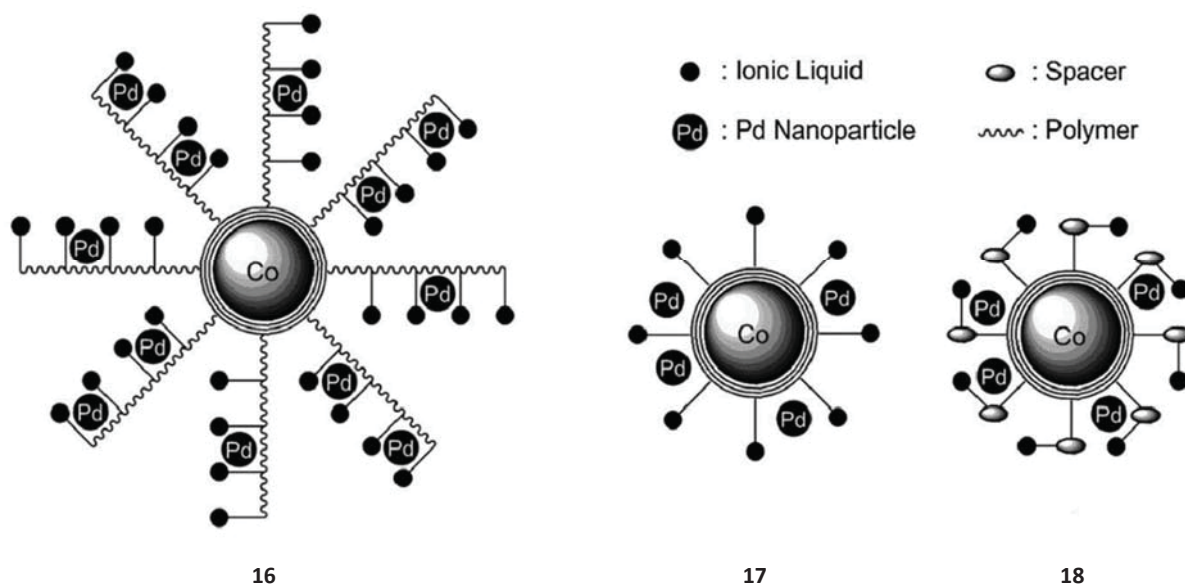
Scheme 9. Pd@PS-IL@Co/C **16**, Pd@Bz-IL@Co/C **17**, and Pd@Spacer-IL@Co/C **18**. Reproduced with permission from reference [5]. Copyright 2011, Royal Society of Chemistry.

Notably, introducing microporous organic polymers (MOPs) provides a versatile supporting network. The main advantage of microporous materials is distributing Pd nanoparticles uniformly with enhanced loadings together with controlling their size which prevents Pd nanoparticles from agglomeration. Moreover, magnetic nanocatalysts with high surface-to-volume ratio and facile recycling are considered excellent support in heterogeneous catalysis applications [2] .

Taking the lead from Tan et. al [6] who generated porous polymers by polymerizing arenes with formaldehyde dimethyl acetal (FDA) as a low-cost and commercially available external cross-linker, we synthesized MOPs with diverse functional groups, surface areas, pore diameters, and different external cross-linker contents. Combining the advantages of MOPs with the high magnetization value of the cobalt nanobeads (Co/C) turned out to be well-dispersed Pd nanoparticles onto the magnetic platform for which the catalysts could be easily separated from the reactions.

1.1.2. Results and discussion

A new hybrid material was synthesized combining carbon-coated cobalt nanobeads (Co/C) as magnetic support with porous polymers.[*] Stark et.al developed this magnet support by a one-step procedure *via* reducing flame-spray pyrolysis on a large scale (>30 g.h^{-1}). Compared to metal oxide based magnetic nanoparticles such as F$_3$O$_4$, Co/C not only possesses a high magnetization value (158 emu.g^{-1}, almost five times higher) but also to be protected against oxidation by the carbon shell (Figure 6) [7]. In addition to high chemical stability, the particles can be recovered by an external magnet readily and rapidly.
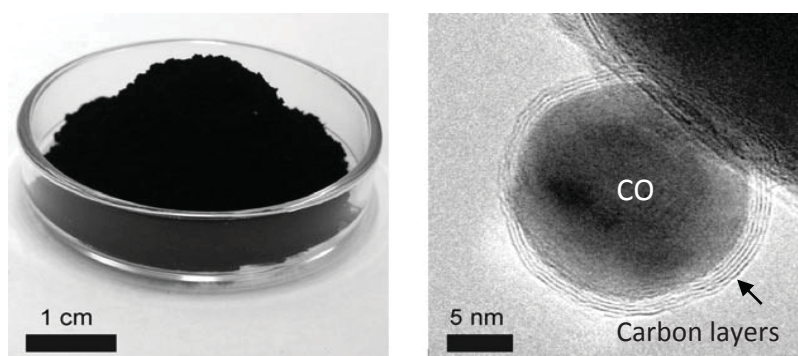
Figure 6. Carbon-coated nanoparticles and TEM image of homogeneous graphene layers. Reproduced with permission from reference [7]. Copyright 2007, Wiley-VCH Verlag GmbH & Co. KGaA, Weinheim.

The homogeneous shell surrounding Co, provides opportunities for introducing functional groups, which can further be used as anchors for attaching a polymer matrix.

In the first step, Co/C nanoparticles **11** were functionalized with a arylamine in *situ* formed aryl radicals from their corresponding diazonium salts [7]. Thus, the Co/C **13** were covalently functionalized according to the general procedure A *via* diazonium chemistry by dispersing **11** in water together with hydrochloric acid as catalyst and different arylamines such as *p*-toluidine **a**, aniline **b,** and *p*-aminophenol **c**. Subsequently, a pre-cooled solution of sodium nitrite was added

---

[*] The preliminary investigations were performed on toluene monomer **14g** in Heck coupling reaction by J. Zhi (Postdoctoral research) and continued by S. Ranjbar (PhD thesis). Hydrogenation of *trans*-stilbene, Suzuki cross-coupling of 4-idoanisole, idobenzene, 4-bromoanisole, and the preliminary recycling test of **14g** with 0.43 wt% Pd were performed by S. Ranjbar [8]. Synthesis and all reactions utilizing **13a-c**, **14d-14l**, and **15d-15l** were performed by M. Homafar. L. Stadler carried out screening of reaction conditions and substrate scope (Master thesis) and A. Hartl investigated the recyclability of the catalyst **14g** (Master thesis). These investigations were performed at the University of Regensburg under supervision of Prof. Dr. O. Reiser.

dropwise at 0°C, followed by stirring for a given time. Best results were obtained with *p*-toluidine **a**, for which a loading of 0.1 mmol toluene units per gram was obtained **13a** (Scheme 10).
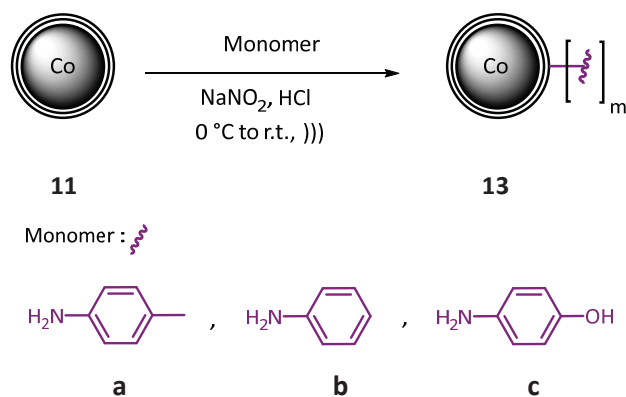
Scheme 10. General procedure A. Stabilizing of the diazonium salt of arylamine onto carbon-coated cobalt particles.))) = ultrasound.

In order to determine the effect of functional groups on the pore sizes and catalyst activity, different polymeric networks were grown on the surface of nanoparticles with various external cross-linker and monomer ratios. Microporous polymers were synthesized according to the general procedure B by "knitting" rigid aromatic building blocks with different equivalents of FDA (**α**:1.25, **β**: 2.50, **γ**: 3.00) and various monomer building blocks **d-l** (Scheme 11).
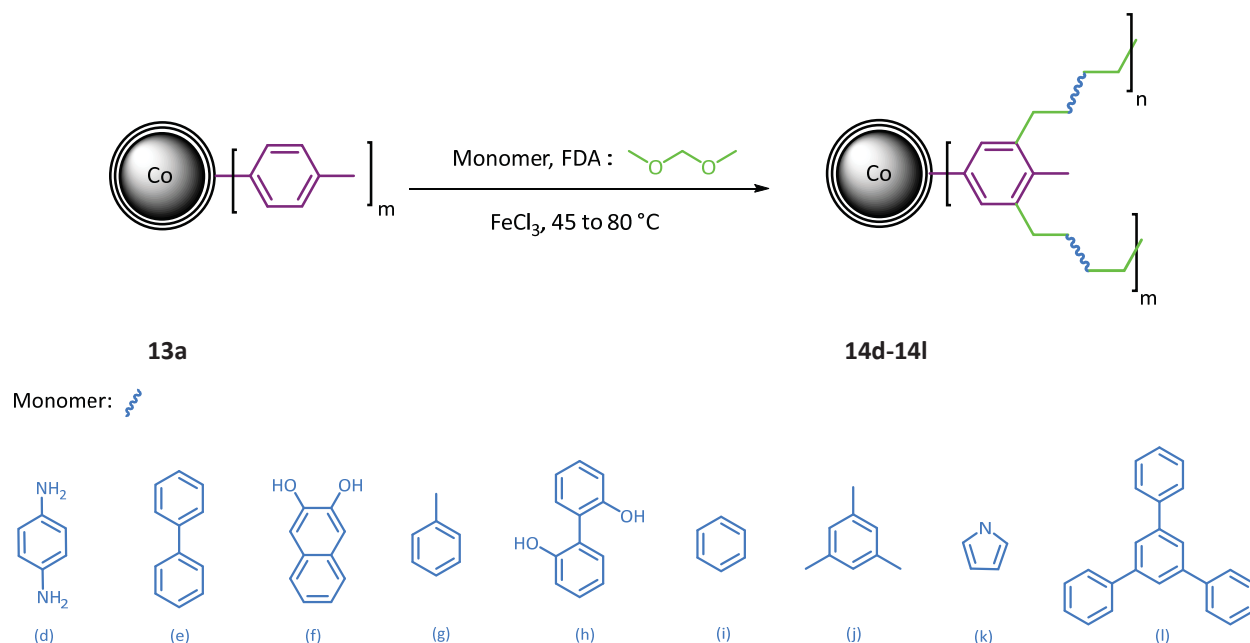
Scheme 11. General procedure B. A range of MOP$_S$@Co/C was synthesized around the **13a** with various monomers (**d-l**), FDA, and anhydrous iron(III)chloride (FeCl$_3$) in 1,2-dichloroethane (DCE).

Table 1. Yield of MOP$_S$@Co/C, entries 5-7, **14h** was synthesized with various equivalents of FDA (**α**:1.25, **β**: 2.50, **γ**: 3.00).

Entry	No.	Co-C (g)	Product (g)	Expected product (g)	EA (%) [a]	Product (%)
1	**14d-β**	0.100	0.110	0.174	22.71 C, 2.03 H, 5.60 N	51
2	**14e-β**	0.100	0.156	0.200	42.97 C, 2.50 H, 0 N	56
3	**14f-β**	0.100	0.136	0.196	30.22 C, 2.11 H,0 N	38
4	**14g-β**	0.101	0.130	0.160	28.63 C, 1.94 H,0 N	50
5	**14h-α**	0.100	0.128	0.217	18.23 C, 1.87 H, 3.40 N	38
6	**14h-β**	0.101	0.171	0.217	38.11 C, 2.93 H, 0 N	61
7	**14h- γ**	0.100	0.170	0.217	38.29 C, 3.11 H, 0 N	61
8	**14i-β**	0.100	0.125	0.157	27.42 C, 1.5 H,0 N	43
9	**14j-β**	0.100	0.109	0.184	13.23 C, 0.76 H,0 N	trace
10	**14k-β**	0.101	0.108	0.147	12.31 C, 0.85 H, 1.4 N	trace
11	**14l-β**	0.100	0.152	0.267	44.77 C, 3.24 H,0 N	32

[a] Determined by elemental microanalysis.

Monomers, 2,2'-biphenol **14h**[†], 1,1'-biphenyl **14e,** and toluene **14g**[‡] with high polymerization and acceptable results in elements loading based on the elemental microanalysis were chosen for further investigation. Thus, MOPs 2,2'-biphenol@Co/C **14h** and toluene@Co/C **14g** were synthesized with 1.25 to 3.00 equivalents of FDA, aiming to further improvement in the surface area and pore value.

MOPs 2,2'-biphenol @Co/C **14h** with 1.25, 2.50, 3.00 equivalents of FDA and toluene@Co/C **14g** with 1.25, 2,00, 2.50 equivalents of FDA were denoted (**14h-α**), (**14h-β**), (**14h-γ**), (**14g-α**), (14g-**β**), and (**14g-γ**), respectively.

The porous properties of the microporous polymer toluene@Co/C **14g** with various equivalents of FDA and the microporous polymer **14h-β** were investigated by N$_2$ sorption[§] analysis at 77.3 K (Table 2, Figure 7, see Figure 25 in Experimental Part).

The rise of the adsorbed nitrogen in the low relative pressure area (P/P$_0$ < 0.1) indicates the presence of micropores, while the steep nitrogen uptake in the middle and high relative pressure

---

[†]**14h, 15h** and their reactions were performed by M. Homafar. Hydrogen reaction of these catalysts was published by Reiser et al. [9] and is available online.

[‡]**14g**, **15g**, and their reactions were also carried out by L. Stadler [9].

[§] Evaluation and graphical presentation of BET measurements of polymers **14h** and **14g** were carried out by L. Stadler in consultation with Dr. S. Najafishirtari.

region (0.8 < P/P$_0$ > 1.0) is characteristic for macropores [10, 11]. The appearance of hysteresis and the shape of the hysteresis loop is associated to mesopores strcture [12], but soft microporous materials can also exhibit this kind of loop in the swollen and deformed state at 77.3 K by N$_2$ (Figure 7A) [13]. The Barrett-Joyner-Halenda (BJH) pore size distribution of **14h** in Figure 7B indicates micro-, meso- and microporous structures and offers promising heterogeneous properties for catalytic reactions. Consequently, micro- and mesoporous structures can trap metal catalysts, and the macroporous structure is capable of accelerating the mass transfer of reactants to the embedded metal catalysts and of the corresponding products [14].

Table 2. Nitrogen adsorption isotherms at 77.3 K of toluene@Co/C **14g-α** to **14g-γ** and 2,2'-biphenol@Co/C **14h**.

No.	FDA[a)]	S$_{BET}$[b)] (m^2/g)	S$_{BJH}$[c)] (m^2/g)	V$_{0.1/tot}$[d)] (cm^3/g)
14g-α	1.25	43	15	0.14
14g-β	2.00	85	22	0.23
14g-γ	2.50	277	55	0.37
14h-β	2.50	389	74	0.63

[a)] Molar ratio with respect to the monomer. [b)] Surface area calculated using BET equation. [c)] Surface area calculated using BJH equation. [d)] Ratio of micropore volume over the total pore volume.

The BET surface areas were calculated to be 277 m$^2 \cdot$g^{-1} and 389 m$^2 \cdot$g^{-1} for **14g-γ** and **14h-β**, respectively. The micropore content was calculated by the ratio of micropore volume (P/P$_0$ = 0.1) over the total pore volume to be 0.63 and 0.37 for **14h-β** and **14g-γ,** respectively. This indicates mainly **14h-β** polymer structure possesses micropores rather than meso/macropore structures. Moreover, the obtained results show that in polymer **14g-γ**, meso-and macropores are predominant, unlike **14h-β** structure which micropores are outnumbered [15].

A

B
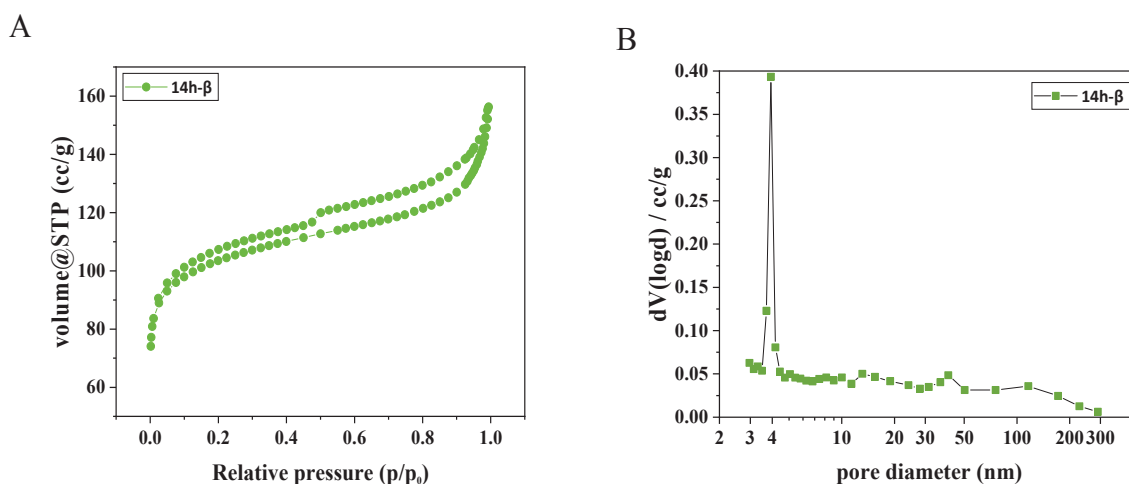
Figure 7. N$_2$ sorption data of **14h-β** A) Brunauer-Emmett-Teller (BET) method, B) Barrett-Joyner-Halenda (BJH) method.

The palladium NPs were incorporated into the porous supports **14h** and **14g** through decomposition method [16] modified by Reiser *et al*. [2]. Accordingly, Pd$_2$(dba)$_3$·CHCl$_3$ was introduced to **14h** and **14g** (1 mg Pd$_2$(dba)$_3$·CHCl$_3$ per 50 mg of the MOPs 2,2'-biphenol@Co/C and toluene@Co/C, **14h-α** to **14h-γ** and **14g-α** to **14g-γ,** respectively) using microwave irradiation and **15h-α** to **15h-γ** and **15g-α** to **15g-γ** were obtained with palladium loadings of 0.2 to 0.4 wt % and incorporation rates between 36% and 95% (Scheme 12, Table 3, entries 1-12). The palladium incorporation rate of 95% for **15h-β, 15h-γ,** and 87% for **15g-γ** (Table 3, entries 2, 3, and 6) indicate a higher capacity uptake for the metal nanoparticles and reflects the results of the nitrogen adsorption measurements (Figure 7).
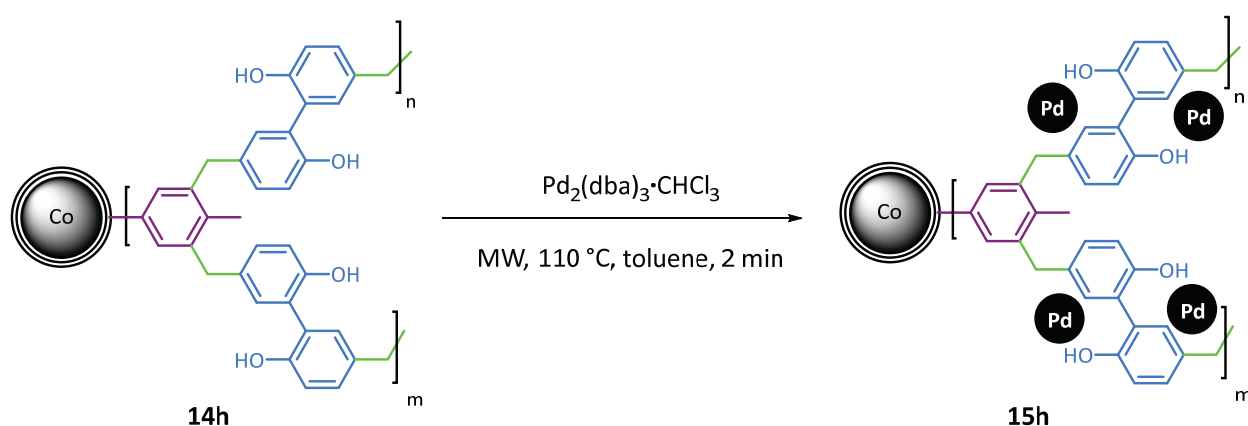
Scheme 12. General procedure C, synthesis of Pd@2,2'-biphenol@Co/C **15h**. Analogous to **15h**, Pd catalyst **15d-l** were synthesized corresponding to the monomer building block **d-l**.

Table 3. Palladium incorporation into 2,2'-biphenol@Co/C **14h-α** to **14g-γ** and toluene@Co/C **14g-α** to **14g-γ**, resulting in the materials **15h-α** to **15h-γ** and **15g-α** to **15g-γ** with various Pd wt % loadings.[**]

Entry	No.	FDA (equiv.)	Pd$_2$dba$_3$·CHCl$_3$ (mg)	Pd incorporation[a] (%)	Pd[a] (wt %)
1	**15h-α**	1.25	1.0	84	0.20
2	**15h-β**	2.5	1.0	95	0.38
3	**15h-γ**	3	1.0	95	0.40
4	**15g-α**	1.25	1.0	36	0.20
5	**15g-β**	2.00	1.0	71	0.30
6	**15g-γ**	2.50	1.0	87	0.40
7	**15g-γ**	2.50	0.5	97	0.20
8	**15g-γ**	2.50	1.0	87	0.40
9	**15g-γ**	2.50	2.5	91	1.0
10	**15g-γ**	2.50	5.0	81	1.7
11	**15g-γ**	2.50	10	91	3.9
12	**15g-γ**	2.50	50	67	14

[a] Determined by ICP-OES.

In order to investigate palladium uptake limit into porous material **15g-γ,** up to 50 mg of palladium precursor per 50 mg of **15g-γ** were synthesized. An appreciable decline was observed with employing 50 mg of palladium precursor (entry 12, 67% incorporation, corresponding to 14 wt% Pd). According to the TEM images, the Pd nanoparticle size distribution for the materials containing 0.4 to 1.7 wt% was found to be quite narrow with particle sizes of 3 and 4 nm. The Pd nanoparticles in the materials with 0.2 wt% Pd were not observable. For entries 11 and 12 with higher Pd loadings, the agglomeration phenomenon was detected (see Experimental Part).

Afterward, to find the optimal reaction solvent, some experiments were performed taking the hydrogenation of *trans*-stilbene as a model reaction (Scheme 13). A solvent screening[††] reveals

[**] Various Pd loadings were utilized in **14g** (Table 3, entry 4-12) by A. Hartl and L. Stadler. See the experimental part for TEM images of these materials.
[††] The preliminary catalyst based on toluene **15g** was investigated with aforementioned solvents by S. Ranjbar (PhD student) and L. Stadler (Master thesis).

that 2-propanol was the best solvent, while MeOH, toluene, DCM, CH_2Cl_2, or $CHCl_3$, gave lower conversions (Table 4).

Catalyst 15h-β

H_2 (1 atm), solvent, r.t.

19f   **20f**
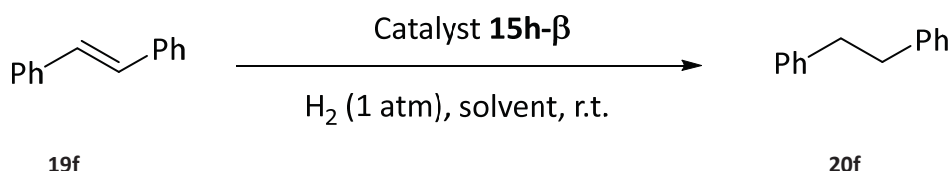
Scheme 13. Hydrogenation of *trans*-stilbene.

Table 4. Different solvents in the hydrogenation of *trans*-stilbene **19f**.[a]

Entry	solvent	Conversion [b] (%)
1	MeOH	67
2	Toluene	60
3	CHCl$_3$	48
4	DCM	78
5	^{i}PrOH	94

[a] *Trans*-stilbene in 4 ml solvent was hydrogenated by 0.2 mol% (0.4wt%) catalyst **15h-β**.
[b] Conversion was determined by GC analysis using dodecane as an internal standard.

To determine the optimal catalyst loading for the hydrogenation of *trans*-stilbene, different amounts of the catalyst were examined (0.1 mol% to 0.3 mol%). Furthermore, control experiment with the microporous polymer 2,2'-biphenol@Co/C **14h-β** having no palladium incorporated did not promote the hydrogenation. All reactions were performed at ambient hydrogen pressure at room temperature.

Full conversion was observed after 30 min with 0.2 mol % catalyst. The increase in the amount of catalyst to 0.3 mol% has no effect on the reaction time (Table 5, entry 4). Notably, no conversion was obtained in the absence of molecular H_2, proving that 2-propanol is not acting as a hydrogen donor in this catalyst system. Other hydrogen donor sources like formic acid /triethylamine or sodium formate were examined but no product was detected.

Table 5. Different catalyst loadings in the hydrogenation of *trans*-stilbene **19f**.

Entry	Pd (mol%)	Time (min)	Conversion [a] (%)
1	0	30	n.d.
2	0.1	30	65
3	0.2	30	98
4	0.3	30	98

Hydrogenation of *trans*-stilbene with catalyst **15h-β** (0.4 wt%) in 4 ml 2-propanol as a solvent.
[a] Conversion was determined by GC analysis using dodecane as an internal standard. n.d. = not determined.

Based on these investigations, the molar ratio of further polymers and the external cross-linker were adjusted. A series of polymers was synthesized using 2 mg $Pd_2(dba)_3 \cdot CHCl_3$ and 3 equivalents of FDA. The palladium incorporation rates were obtained between 64 % and 97 % (Table 6). The hydrogenation of *trans*-stilbene in 2-propanol was selected as a model reaction in order to investigate the catalytic activity of the resulting hybrid materials **15d-γ, 15e-γ, 15h-γ, 15f-γ**. In this regard, when low palladium amounts were used in the synthesis, monomers 1,4-diaminobenzene and 1,1'-biphenyl showed unsatisfactorily results in palladium incorporation (entries 1 and 2), while 2,2'-biphenol and 2,3-naphthalenediol (entries 3 and 4), showed promising results. Notably, phenol monomers possess the capacity to stabilize the palladium nanoparticles even more than strong donor groups (**15d**) or chelators (**15f**).

Table 6. Synthesis of various Pd@MOPs@Co/C following the procedure C in Scheme 12 and their evaluation in the catalytic hydrogenation of *trans*-stilbene **19f**.

Entry	Catalyst	Monomer	FDA[a]	Pd incorporation[b] (%)	Pd[b] (wt %)	Conversion[c] (%)	TOF (h^{-1})
1	**15d-γ**	1,4-diaminobenzene	3	64	0.3	traces	n.d.
2	**15e-γ**	1,1'-biphenyl	3	73	0.3	100 (94)	940
3	**15h-γ**	2,2'-biphenol	3	95	0.4	94 (93)	930
4	**15f-γ**	2,3-naphthalenediol	3	93	0.4	57 (47)	470

[a] Molar ratio with respect to the monomer. [b] Determined by ICP-OES. 2.0 mg (1.9 μmol) Pd$_2$dba$_3$·CHCl$_3$ was employed [c] Hydrogenation of *trans*-stilbene with 0.2 mol % Pd after 30 min. Conversion and yield (in brackets) were determined by GC analysis using dodecane as an internal standard. TOF is calculated as mmol substrate per mmol palladium (this value was obtained by ICP-OES measurements) per time.

In order to further evaluate the new hybrid materials catalyst **15h-γ** (0.4wt%) and catalyst **15e-γ** (0.3wt%), their recyclability and metal leaching in the hydrogenation of *trans*-stilbene to the fully hydrogenated 1,2-diphenylethane were tested.

The catalysts showed overall activities of >300 up to 990 turnover numbers/h (TOF is calculated as mmol substrate per mmol palladium (this value was obtained by ICP-OES measurements) per time). On average, low palladium contamination of about 3 ppm in the product of catalyst **15h-γ** was detected (Table 7), while the leaching palladium in catalyst **15e-γ** showed a higher average of 11 ppm (Table 8). The leached Co was observed on average 6 ppm and 12 ppm in the products of **15h-γ** and **15e-γ**, respectively. It is noteworthy that hydroxyl groups play a decisive role in this phenomenon. They not only capable to stabilize the Pd nanoparticles efficiently but also protect cobalt ions from leaching as an internal scavenger.
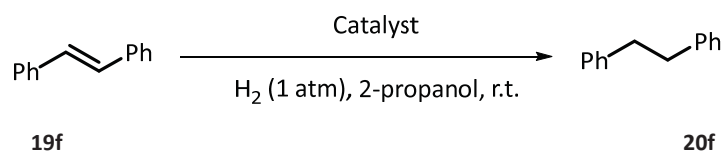
Scheme 14. Consecutive hydrogenation of *trans*-stilbene **19f**.

Table 7. Consecutive hydrogenation of *trans*-stilbene **19f** with catalyst **15h-γ** (0.4 wt %) in 2-propanol and determination of the leaching. [a]

Run	TOF (h⁻¹)	Time (min)	Yield [b] (%)	Leaching Pd[c] (ppm)	Leaching Co[c] (ppm)
1	990	30	99	2	3
2	666	45	93	4	3
3	500	60	98	5	18
4	400	75	97	2	5
5	354	85	96	6	3
6	301	100	95	<2	2

[a] Hydrogenation of *trans*-stilbene (0.5 mmol) using 0.2 mol% catalyst **15h-γ**, [b] Yield was determined by GC analysis using internal standard [c] Leaching was determined by ICP measurement, in µg per g of product.

Table 8. Consecutive hydrogenation of *trans*-stilbene **19f** with catalyst **15e-γ** (0.3 wt %) in 2-propanol and determination of the leaching.[a]

Run	TOF (h⁻¹)	Time (min)	Yield [b] (%)	Leaching Pd[c] (ppm)	Leaching Co[c] (ppm)
1	980	30	98	7	25
2	757	40	90	6	4
3	666	45	93	9	39
4	602	50	91	18	4
5	354	85	90	20	2
6	300	100	94	9	3

[a] Hydrogenation of *trans*-stilbene (0.5 mmol) using 0.2 mol% catalyst **15e-γ**, [b] Yield was determined by GC analysis using internal standard Leaching was determined by ICP measurement, in µg per g of product.

Figures 8 and 9 show a graphical representation of catalyst **15h-γ** and **15e-γ** of the presented reaction in the six following runs.
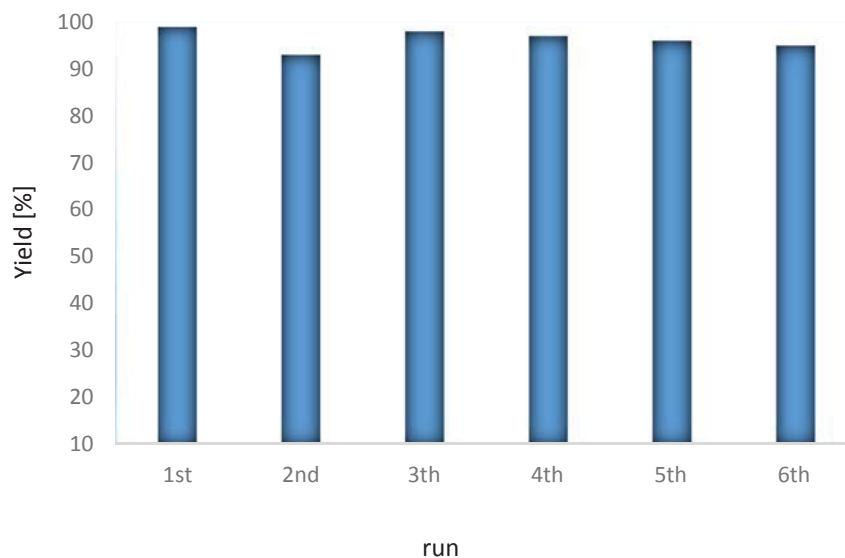
Figure 8. Recycling regarding the hydrogenation of *trans*-stilbene **19f** with catalyst **15h-γ**.
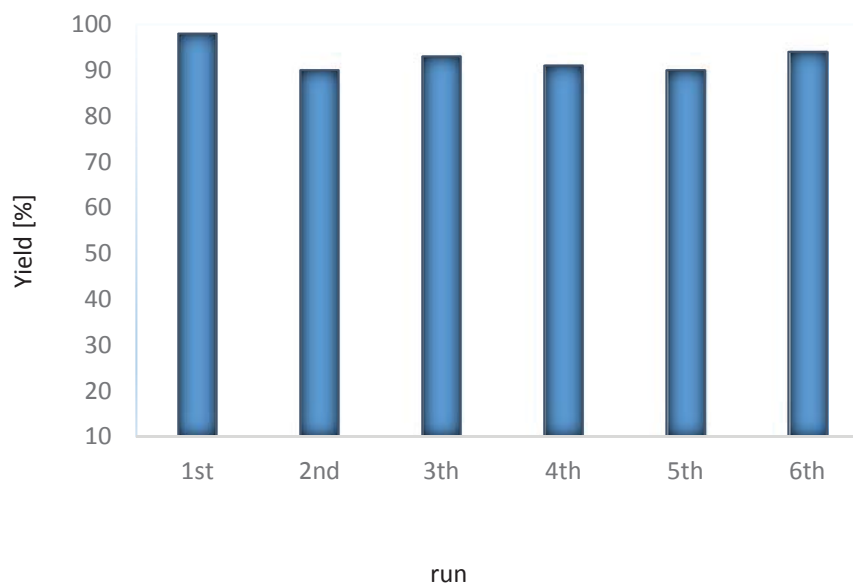
Figure 9. Recycling regarding the hydrogenation of *trans*-stilbene **19f** with catalyst **15e-γ**.

Taking into account a large scale of catalyst **15h-β** and **15g-γ** (500 mg) was synthesized out of **14h-β** and **14g-γ**, resulting in 2.0 wt % Pd (97% Pd incorporation) and 1.9 wt % (89% Pd

incorporation), respectively. The palladium nanoparticle size of **15h-β** was examined by TEM and found to be quite narrow with main particle sizes of 2 and 3 nm (Figure 10, 11 and 12).
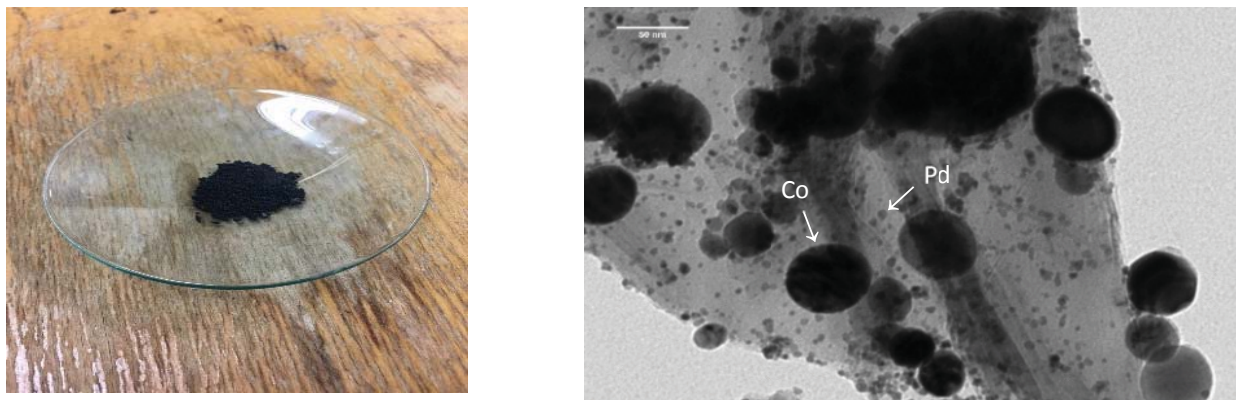
Figure 10. Catalyst **15h-β** with 2.0 wt% Pd.
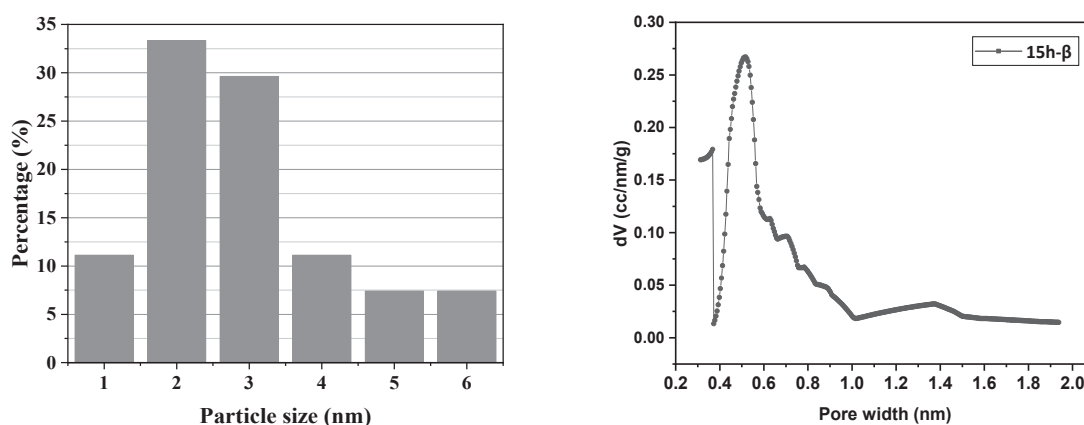
Figure 11. The particle size distribution of palladium nanoparticles. **Figure 12.** The size distribution of the microporous of **15h-β** obtained by the Horvath-Kawazoe (HK) method.

After loading the palladium onto the nanoparticles, the BET surface areas of **15h-β** and **15g-γ** were reduced to 248 $m^2 \cdot g^{-1}$ and 224 $m^2 \cdot g^{-1}$, respectively (Table 9, Figure 13, see Experimental Part for **15g-γ,** Figure 26). In other words, 36% and 19% loss of surface area was observed compared to MOPs **14h-β** and **14g-γ**. The micropore volume ($V_{0.1}$) of **15h-β** showed a decrease of 35%, in contrast to **15g-γ** (18%). The results of **15h-β** showed that the loss of surface area and micropores is related to each other, which can indicate a significant contribution of micropores to the total

34

surface area. Thus, changing the meso/macropore volume ($V_{tot-0.1}$) was not affected by metal leaching of **15h-β** to a great extend (0.04%), in contrast to **15g-γ** (18%).

Table 9. Nitrogen sorption data of **14h-β**, **14g-γ** polymers, and **15h-β**, **15g-γ** catalysts.

No.	FDA (equiv.)	mass (g)	surface area[a] ($m^2 \cdot g^{-1}$)	$V_{0.1/tot}$[b] ($cm^3 \cdot g^{-1}$)	multi-point BET plot considering
14h-β	2.50	0.0850	389	0.63	0.002<P/P_0<0.076
15h-β	2.50	0.0696	248	0.52	0.020<P/P_0<0.151
14g-γ	2.50	0.1218	277	0.37	0.05<P/P_0<0.126
15g-γ	2.50	0.0730	224	0.37	0.032<P/P_0<0.150

[a] Surface area was calculated by multi-point BET plot having a relative error <1.0%. [b] Ratio of micropore volume over the total pore volume at 77.3 K.

Indeed, the results obtained suggest that Pd nanoparticles were incorporated more efficiently into the micropores of the material in the catalyst **15h-β**, which causes more stabilization of Pd nanoparticles and consequently, turns out to suppress Pd leaching.

A   B
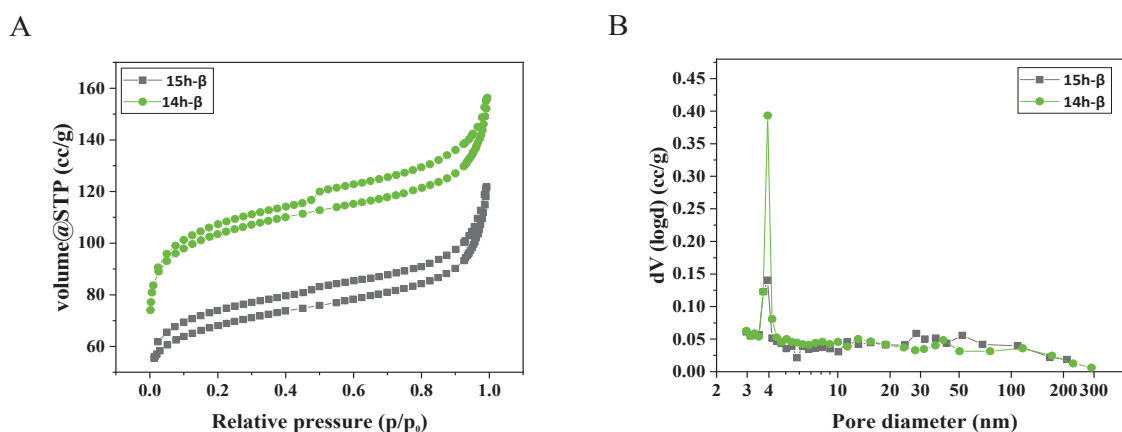
Figure 13. A) N_2 adsorption-desorption isotherms of **14h-β** (green) and **15h-β** (grey). B) Logarithmic presentation of the pore size distribution calculated by the Barrett-Joyner-Halenda (BJH) method for **14h-β** (green) and **15h-β** (grey).

Catalyst **15g-γ** components were characterized by the high-angle annular dark-field scanning transmission electron microscopy (HAADF-STEM). The element mapping shows Pd nanoparticles were distributed within the carbon-based polymer uniformly. The presence of nitrogen and iron

nanoparticles are contributed to the polymer synthesis process (1.4 wt % Fe, corresponding to 2% incorporation of the original FeCl₃ (the graph was shown in the Experimental Part)), and these
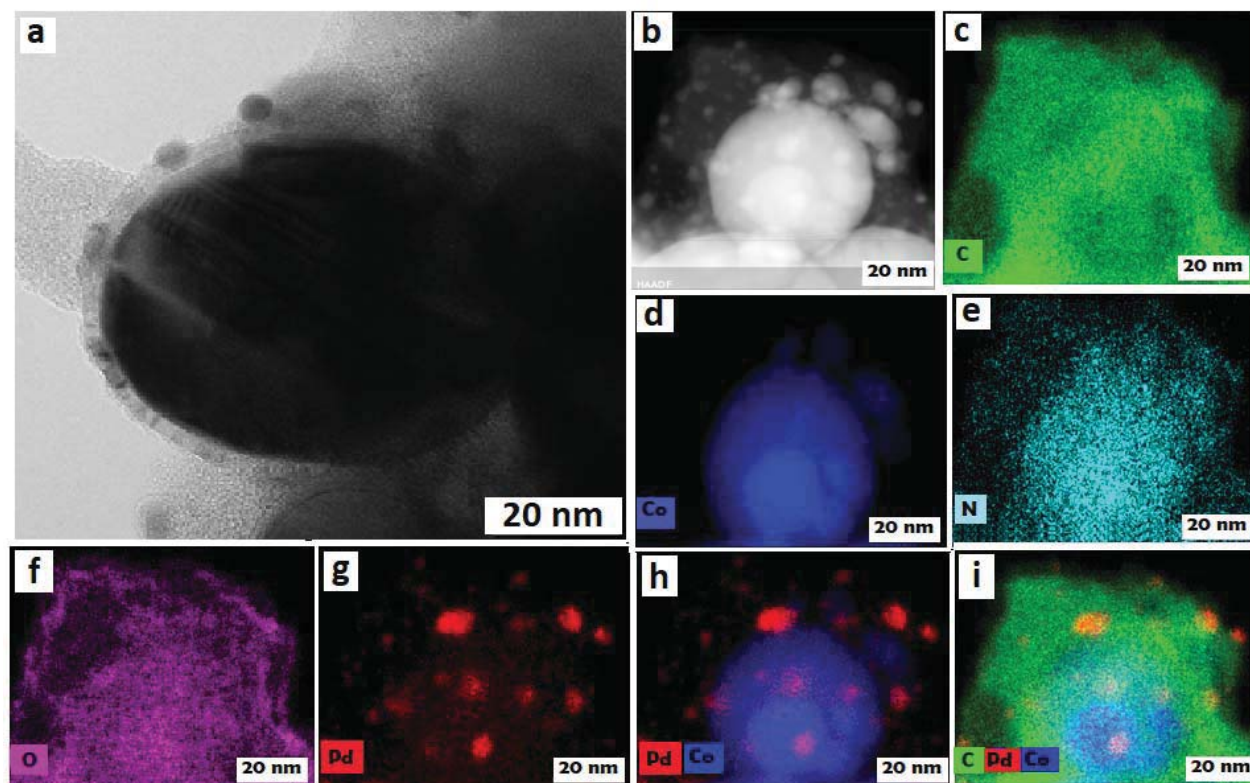
Figure 14. HAADF images and EDS chemical mapping of **15g-γ** (1.9 wt %) a) HRTEM image showing cobalt single nanoparticle covered with carbon and Pd NPs. (b-i) showing the elemental mapping of C, Co, N, O, Pd, Pd-Co, and C-Pd-Co together.

particles were not active for hydrogenation reactions. The distribution of oxygen, predominately present near the iron nanoparticles, suggests an oxidized form of iron (Figure 14).

Afterward, in order to benchmark the fresh and recycled catalyst characterizations, the hydrogenation of diphenylacetylene was performed with catalyst **15h-β** 2.0 wt% (97% Pd incorporation) and **15g-γ** 1.9 wt% (89% Pd incorporation) in 20 ml 2-propanol (Scheme 15, Table 10 and 11).
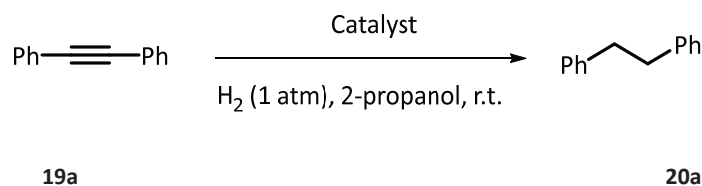
Scheme 15. Hydrogenation of diphenylacetylene **19a** with catalyst **15h-β** and **15g-γ.**

Table 10. Consecutive hydrogenation of diphenylacetylene **19a** with catalyst **15h-β** (2.0 wt %) in 2-propanol and determination of the leaching.[a)]

Run	TOF (h^{-1})	Time[b)] (min)	Yield (%)	Leaching Pd[c)] (ppm)	Leaching Co[c)] (ppm)
1	2000	15	94	2	6
2	1500	20	91	2	3
3	1200	25	84	2	3
4	1000	30	96	3	5
5	1000	30	87	2	5
6	857	35	85	2	2

[a)] Diphenylacetylene **19a** (1 mmol) in 2-propanol (20 mL) was hydrogenated by 0.2 mol % of **15h-β**. Each run was stopped after full conversion in order to determine the leaching. TOF is calculated as mmol substrate per mmol palladium (obtained by ICP-OES measurements) per time until full conversion was reached in hours [b)] Hydrogenation carried out until complete conversion was determined by GC analysis. [c)] Leaching was determined by ICP-OES. Calculated in µg per g of product.

Table 11. Consecutive hydrogenation of Diphenylacetylene **19a** with **15g-γ** (1.9 wt %) in 2-propanol and determination of the leaching.[a)]

Run	TOF (h^{-1})	Time[b)] (min)	Yield (%)	Leaching Pd[c)] (ppm)	Leaching Co[c)] (ppm)
1	1500	20	94	9	25
2	1200	25	89	<2	34
3	1000	30	76	4	13
4	857	35	93	38	42
5	667	45	96	28	27
6	667	45	93	10	15

[a)] Diphenylacetylene 19a (1 mmol) in 2-propanol (20 mL) was hydrogenated by 0.2 mol % 15g-γ (1.9 wt %). Each run was stopped after full conversion in order to determine the leaching. TOF is calculated as mmol substrate per mmol palladium (obtained by ICP-OES measurements) per time [b)] Hydrogenation carried out until complete conversion was determined by GC analysis. [c)] Leaching determined by ICP-OES. Calculated in µg per g of product.

37

Six consecutive cycles of catalyst **15h-β** showed overall a high activity of >800 up to 2000 turnover numbers/h (TOF is calculated as mmol substrate per mmol palladium (this value was obtained by ICP-OES measurements) per time). A negligible amount of Pd and Co leaching of approx. 2 ppm was observed in every run for catalyst **15h-β** as confirmed by ICP-OES (detection limit 2 ppm). No agglomeration of the Pd nanoparticles was observed for both catalysts by TEM analysis after six consecutive hydrogenation runs (Figure 15). Being below the limit of heavy metal contamination (< 10 ppm) is a substantial aspect of our desired catalyst which can be useful in the pharmaceutical industry [16]. After six runs, 90% of the original catalyst **15h-β** (9 mg, 1.76 µmol) and 88% of the original catalyst **15g-γ** (10 mg, 1.8 µmol) were retrieved.
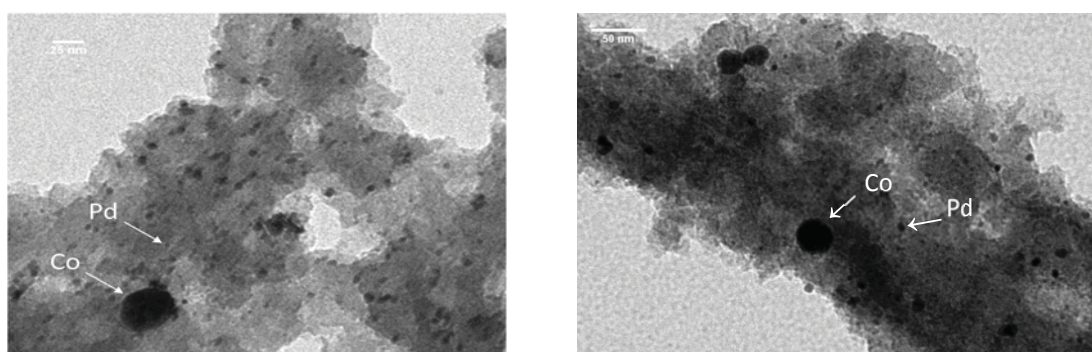
Figure 15. TEM images of the Pd catalyst **15g-γ** (1.9 wt %)(left) and Pd catalyst **15h-β** (2.0 wt %) (right) after six consecutive recycling steps.

X-ray photoelectron spectroscopy (XPS) spectra of Pd(0)/Pd(II) indicated significantly less Pd(II) was detected during preparation and recycling, the Pd(0)/Pd(II) ratio 80:20 upon preparation of **15h-β** and 100:0 after six runs) and catalyst **15g-γ** showed the Pd(0)/Pd(II) ratio 64:35 upon preparation and 82:18 after six runs (see Experimental Part). Increasing the Pd(0)/Pd(II) ratio in a pretreatment experiment shows an *in situ* reduction of the oxidized palladium species upon hydrogenation. Moreover, the higher Pd(0) ratio in catalyst **15h-β** shows that the hydroxyl groups present can protect Pd(0) from oxidation trough coordination (Figure 16) which again demonstrates that the microporous polymer counts as protective support.

Thermogravimetric analysis (TGA) of catalyst **15h-β** detected no serious weight loss up to 200 °C and the polymer can be stable until 200 °C (Figure 17). As a result, the catalyst can be used in various reactions at high temperatures.
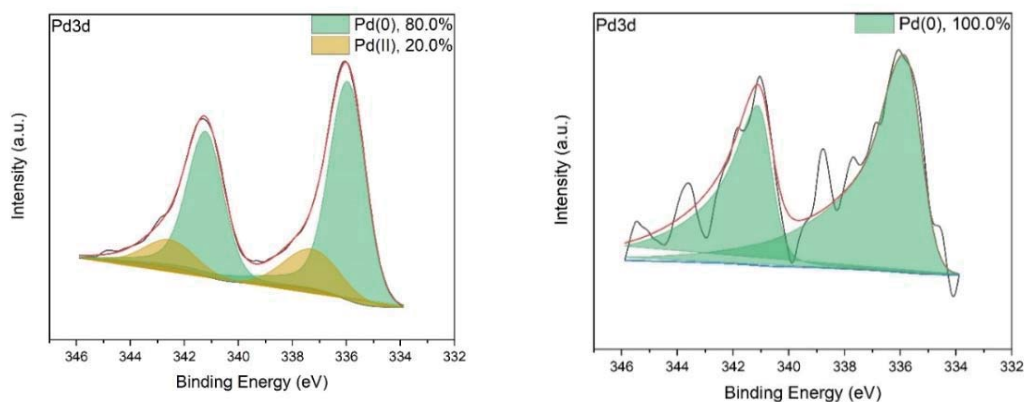
Figure 16. XPS spectra of Pd3d of the catalyst **15h-β** with 2.0 wt % Pd**:** fresh catalyst (left) and after six recycling steps (right).
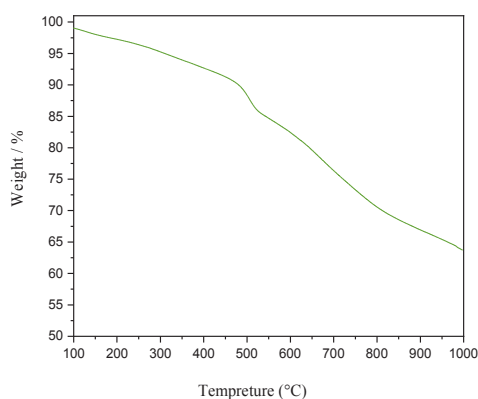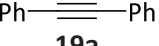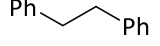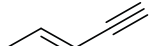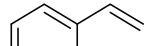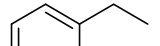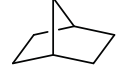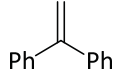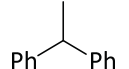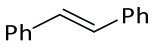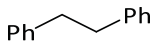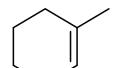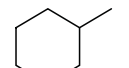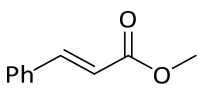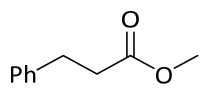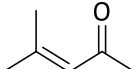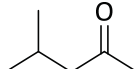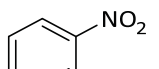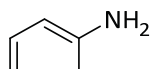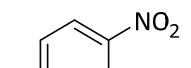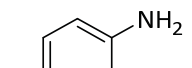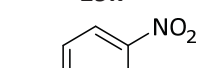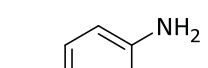

Figure 17. TGA measurement of catalyst **15h-β**.

The catalytic activities of **15h-β** and **15g-γ** was examined with other substrates, various alkynes, alkenes, α,β-unsaturated compounds, and nitroarenes with molecular hydrogen under atmospheric pressure. Primary and strained alkenes were successfully hydrogenated within short reaction times, yielding high TOFs up to 3000 h^{-1} (Table 12, entries 1-4). Corresponding alkanes of di- and tri-substituted olefins were obtained by prolonging the reaction time (65-480 minutes, Table 11, entries 5-9). Furthermore, the double bond was hydrogenated selectively in α,β-unsaturated carbonyl compounds. The hydrogenation of the important class of chemicals, i.e. nitroarenes, proceeded in reaction time of 65-110 minutes (Table 11, entries 10-12).

Table 12. Hydrogenation of alkenes, alkynes, and nitro compounds with **15h-β** (2.0 wt %) and **15g-γ** (1.9%).

Entry[a]	Substrate	Product	Catalyst 15h-β		Catalyst 15g-γ	
			t (min)	TOF (h^{-1})	t (min)	TOF (h^{-1})
1	Ph≡Ph **19a**	Ph⁀Ph **20a**	15	2000	20	2000
2	**19b**	**20b**	30	1000	30	1000
3	**19c**	**20c**	10	3000	10	3000
4	**19d**	**20d**	10	3000	10	3000
5	Ph₂C=CH₂ **19e**	Ph₂CH **20e**	70	429	40	750
6	Ph⁀Ph **19f**	Ph⁀Ph **20f**	65	462	70	429
7	**19g**	**20g**	480	63	540	56
8	**19h**	**20h**	45	667	30	1000
9	**19i**	**20i**	65	462	90	333
10	**19j**	**20j**	110	273	120	250
11	**19k**	**20k**	100	300	110	273
12[b]	**19l**	**20l**	65	92	60	100

[a] Substrate (0.5 mmol) in 2-propanol (10 mL) was hydrogenated by 0.2 mol % **15h-β** (2.0 wt %) or **15g-γ** (1.9%) until full conversion was determined by GC analysis using dodecane as an internal standard. [b] 1 mol % catalyst **15h-β** (2.0 wt %) or **15g-γ** (1.9%) , 50 °C.

1.2. Suzuki cross-coupling reaction

1.2.1. Introduction

C-C bond formation is one of the influential reactions in pharmaceutical and agrochemical chemistry, natural products, and advanced materials [18]. The 2010 Nobel prize in chemistry was granted to Akira Suzuki, along with Richard F. Heck and Ei-ichi Negishi for their achievements in palladium-catalyzed cross-couplings in organic synthesis. In this method, biaryl compounds are synthesized by coupling aryl halides and aryl boronic acid in the presence of Pd and base [19]. This type of reaction not only benefits from a broad tolerance of functional groups but also from mild reaction and sustainable products. Since that time, many studies have been conducted aiming to design a new catalyst with high catalytic performance.

Various solid supports such as magnetic nanoparticles [20], organic polymers [21], dendrimers [22] were used as platforms for molecular Pd complexes or Pd nanoparticles. Diverse ligands were applied to assist the palladium-catalyzed cross-coupling reactions for instance phosphine ligands [23], N- heterocyclic carbenes (NHCs) [24], N,N,O-Tridentate [25], imines [26], oxime palladacycles [27], and diazabutadienes [28].

Although phosphine ligands showed high catalytic activity in palladium-catalyzed cross-coupling reactions, from a practical view some of these catalysts suffer from air and moisture sensitivity during manufacturing in addition to being toxic [29]. Figure 18 shows some examples of phosphine ligands like monodentate, bulky, and electron-rich dialkylbiaryl phosphines which have been used as supporting ligands in the transformation [30].
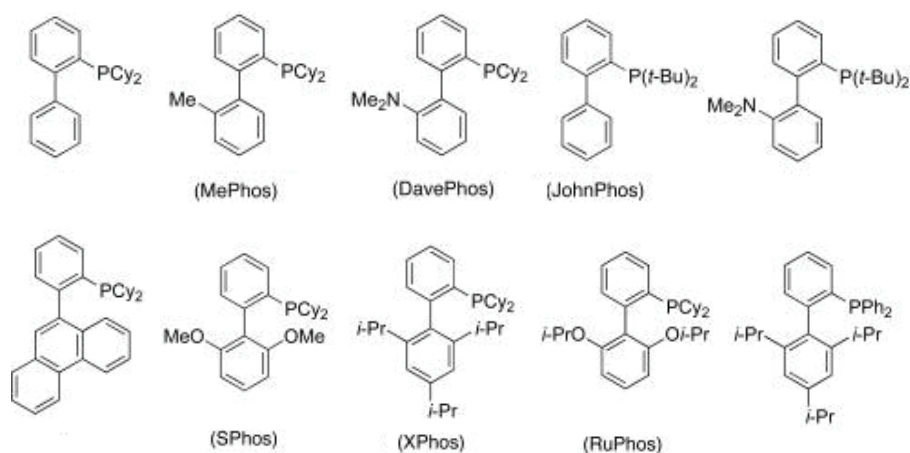
Figure 18. Supporting phosphine ligands.

41

Moreover, investigation of NHCs showed that they are stronger electron-donating than phosphine ligands. The first example NHCs (Figure 19, **A**) was discovered by Ölefe and Wanzlick in 1968. Later, Arduengo et al. have isolated these free NHCs in 1991. Hence, it was called the Wanzlick-Arduengo type carbine [31].
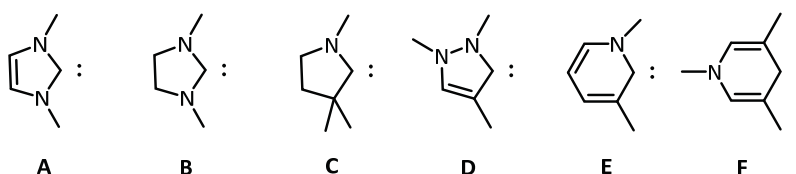

Figure 19. Various N- heterocyclic carbenes.

NHCs showed good activity not only in free form but also in coordinated species. Special properties of NHCs like ease, stability, and efficiency caused them to be applied as a ligand in catalysts. The first example of the Pd-NHCs complex was developed by Herrmann et al. in 1995 in the Suzuki-Miyaura cross-coupling reaction (Scheme 16) [32].
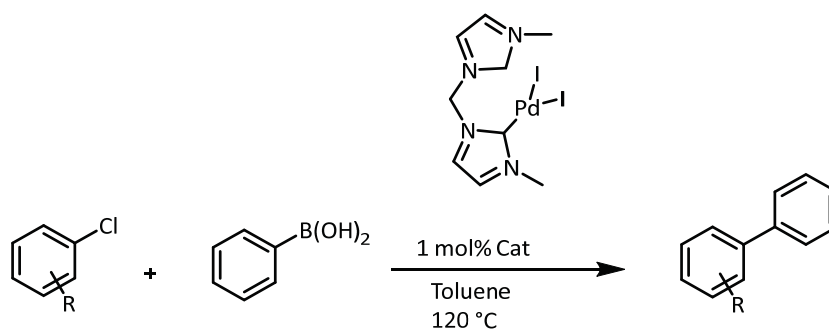
Scheme 16. Pd-NHCs complex.

As isolation of single carbene monomer NHC is a challenging task due to their easy dimerization or decomposition in water, bulky substituents are introduced on the nitrogen atoms of NHCs to prevent them from dimerization.
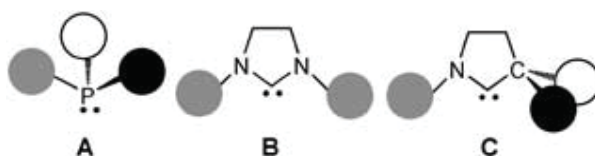
Figure 20. The CAACs structures.

Bertrand et al. demonstrated that the presence of only one nitrogen atom in the N-heterocyclic carbene structure results in a stronger donor than two nitrogen atoms. Notably, they reported that CAACs (Figure 20, **C**) are more efficient complexes than **A** and **B** due to the presence of a quaternary carbon atom in a position α to the carbon center. Inspired by this, the CAAC-palladium-catalyzed α-arylation of carbonyl compounds has been found a useful synthetic method and they were used as an interesting ligand for transition metal in catalysts [33].

Catalysts used in the Suzuki-Miyaura cross-coupling reactions are generally based on homogenous Pd complexes containing ligands such as phosphine or carbenes, which are rarely recoverable. Therefore, the development of cost effective and easily recyclable catalyst systems is highly desirable. Many efforts have been performed to design Pd-based heterogeneous catalysts to improve their recycling performance along with catalytic ability.

Kato et al. developed a microporous polymer network with a monomer having a dendrimer ligand based on polymerization-induced phase separation (PIPS) techniques. They captured the Pd nanoparticles concurrently with polymerization in order to suppress Pd leaching. The catalyst was applied for Suzuki-Miyaura cross-coupling of 4'-bromoacetophenone and phenylboronic acid in water and the desired products were obtained along with a low amount of Pd leaching (0.27% of initial catalyst). As they mentioned the plausible platform of microporous polymer which most contains mesoporous with the surface area of 511 $m^2 \cdot g^{-1}$, was the reason for this achievement [22].

$Pd/Fe_3O_4@SiO_2@KCC-1$ as a novel core-shell magnetic fibrous nanocatalyst reported by Ma et al. in 2014. The resulting catalyst had two efficient properties. First, the support included fibrous silica nanospheres (KCC-1) with a high BET surface area which was functionalized with robust anchors like amino groups. As a result, Pd nanoparticles could be captured by these centers so that the catalyst revealed good dispersion with no aggregation. Second, the presence of core-shell magnetic fibrous caused the catalyst separation and recovery were performed readily. The reduction of 4-nitrophenol and Suzuki-Miyaura cross-coupling of aryl halides were studied to evaluate their catalytic activity. The investigation displayed good catalyst activity in both reactions. Notably, the catalyst not only showed good activity for the Suzuki-Miyaura cross-coupling reaction of aryl iodides and bromides but also displayed good activity with aryl chlorides

after optimizing the reaction condition. At last, the catalyst was reused conveniently for five runs without a significant decrease in the catalytic activity [34].

1.2.2. Results and discussion

The results obtained from the hydrogenation reactions further motivated us to evaluate the catalyst performance of the catalyst **15h-β** for the C-C coupling reaction. Suzuki-Miyaura cross-coupling reactions of various aryl halides were examined with phenylboronic acid **22** in the presence of potassium phosphate as a base.[‡‡]

R: NO$_2$, OMe, OH, Me
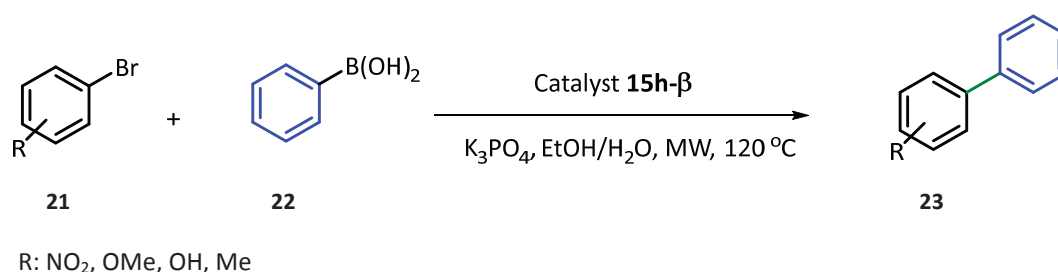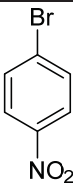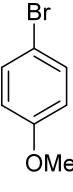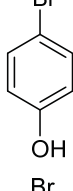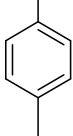
Scheme 17. Suzuki-Miyaura cross-coupling reaction of aryl bromides **21**.

The reactions were performed under microwave irradiation. The advantages of using microwaves irradiation as a heating source include increasing the rate of reactions and improving the product yields, which in turn also saves energy [35]. Suzuki-Miyaura cross-coupling reaction was performed by aryl halides bearing both electron-donating and electron-withdrawing groups (Scheme 17).

The optimal condition was found by using a mixture of water/ethanol (5:5) and microwave heating at 120 °C. The reaction progress was monitored by Thin-layer chromatography (TLC).

[‡‡] The preliminary Suzuki cross-coupling reaction of **15g** (0.43 wt% Pd) with aryliodide as well as arylbromide, related recycling test applying aryl iodide, and screening of reaction conditions were performed by S. Ranjbar [8].

Table 13. Suzuki-Miyaura cross-coupling reaction of aryl bromides **21** with catalyst **15h-β** (2.0 wt %). [a]

Entry	Substrate	t (min)	Yield [b]	TOF (h^{-1})
1	**21a**	10	92	2875
2	**21b**	10	90	2812
3	**21c**	10	80	2500
4	**21d**	30	20	200

[a] Reactions carried out with substrate **21** (0.5 mmol), phenylboronic acid **22**, (0.75mmol), K$_3$PO$_4$ (1.25 mmol) in water (5 mL) and ethanol (5 mL) and 0.2 mol % **15h-β** (2.0 wt %).
[b] Isolated yield.

As listed in Table 13, the coupling of aryl bromides **21** and phenylboronic acid **22** for strong electron-donating and electron-withdrawing groups were obtained in high yields with 0.2 mol% catalyst **15h-β** (2.0 wt%) (entry1-3) while for substrate bearing electron-neutral substituent showed low yield.

R: NO$_2$, OMe, OH, Me
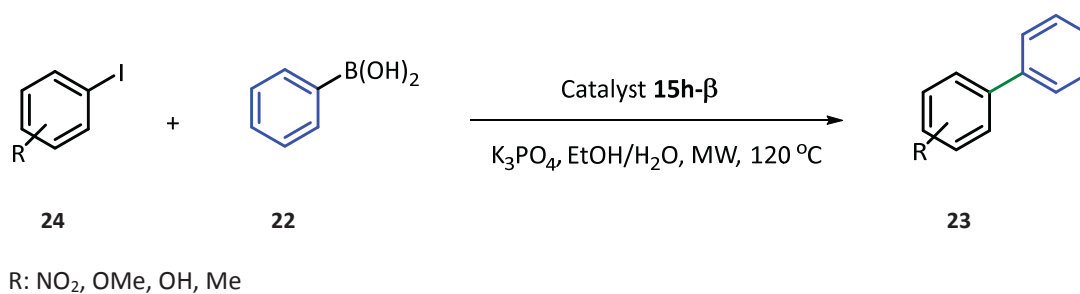
Scheme 18. Suzuki-Miyaura cross-coupling reaction of aryl iodides **24.**

Table 14. Suzuki-Miyaura cross-coupling reaction of aryl iodide **24** with catalyst **15h-β** (2.0 wt %). [a]

Entry	Substrate	t (min)	Yield [b]	TOF (h^{-1})
1	NO$_2$ **24a**	10	95	2968
2	OMe **24b**	10	91	2843
3	OH **24c**	10	82	2562
4	**24d**	30	20	200

[a] Reactions carried out with substrate **24** (0.5 mmol), phenylboronic acid **22** (0.75 mmol), K$_3$PO$_4$ (1.25 mmol) in water (5 mL) and ethanol (5 mL) and 0.2 mol % **15h-β** (2.0 wt %).
[b] Isolated yield.

The catalysts revealed overall a high activity of >200 up to 2875 h^{-1} (TOF is calculated as mmol substrate per mmol palladium (this value was obtained by ICP-OES measurements) per time). Further evaluation of the catalytic activity for the coupling between aryl iodides and

phenylboronic acid indicated comparable results with TOFs of >200 up to 2968 h^{-1} for coupling of aryl iodides (Table 14).

The data in Tables 13 and 14 show the effect of substitutes on the aryl halides. Notably, the presence of strong electron-donating and electron-withdrawing moieties influences significantly the catalytic activity. The data of entries 4 of Table 13 and Table 14 illustrate the remarkable decrease of catalytic activity with substituents such as methyl.

In order to extend the scope of our catalytic system, we performed the coupling of deactivated aryl chlorides through the aforementioned condition. Unfortunately, the coupling of aryl chloride did not proceed under this condition. It is already known that an appropriate solvent can efficiently affect the coupling in the Suzuki-Miyaura cross-coupling reaction [36]. To do so, various solvents (EtOH/H$_2$O, DMA/H$_2$O, DMF/H$_2$O, DCM, Toluene/H$_2$O/^{i}PrOH) were tested but just biphenyl as a side product was obtained.

We subsequently performed different catalysts loadings like 0.5 mol%, 1.0 mol%, 1.5 mol%, 2.0 mol% as well as various bases K$_3$PO$_4$, K$_2$CO$_3$, Na$_2$CO$_3$. Besides these experiments, the reactions were carried out for 3 h with microwave or 24 h with conventional heating, but no product was observed.

As the efficient catalyst is considered with the minimum amount of heavy metal in products, the recyclability of catalyst **15h-β** was investigated in six consecutive cycles.
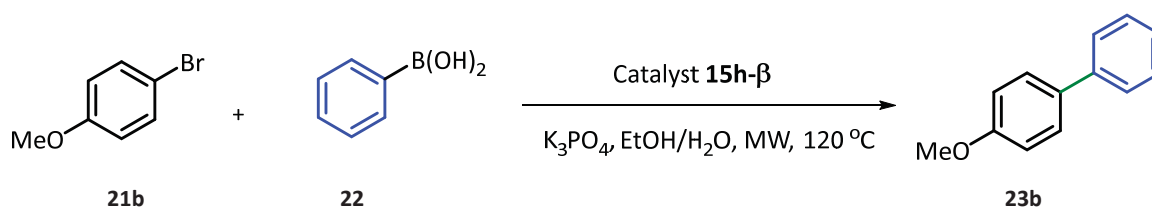
Scheme 20. Consecutive Suzuki-Miyaura cross-coupling of 4-bromoanisole **21b**.

Table 15. Consecutive Suzuki cross-coupling of 4-bromoanisole **21b** with catalyst **15h-β** in water and ethanol for 10 min and determination of the leaching.[a]

Run	TOF (h^{-1})	Yield (%)	Leaching Pd[b] (ppm)	Leaching Co[b] (ppm)
1	1118	95	4	3
2	1125	90	2	6
3	1087	87	2	4
4	1000	80	3	6
5	925	74	4	2
6	875	70	3	2

[a] 4-bromoanisol **21b** (1 mmol), phenylboronic acid **22** (1.5mmol), K_3PO_4 (2.5 mmol) in water (7 mL) and ethanol (7 mL), and 0.5 mol % of **15h-β** (2.0 wt %) were used for recyclability test. After each run, the leaching was determined. TOF is calculated as mmol substrate per mmol palladium (obtained by ICP-OES measurements) per time. [b] Leaching was determined by ICP-OES. Calculated in µg per g of product.

In order to find the possible impact of aryl halides on Pd leaching, the Suzuki-Miyaura cross-coupling reaction of 4-iodoanisole and 4-bromoanisole was examined. The reactions were performed with microwave heating at 120 °C and after each run, the catalyst was separated from the reaction mixture by an external magnet. As the result, 73% of the original catalyst was regained (19 mg, 1.8 µmol) in the coupling reaction of 4-iodoanisole, and retrieval catalyst was obtained 76% (21 mg, 2.0 µmol) in the coupling reaction of 4-bromoanisole.

On average, low palladium contamination of about 3 ppm in the coupling reaction of 4-bromoanisol **21b** was detected (Table 15), while the leaching palladium in the coupling reaction of 4-iodoanisol **24b** showed a slightly higher average of 4 ppm (Table 16).
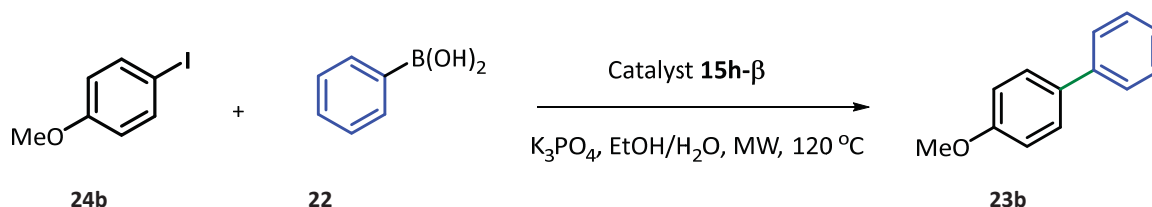
Scheme 19. Consecutive Suzuki-Miyaura cross-coupling reaction of 4-iodoanisol **24b**.

Table 16. Consecutive Suzuki cross-coupling of 4-iodoanisol **24b** with **15h-β** catalyst in water and ethanol for 10 min and determination of the leaching.[a]

Run	TOF (h^{-1})	Yield (%)	Leaching Pd[b] (ppm)	Leaching Co[b] (ppm)
1	1225	98	2	3
2	1125	92	3	15
3	1030	88	7	8
4	987	79	3	6
5	875	70	4	5
6	875	70	3	4

[a] 4-iodoanisol **24b** (1 mmol), phenylboronic acid **22** (1.5mmol), K_3PO_4 (2.5 mmol) in water (7 mL) and ethanol (7 mL), and 0.5 mol % of **15h-β** (2.0 wt %) were used for recyclability test. After each run, the leaching was determined. TOF is calculated as mmol substrate per mmol palladium (obtained by ICP-OES measurements) per time. [b] Leaching was determined by ICP-OES. Calculated in µg per g of product.

Approximately 3% and 2% of Pd were leached from the supports in total within all runs (in 4-iodoanisole and 4-bromoanisole reactions, respectively). The leached Co was observed on average 7 ppm and 4 ppm in the products of 4-iodoanisol **24b** and 4-bromoanisol **21b**, respectively. The negligible amounts of leached Co and Pd show the catalyst structures are stable and resistant after six runs. The results indicated that Pd leaching occurs independently of aryl halides performance. Moreover, TOF (h^{-1}) of reactions showed, the coupling of 4-iodoanisole **24b** proceeded slightly faster. The same trend for the Pd@toluene@Co/C **15g** with 0.43 wt% Pd has been observed by a former colleague, S. Ranjbar. This tendency can be attributed to the weak

bond dissociation energy of C-I (PhI: 65 kcal.mol^{-1}) compared to C-Br (PhBr: 81 kcal.mol^{-1}) which leads to faster reactivity in the oxidation step [8].

1.3. Conclusion

In summary, to take advantage of the unique properties of MOPs materials along with magnetic catalysts, we have developed a new magnetically retrievable palladium nanocatalyst with a microporous organic polymer network. A range of microporous organic polymers was synthesized to find an efficient network for stabilizing palladium nanoparticles. Among them, the microporous polymer 2,2'-biphenol@Co/C **14h** provided a higher surface area and appropriate pore size for uniform distribution of palladium nanoparticles. This platform prevents the agglomeration and deactivation of the catalytically active sites. The resulting catalyst showed low Pd and Co leaching in the products in hydrogenation and Suzuki-Miyaura cross-coupling reactions. Another approach of the porous material **14h**, employing this polymer as scavenger for various heavy metal ions such as Hg^{+2}, Cu^{+2}, Cr^{+2}, and Pb^{+2} which was performed in our group [37]. Notably, the magnetic character of the catalyst allows its easy recovery from the reaction by a simple external magnet and could be reused for six consecutive runs.

2. Bimetallic Zn@Pd@MOP@Co/C Catalyst for Selective Hydrogenation
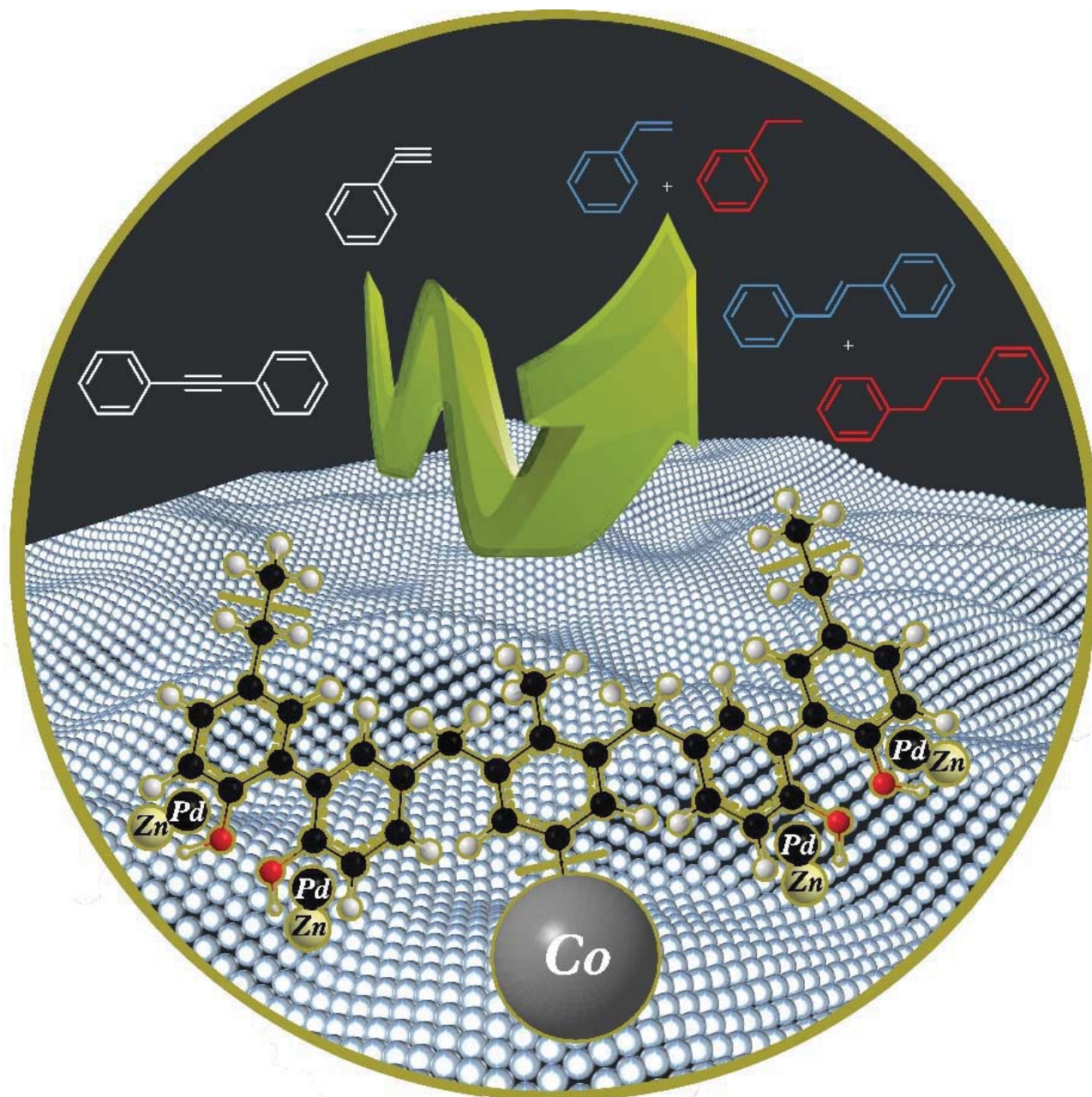
2.1. Introduction

One of the most prominent categories of heterogeneous are bimetallic catalysts [38]. Bimetallic catalysts are composed of two different metals that in addition to the individual properties of metals reveal new and distinctive properties. These new properties derived from synergistic effects between the two different metals in the bimetallic systems. Their tunable chemical/physical properties have attracted attention in a wide range of applications. Hence, the development of bimetallic catalysts has been a research focus for many years, and the library of bimetallic catalysts has been enriched significantly in the last decade [39].

The most prominent and earliest example of utilizing bimetallic materials back to the Bronze age when Cu-Sn alloy have been replaced stone as the material of choice in the manufacturing of tools and weapons, and also as buildings materials [40]. In the succeeding centuries, a wide range of bimetallic materials has been produced and their properties characterized, thanks to modern technology.

The first "bimetallic cluster" was introduced by John H. Sinfelt through bimetallic nanocatalysts supported on silica or alumina [41]. Later, bimetallic catalysts like Ni-Cr, Ru-Cu, Os-Cu, Pt-Ir, and Pt-Ru with high valence electronic configuration were evaluated and showed high activity and selectivity in reactions [38]. Despite that monometallic catalysts have been employed for selective hydrogenation, they suffer from insufficient selectivity in reactions. In addition to the low selectivity, it is widely known that noble metal catalysts are significantly more expensive. Thus, bimetallic nanoparticles (BNPs) that contain noble metals have the potential to decrease the noble metal content, leading to cost reduction. BNPs have been considered to be more efficient than their monometallic counterparts in catalytic applications, due to their reduced size and increase in the surface area [42]. Although the activity of bimetallic catalysts was reported lower than monometallic catalysts, the high selectivity of these catalysts has received considerable attention in this field. Under these premises, BNPs have been explored for a range of reactions such as selective oxidation [43], selective hydrogenation [44], hydrogenolysis [45], and reforming reactions [46]. For instance, hydrogenation products of alkyne alcohols or unsaturated ketones which are important intermediates in the production of vitamins (A, E, B_6, and K), fragrant substances, textile, and resin industries are produced by bimetallic catalysts [47].

Generally, two common strategies can be employed for the synthesis of bimetallic nanostructures, the so-called bottom-up and top-down approaches. From economic point of view, the bottom-up method is preferred, offering an economical synthetic method, compared to the top-down technique which requires expensive types of equipment for the synthesis.

Bimetallic nanoalloy catalysts can be developed through the following methods: chemical reduction, thermal decomposition of appropriative precursors, electrochemical synthesis, radiolysis and sonochemical synthesis. The chemical reduction method is subclassified into co-reduction, reduction of bimetallic metal complexes, successive reduction. The method described here is limited to the chemical reduction technique. This method is performed by a reducing agent like $NaBH_4$ or N_2H_4 or H_2 gas. Moreover, stabiliser molecules such as surfactant ligands (e.g. alkyl thiols) or polymer ligands (e.g. polyvinyl pyrrolidone (PPV), polyvinyl alcohol (PVA), dendrimers) can be used to prevent the nanoparticles from aggregation [48, 49, 50]. In this method, controlling the reduction process is critical because of the difference in the reduction potentials of two metals. Nevertheless, the modification of catalysts is very challenging since it requires correlating the characteristics of the active phase and the catalytic performance.

Several structures were reported for bimetallic nanoparticle systems: crown-jewel structure, alloyed structure, core@shell, hetero-structure, and hollow structure (Figure 21) [51]. The fundamental structure of the bimetallic catalysts is related to the spatial distribution of two metals.
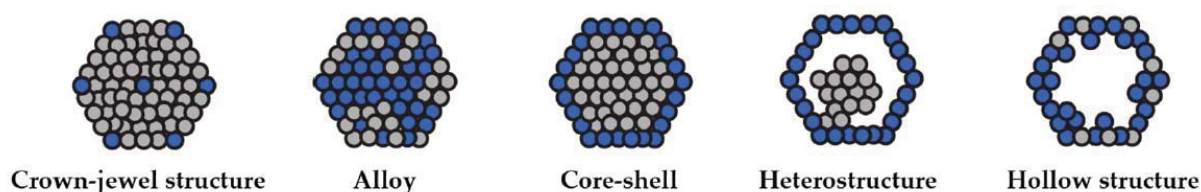
Figure 21. Different bimetallic systems.

The commonly used methods for preparing crown-jewel structures are chemical vapor deposition (CVD) and the solution state methods. The precious metal atoms serve as the jewel

and locate at the surface of none-noble metals (M= Ni, Cu, Fe, etc.). Hence, expensive metals can engage in chemical reactions [52].

The other structure which has attracted increasing attention in oxidation reduction reaction (ORR) and in proton-exchange membrane fuel cells (PEMFCs) is the bimetallic hetero-structure system. Bimetallic hetero-structures are produced through growth mechanisms like seed mediated co-reduction, hydrothermal, galvanic replacement reactions, and antigalvanic reactions [53]. For example, Pt-on-Pd heterogeneous bimetallic nanostructures have been produced by a reducing agent in an organic medium in the presence of Pd nanoparticles as seeds. Considering that synthesis through growth methods is time-consuming and needs pre-formed seeds, much research has been devoted to develop a direct synthesis method. Yamauchi and co-workers proposed a simple method with high yield for the direct synthesis of Pt-on-Pd nanostructure in an aqueous solution. Mixtures of K_2PtCl_4, $NaPdCl_4$, and Pluronic P123 were introduced to ascorbic acid as a reducing agent at room temperature for 30 minutes. The bimetallic hetero-structure was obtained with a dendritic shape which Pt distributed as a nanoarms branching in various directions and Pd in the core domain [54].

Hollow structures are another bimetallic systems that have gained considerable interest owing to their high surface-to-volume ratio and large pore volume. Bimetallic nanomaterials with hollow structures are produced by the template-mediated strategy which includes hard-templating, soft-templating, and sacrificial templating methods [55, 56]. Albeit template-mediated methods are effective and controllable approaches, the high cost and tedious synthetic procedures are one of their disadvantages [57]. Hence, Yang and coworkers introduced a novel one-pot template-free approach to the synthesis of hollow PdCu alloyed nanocubes through tuning the surface energy difference of the main crystal planes by alloying. In this method, palladium (II), copper (II), salt, glutamate, and multi-walled carbon nanotubes (MWCNTs) were added into ethylene glycol (EG) and heated at 160 °C for 6 h. Their results revealed that the hollow PdCu nanocubes have a higher accessible surface area and superior electrocatalytic activity than the solid PdCu nanoparticles [58].

Among bimetallic structures, core@shell and alloyed systems are most intuitive, owing to the interaction and dispersion between the two metals. From a synthetic point of view, the reduction method has a significant role in the resulting structures. For example, the alloyed system is obtained when both metal precursors are reduced simultaneously, contrasting core-shell structures for which reduction is performed sequentially. In the core-shell system, the noble metal is initially reduced, followed by the subsequent addition of second metal. [59, 60, 61]. Moreover, core@shell structured nanomaterials are considered the kinetically stable structures whereas, the corresponding alloy nanostructures are the thermodynamically stable species. Core- shell structures are able to transform to their corresponding alloy counterparts by heating [62]. Generally, the final structure of bimetallic catalysts strongly depends upon the composition, their synthesis method and condition, relative strengths of metal-metal bond, and surface energies of bulk elements [38].

Several factors have been identified as an effective means of influencing the catalytic activity/selectivity of a bimetallic catalyst. The effect of some factors will be discussed in the following.

2.1.1. Metal particle size and shape effects

As the majority of the chemical reactions occur on the surface of the catalyst, decreasing the size of particles and increasing the surface area can increase catalytic activity [63, 64].

In 1986, Sárkány et al. investigated the Pd dispersion on the competitive hydrogenation of an acetylene and ethylene mixture over Pd/Al_2O_3 as a catalyst. They observed that increasing the Pd dispersion, i.e., decreasing the size of Pd particles has a significant influence on the selectivity for ethylene formation and the turnover frequency (TOF) of acetylene hydrogenation. Since more acetylene is adsorbed on smaller Pd crystallites in a less crowded manner, more hydrogen can be absorbed between the hydrocarbon layers on the catalyst surface and leads to more activity [65]. Moreover, the Pd surface structure can also have an impact on catalytic performance. In this regard, Moon groups revealed that catalysts with bigger particles such as cubic Pd NPs have higher selectivity and conversion than catalysts with spherical particles in acetylene hydrogenation. In other words, the cubic Pd particles need a lower temperature towards the

spherical particles for the hydride decomposition and desorption of C_2 hydrocarbons on the catalyst surface [66].

2.1.2. Surface area and porosity

The surface area and porosity play an important role in catalytic performance. For example, porous structured alloys with a high surface area are significantly more promising support in catalytic applications than their solid counterparts [67]. The porous alloy system was first produced using dealloying by Murray Raney. The developed porous alloy was synthesized *via* selective leaching of a block of nickel-aluminium alloy ($NiAl_3$ and Ni_2Al_3) with concentrated sodium hydroxide and used for the hydrogenation of vegetable oils. The dealloying approach was utilized for more than 80 years to generate nanoporous alloys with large surface areas and small pores in heterogeneous catalyst applications. This approach contains electrochemical and chemical dealloying. Noble and non-noble metals could be applied with this method to produce alloy nanoporous NPs. In this technique, the less-noble component is selectively dissolved with an excess amount of concentrated nitric acid to leave a nanoporous residue [68]. The nanoporous alloys fabricated by the dealloying method have been widely reported recently. For instance, Wang et al. produced bimetallic nanocrystals *via* a chemical dealloying process using nanocrystalline alloys Au-, Pd-, Pt-, Ir-, Ru-, Rh- as precursors. As the precursor itself has small particle size and large surface area, the as-obtained dealloyed product (such as nanoporous Pd-Ni alloys) not only has ideal surface area and pore size, but also unique structural properties [69]. A nanoporous PdNi(np-PdNi) catalyst is an example of a bimetallic catalyst that produced *via* electrochemical dealloying a $Pd_{20}Ni_{80}$ alloy as the precursor in an acid solution by Chen group [70]. It should be stated that the large surface area and small pores of alloy nanoporous nanoparticles make them superior to the various fields such as electrochemical catalysis, heterogeneous catalysis, and semi-homogeneous catalysis [69].

2.1.3. Second metal effects

The addition of the second metal can modify the electronic state of the primary catalytic component and improve its catalytic properties. Hence, the interaction between the active site and the second metal plays an important role in the catalytic performance of bimetallic catalysts [71]. Zhang et al. showed that an *in situ* treated Pt–Re/C bimetallic catalyst involved positively

charged Pt of which the extent of electron deficiency increased with the Re amount, suggesting electron transfer from Pt to Re [72].

Another crucial factor in the bimetallic systems is the molar ratio of the second metal. It should be stressed that various molar ratios of the second metal can make a different selectivity and specific activity (TOF) in catalytic performance. For example, Fang and coworkers compared magnetic core-shell monometallic $Fe_3O_4@SiO_2$/Pd and bimetallic $Fe_3O_4@SiO_2$/Pd-M (M = Ag, Cu, and Zn) catalysts with various loadings and shell thickness in the hydrogenation of phenylacetylene. They reported that $Fe_3O_4@SiO_2$ (c,80)/$PdZn_6$ exhibits the best selectivity of 86.1% for the formation of styrene at a phenylacetylene conversion around 99.5% compared to aforementioned catalysts or $Fe_3O_4@SiO_2$(c,80)/$PdZn_{0.6}$ (with a Zn/Pd molar ratio of 0.6). The stability of the catalyst was tested for 10 consecutive cycles and no metal leaching was observed [73]. Similarly, Wang et.al reported that Pd-Zn_6/Al_2O_3 is more selective for the hydrogenation of phenylacetylene to styrene by comparison with Pd-$Zn_{0.6}$/Al_2O_3, $PdCu_{0.6}$/Al_2O_3, and $PdCu_6$/Al_2O_3. The high selectivity of Pd-Zn_6/Al_2O_3 was attributed to the maximum modification degree of Zn on Pd [74].

2.2. Supported bimetallic catalysts

A number of active metals such as Pd, Ni, Au was modified with a wide range of elements (Ag, Cu, Si, Ga, Sn, Zn) and supported on different carriers. Solid oxide carries such as Al_2O_3 [75], SiO_2 [76], TiO_2 [77], ZnO [78], activated carbon (AC) [79], and magnetic NPs [80] have been explored as potential supports for bimetallic catalysts. PdZn was developed on the metal oxide support (e.g. ZnO-based) through the reduction method (Figure 22). In this regard, during reduction, Zn metal can alleviate the number of Pd active sites on the surface by diluting and consequently, the PdZn intermetallic phase can be produced [78].

Figure 22. Selective hydrogenation of alkyne with PdZn alloy catalyst on Zno support. Reproduced with permission from reference [78]. Copyright 2011, American Chemical Society.

Among developed alloys, catalysts based on Pd-Zn alloy have been reported to be promising and effective catalysts in selective hydrogenation of alkynes to alkenes. Stakeev et al. compared the selectivity of Pd/C and Pd-Zn/C catalysts in acetylene hydrogenations. The Pd-Zn/C catalyst was synthesized using the heterobimetallic $PdZn(OAc)_4(OH)_2$ complex *via* the incipient-wetness impregnation method. They reported that the presence of Zn improves the selectivity of the catalyst for the semi hydrogenation of alkynes as compared to the monometallic catalyst Pd/C. Although TEM and SEM analysis indicated that the Pd dispersion in the Pd-Zn/C catalyst is lower than in the Pd/C catalyst, the favorable selectivity derives from homogeneous formation of Pd-Zn bimetallic nanoparticles [81]. This result was in contrast with the previous reports in monometallic catalysts showed that high Pd dispersion leads to better selectivity in alkyne hydrogenation reactions [82, 83].

Pd-Ni alloy with two different supports such as alumina (Al) and activated carbon (AC) was also synthesized using different catalyst loadings for alkyne selective hydrogenation. The obtained results showed that Pd-Ni with Al_2O_3 support is more active and selective than Pd-Ni with activated carbon (AC) support even at low loadings. Catalysts characterization exhibited that γ-Al_2O_3 support has a poor contribution of supermicro-, mirco-and macropores, in contrast to the activated carbon (AC) support [84].

Ru-Ni/Fe_3O_4 catalyst was the other catalyst that was prepared for selective hydrogenation. To do so, diformyltricyclodecanes (DFTD) was reduced to tricyclodecanedimethylol (TDDMO) under

mild conditions. The developed bimetallic catalyst showed good conversion and selectivity even at a very low Ru loading (97% selectivity at 98% conversion). Notable, adding PPh$_3$ as a ligand had a positive effect on catalytic performance [85].

2.3. Application of bimetallic catalysts

The intrinsic electronic/geometric structures of bimetallic catalysts have attracted academic and industrial interest over the last decades. Bimetallic catalysts play an important role in a wide variety of chemical and electrochemical reactions. The range of their applications was detailed studied by Hutchings's group [86]. It is worth mentioning that bimetallic catalysts have been considered as superior catalysts for high purity hydrogen production *via* steam reforming techniques [87]. Bimetallic catalysts are widely used for certain reactions like vinyl acetate (VA) synthesis. In the United States, 4.8 million tons of vinyl acetate (VA) are generated over Pd-Au catalysts [88]. It should be stressed that the tiny size and large surface areas of bimetallic nanoparticles provide them high conductivity, which helps in the production of electronic devices such as memory chips, display screens, and transistors. In pharmaceutical sciences, magnetic bimetallic nanocatalysts are used in drug delivery, the early diagnosis of disease, and its treatment [89]. For example, Iron based bimetallic nanoparticles coated with peptides are being bound to the tumor cells for improving magnetic resonance imagine (MRI) [90]. In a word, bimetallic catalysts have significant economic value because of their high durability and performance. Hence, they are utilized in various applications such as medicine, engineering, catalysis, and other industrial fields.

With the development of artificial chemicals, selective reactions play an important role in reducing byproducts. For example, in selective hydrogenation reactions by using a selective catalyst, only one target functional group is reduced and all other functional groups remain in the substrate which in turn decreases undesired byproducts. Over the last decades, many efforts have been devoted to the development of highly selective and efficient catalysts. Pd-based catalysts are known as active catalysts for hydrogenation reactions as hydrogen is easily dissociated on the palladium surface [91, 92]. Moreover, several studies have reported the selectivity of Pd catalyst can be increased by modification of second metal. To date various

additional metals (e.g., Co [93], Fe [94], Cu [95], Ni [96], Ag [97], Zn [98]) were introduced to monometallic Pd catalysts.

However, Pd-Zn bimetallic gained significant attention in catalysis due to their high miscibility, high thermal stability, high oxygen binding capability, and high ability to form a uniform structure. PdZn bimetallic nanoparticles were widely used not only in selective hydrogenation reactions but also in a number of applications such as methanol reforming [98], ethanol dehydrogenation [99], hydrodeoxygenation (HDO) [100], and water-gas shift reactions [101]. For example, bimetallic Pd/Zn catalyst was reported as an alternative for Cu/ZnO and Cu/Cr catalysts in ethanol dehydrogenation, because the presense of Zn can improve the stability of the Pd by preventing them from stintering [102].

2.4. Results and discussion

Based on these previous investigations, bimetallic catalyst comprising PdZn nanoparticles into a microporous organic polymer matrix with the magnetic carbon-coated cobalt support may indicate interesting catalytic properties in selective hydrogenation reactions. In this regard, Zn-Pd was synthesized on the carbon-coated fragment cobalt magnetic nanobeads (Co/C) surrounded by a microporous organic polymer shell which has the ability to control the formation of well-defined nanoparticle systems. No toxic stabilizing agents or ligands were used in the synthesis of Zn@Pd@MOP@Co/C. The preparation of Pd nanoparticles precedes the reduction of Zn ions. Afterward, pre-formed monometallic nanoparticles must be surrounded by the second metal. The electron transfer from the transition metal Zn atoms to noble metal Pd atoms supposedly occurs in the ZnPd nanoparticles. Hence, Zn atoms are deposited on the Pd nanoparticles. As a result, the second metal can decrease a tendency of Pd towards adsorption of unsaturated compounds. This process may form the bimetallic Pd(core)-Zn(shell) bimetallic nanoparticles. The so prepared bimetallic catalyst using a low-cost second metal could reduce the usage of costly Pd. In addition, the catalyst can be readily retrievable by an external magnet.

To do so, the results obtained from the hydrogenation reactions in our previous work [9] motivated us to employ the 2,2'-biphenol@Co/C **14h** as the polymeric network. The synthetic strategy for the bimetallic Zn@Pd@MOP@Co/C nanoparticles used in our work involves three

steps. First, 2,2'-biphenol@Co/C **14h** was developed around the Co/C **11**. Second, 300 mg of the 2,2'-biphenol@Co/C **14h** was introduced to 6 mg $Pd_2(dba)_3 \cdot CHCl_3$ by microwave irradiation to produce **15h** with palladium loading of 0.3 wt% and incorporation of 78%. Hydrazine monohydrate solution was added dropwise to the 70 mg of the **15h**, to bring the PH of the mixture to 9, followed by the addition of 0.1 g $NaBH_4$. Subsequently, $Zn(NO_3)_2 \cdot 6H_2O$ was added to the **15h**. Therefore, Zn ions on the pre-formed monometallic nanoparticles **15h** are reduced by the reducing agent to Zn(0). In the end, the reaction mixture was stirred for 24 h at 60°C.
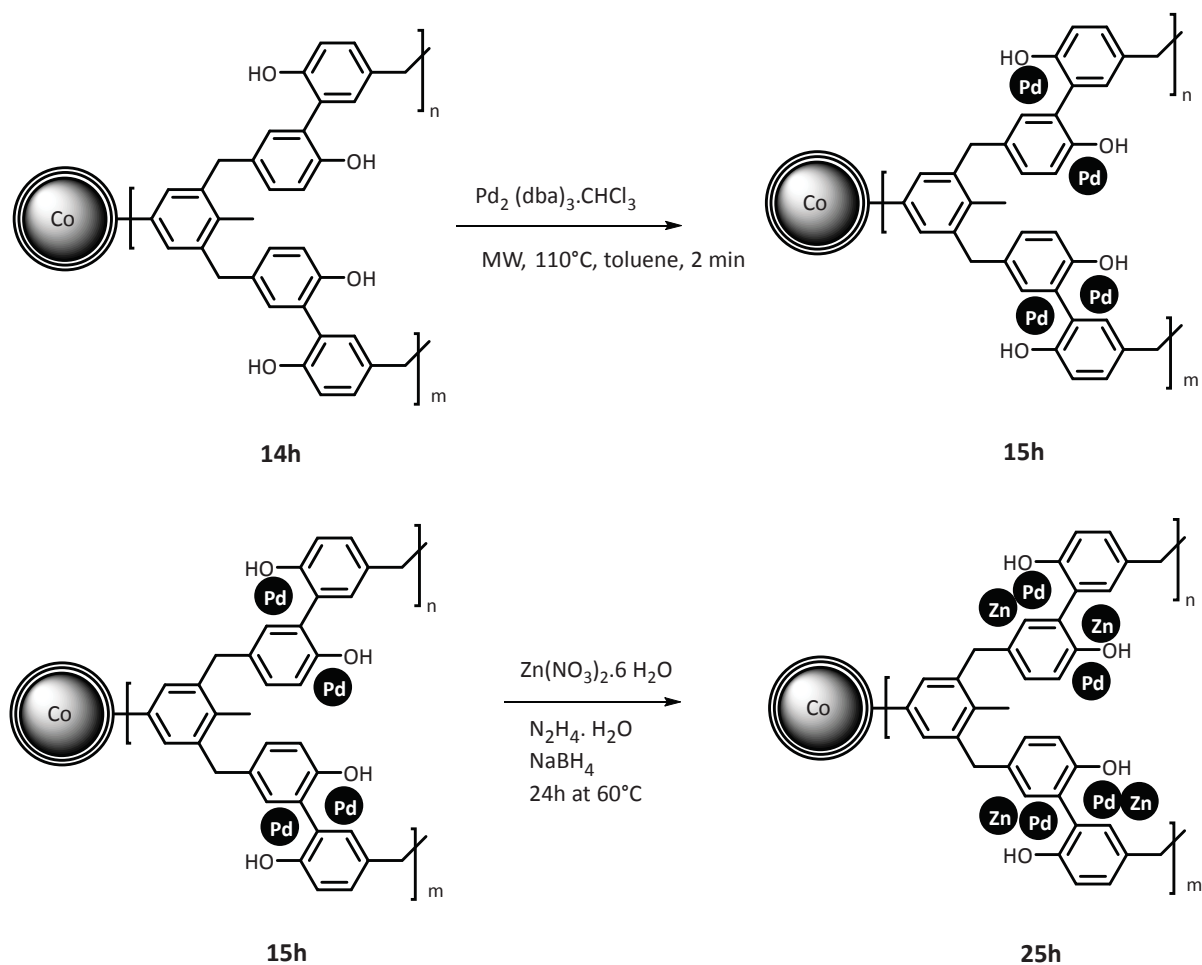
Scheme 21. Synthesis of Zn@Pd@MOP@Co/C.

The formula of the resulting catalyst can be described as $Zn_y@Pd@MOPs@Co/C$, in which y represents the molar ratio of Zn to Pd. Four bimetallic catalysts $Zn_y@Pd@MOPs@Co/C$ were prepared with the molar ratio 1 (**25h-α**), 2 (**25h-β**), 10 (**25h-γ**), and 20 (**25h-δ**). The catalyst compositions were investigated by ICP-OES and the results were shown in Table 18. **25h-α** to

25h-δ were obtained with Zn loadings of 0.2 to 2.2 wt% and Pd loading of 0.3 wt%. Zn incorporation rates were obtained between 14% and 39%. While Pd incorporation rates were found to be between 72% and 79% (Table 17). The BET surface area, pore volume, and pore diameter of Pd@MOP@Co/C **15h** were measured in previous work [9].

Table 17. Pd incorporation into 2,2'-biphenol@Co/C **14h**, following Zn incorporation into **15h**, resulting in the materials **25h-α** to **25h-δ** with various metal loadings.

Entry	No.	14h (mg)	Pd incorporation[a) (%)	Zn incorporation[a) (%)	Metal loading[a) (wt%)	
					Pd	Zn
1	**25h-α**	70	79	14	0.3	0.2
2	**25h-β**	70	74	20	0.3	0.5
3	**25h-γ**	70	72	32	0.3	1.7
4	**25h-δ**	70	78	39	0.3	2.2

[a) Determined by ICP-OES.

The catalytic selectivity of catalysts was investigated first for the hydrogenation of diphenylacetylene **19a** (Scheme 22). Hydrogenation was carrird out with 0.5 mol% catalyst Zn_y@Pd@MOPs@Co/C at room tempreature and ambient hydrogen pressure in ethanol.
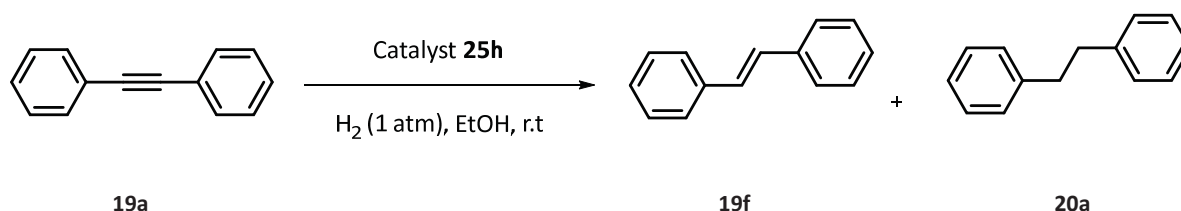
Scheme 22. Selective hydrogenation of diphenylacetylene **19a**.

Table 18. The evaluation of the catalytic activity of Zn_y@Pd@MOP@Co/C in selective hydrogenation of diphenylacetylene **19a**.

Entry	No.	Time (h)	Conversion[a) %	
			Stilbene	Diphenylethane
1	**25h-β**	3	-	100
2	**25h-γ**	3	-	100
3	**25h-δ**	3	-	90

Diphenylacetylene **19a** *(*0.5 mmol) in EtOH (10 mL) was hydrogenated by 0.5 mol % **25h-β**, **25h-γ**, and **25h-δ**.
[a) Conversion was determined by GC analysis using dodecane as an internal standard.

However, the experimental results obtained using different catalysts with varying Zn:Pd molar ratios did not show selectivity to stilbene **19f**.

Further efforts were directed with catalyst **25h-δ** for the selective hydrogenation of phenylacetylene (Scheme 23). The reaction progress was monitored by GC analysis. The results in Table 19 displayed the selective hydrogenation of phenylacetylene to the corresponding alkene, styrene. Comparing the bimetallic Zn_{20}@Pd@MOP@Co/C **25h-δ** with the monometallic Pd@MOP@Co/C **15h-β** in the previous work [9], in resulting the selectivity of catalyst Zn_{20}@Pd@MOP@Co/C is slightly higher than monometallic Pd@MOP@Co/C **15h-β** in the phenylacetylene hydrogenation. On the other hand, the raction time required for conversion of phenylacetylene over bimetallic catalyst **25h-δ** is longer than monometallic catalyst **15h-β**. The catalyst Zn_{20}@Pd@MOP@Co/C **25h-δ** did not exhibit selectivity to other alkynes. Therefore, further catalyst characterization was not performed for this catalyst. Using different Zn precursors (zinc chloride, zinc oxide) and milder reducing agent (borane-*tert*-butylamine complex (TBAB)) in the synthesis method also had no promising impact on catalytic performance.
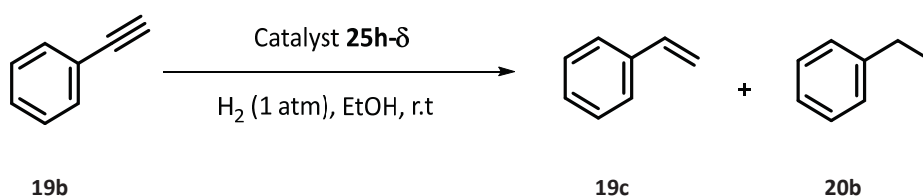
Scheme 23. Selective hydrogenation of phenylacetylene **19b**.

Table 19. The evaluation of the catalytic activity of Zn_{20}@Pd@MOP@Co/C **25h-δ** and Pd@MOP@Co/C **15h-β** in selective hydrogenation of phenylacetylene **19b**.

Entry	No.	Time (min)	Conversion[a] %	
			Styrene	Ethylbenzene
1	**25h-δ**	120	85%	-
2	**15h-β**	10	78%	-

Phenylacetylene **19b**   (0.5 mmol) in EtOH (10 mL) was hydrogenated by 0.5 mol % **25h-δ** (0.3 wt% Pd) and **15h-β** (0.4 wt% Pd).
[a] Conversion was determined by GC analysis using dodecane as an internal standard.

2.5. Conclusion

In conclusion, Pd core-Zn shell bimetallic nanoparticles were prepared by the reduction of a second metal onto the pre-formed core-shell nanoparticles (Pd@MOP@Co/C) (<3 nm). Zn_y@Pd@MOPs@Co/C bimetallic catalysts were evaluated based on their catalytic performance for selective hydrogenation of diphenylacetylene **19a** and phenylacetylene **19b** under 1 atm H_2 (*via* a balloon), ethanol as solvent, and at room temperature. The monometallic Pd catalyst was compared with the bimetallic Zn-Pd catalyst under the same condition. The observation of both mono and bimetallic catalysts indicated the slightly higher selectivity for bimetallic catalyst in selective hydrogenation of phenylacetylene, but no selectivity has been found in the hydrogenation of diphenylacetylene to stilbene and the fully hydrogenated product has been obtained.

A possible explanation for this inactivity might be attributed to the segregation of zinc atoms on the bimetallic surface when ZnO particles are formed. Zakhatser et al. reported that Zn in PtZn nanostructured alloy is not stable in contact with air and has a tendency to leach [103]. As a result, Zn could be segregated from the catalyst, a phenomenon which leads to the remaining of just Pd nanoparticles in the catalyst. Therefore, we observe only the monometallic catalytic behavior of pure Pd. Although the formation of zinc oxide particles on the surface of the NPs has been shown to increase the catalyst activity in some cases, this phenomenon had no efficient effect on our catalyst. Indeed, the catalytic properties of the catalyst can be affected by the morphology of Pd and Zn and their changes during reactions. This work requires preventing the catalyst from exposure to oxygen and further investigation.

3. Palladium Nanoparticles Supported on Electroactive Microporous Organic Polymer (MOP) Based on Triphenylphosphine (TPP)
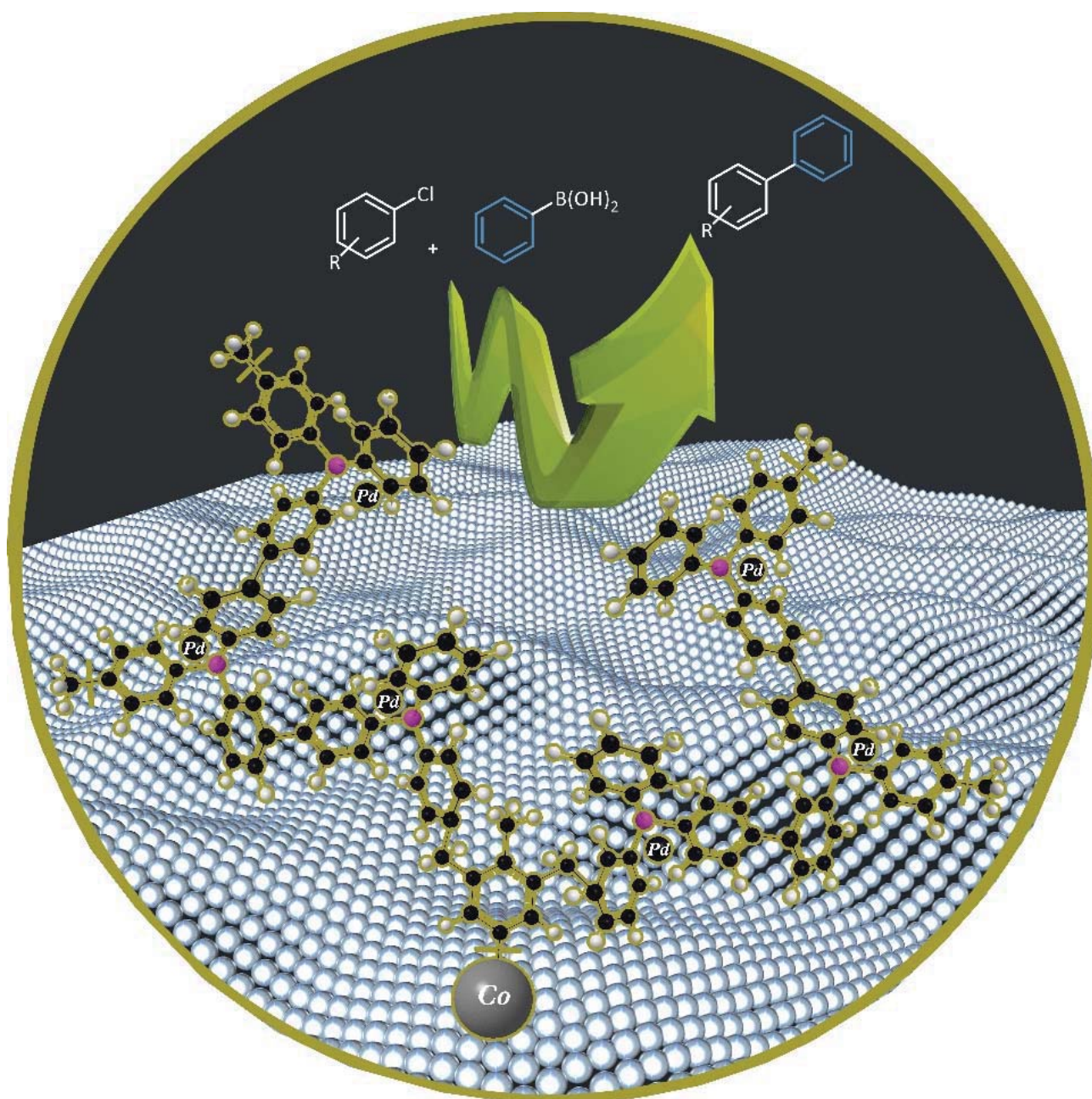
3.1. Introduction

Over the past decades, porous materials have been exploited as catalysts or catalyst supports [104, 9], and proven themselves as excellent materials in sorption, purification, separation [105], gas storage [106, 107], and heterogeneous catalysis [108, 109]. It is widely known that increasing interest in porous materials is due to their special properties such as porosity, surface area, pore size, and density. Apart from these advantages, porous materials require to possess a certain type of physical or chemical function to fulfill in certain applications [110]. For example, in automobile approaches which is powered by a fuel cell, It has been reported that increasing the surface area of porous materials cannot be enough to develop hydrogen storage unless the enthalpy of adsorption of hydrogen to the pore wall is increased by the incorporation of noble metals or heteroatoms [111, 112]. Hence, the surge of interest in developing porous materials has led scientists to produce various porous materials with the ability to adapt to functional groups.

Microporous organic polymers (MOPs) are a family of porous materials which have attracted scientific interest due to their prominent feature of high intrinsic levels of porosity along with excellent chemical stability and capability of introducing a broad range of functional groups. The major advantage of these materials involves the flexibility of monomers to generate new building blocks with high surface area and narrow pore size distribution [113].

Functional MOPs were synthesized through Friedel-Crafts reaction like hypercrosslinked styrene-type polymers (HCPs) [114], hypercrosslinked polypyrrole, polyaniline, or aminobenzene [115, 116]. A range of monomers with various functional groups has been employed for the synthesis of MOPs through the aforementioned methods. However, the use of Friedel-Crafts reaction in MOPs synthesis benefits from direct polymerization of monomers as well as intermolecular and intramolecular post-crosslinking of preformed polymers. In addition, the polymerization performs in the presence of low-cost and commercially available Lewis acid as catalysts [117].

Triphenylphosphine (PPh$_3$) as aromatic ring linkers with strong electron-donating ability was known as a valuable monomer in MOPs due to their extraordinary high surface area and well-defined pore structure [113]. It should be stated that strong interaction between phosphine

ligands and transition metals causes outstanding leaching resistance ability. In recent years, a number of microporous polymers containing PPh_3 and its derivatives were synthesized as catalyst supports [118]. As a result, their air-sensitivity and thermal instability can be addressed by immobilizing onto solid support [119].

In this regard, in 2013 Tan and Li group reported a palladium-phosphine heterogeneous catalyst which was obtained through knitting triphenylphosphine with benzene (Figure 23). Two network polymers were employed, the microporous knitting aryl network polymers (KAPs) and polystyrene (PS) network. Three kinds of catalysts were prepared through one-step knitting and post-modification methods and denoted KAPs(Ph-PPh$_3$)-Pd, KAPs(Ph)-PPh$_3$-Pd, and PS-PPh$_2$-Pd. Among developed catalysts, KAPs(Ph-PPh$_3$)-Pd with 0.7% loading of Pd showed more microporous structure (1025 $m^2 \cdot g^{-1}$) and higher dispersion of Pd compared to KAPs(Ph)-PPh$_3$-Pd (916 $m^2 \cdot g^{-1}$), and PS-PPh$_2$-Pd (33 $m^2 \cdot g^{-1}$). The KAPs(Ph-PPh$_3$)-Pd was applied for the Suzuki–Miyaura cross-coupling reaction of aryl chlorides in an aqueous ethanol solution and indicated high activity under relatively mild condition (80°C).
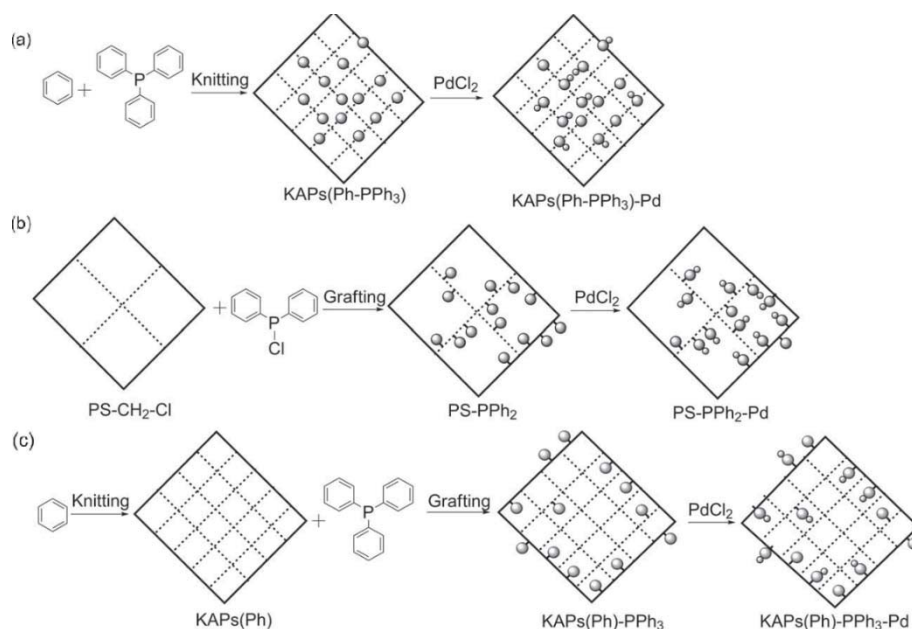
Figure 23 . Synthesis of KAPs(Ph-PPh$_3$)-Pd, KAPs(Ph)-PPh$_3$-Pd, and PS-PPh$_2$-Pd. Reproduced with permission from reference [120]. Copyright 2012, Wiley-VCH.

66

The Pd leaching was low with a total Pd loss of only 1%. In contrast, PS-PPh$_2$-Pd turned black in the first run, which showed the deactivation of the catalyst. By physicochemical characterization of catalyst, it was conferred that PPh$_2$-Pd in PS-PPh$_2$-Pd grafted on the walls of larger inter-pore channels of the spheres. As a result, meso-and macro-pores can not protect Pd^0 species and the catalyst is not reusable for the next run. Also, for the KAPs(Ph)-PPh$_3$-Pd, which PPh$_3$ was grafted on pre-made microporous KAP(Ph), the activity reduced quickly after the first run. This deactivity was attributed to the weak bond between the Pd and PPh$_3$ located in the superficial section. While Pd^0 species in KAPs(Ph-PPh$_3$)-Pd are efficiently dispersed into the microporous structures and are tightly locked inside each micropore alone [120].

The ligand PPh$_3$ was also used for the synthesis of other metal catlysts such as HCP-PPh$_3$-Ru. A hypercrosslinked polymer (HCP)-immobilized ruthenium (HCP-PPh$_3$-Ru) was developed from benzene and PPh$_3$ through a one-step external cross-linking reaction (Scheme 24) [121]. The BET surface area of the polymer network was obtained 993 m^2.g^{-1}.
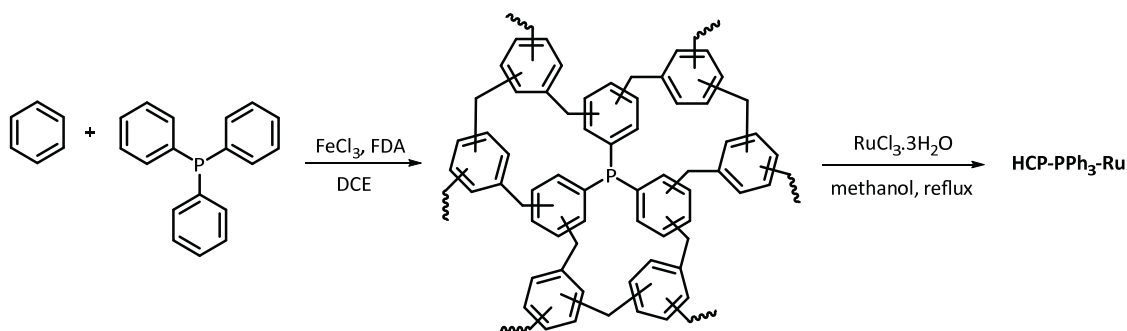
Scheme 24. HCP-Ru catalyst.

The catalyst exhibited outstanding catalytic performance in the synthesis of pyridine from aromatic ketone with ammonium acetate (NH$_4$OAC) (Scheme 25) and also cycloaddition reaction of diazodicarbonyl compounds with olefins. In addition, carbazole derivatives can be produced by combining cycloaddition reaction with an Amberlyst-15 catalyst through a one-pot, step-wise method (Scheme 26).

67
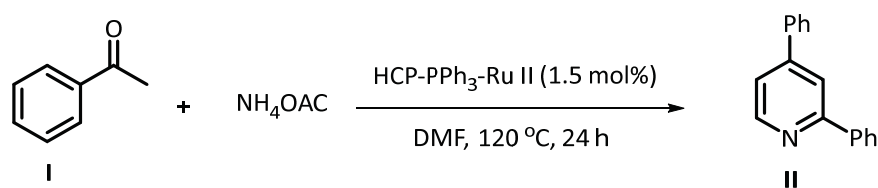
Scheme 25. Cyclization of acetophenone.

The recycling performance of the catalysts showed no significant metal leaching during the recycling process. These results are stem from the strong interaction between PPh$_3$ and the multistage porous structure of the support.
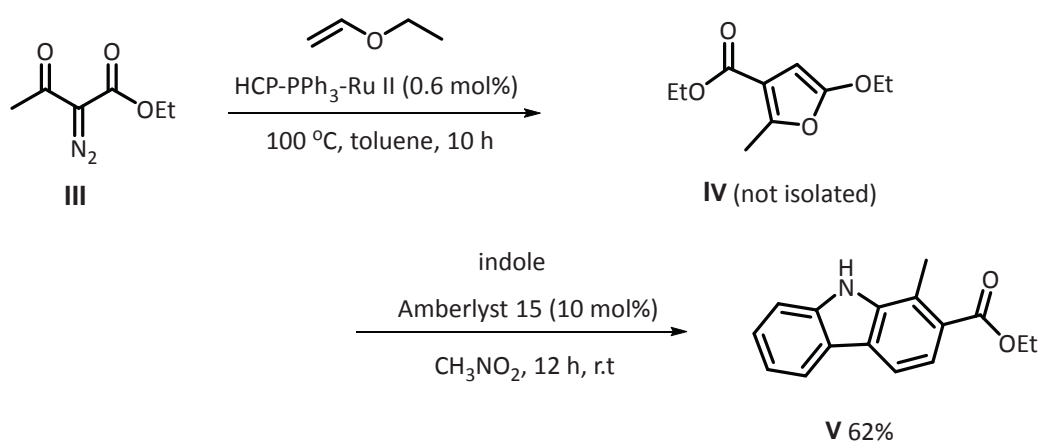
Scheme 26. Synthesis of carbazole derivatives from diazodicarbonyl.

It is worth mentioning that PPh$_3$ was used as aromatic ring linkers in the synthesis of MOPs. Zhang et al. were the first to synthesize the functionalized porous polymer (PP) based on phosphine (PP-P-Pd) and phosphine oxide (PP-PO-Pd). The polymer networks were prepared through the Yamamoto reaction method (Scheme 27) [113]. BET specific areas for PP-P and PP-PO polymers were obtained 1284 $m^2 \cdot g^{-1}$ and 1353 $m^2 \cdot g^{-1}$, respectively. Pd nanoparticles were incorporated into the polymer networks by an impregnation method. The Suzuki–Miyaura cross-coupling reactions were performed to evaluate the catalytic ability of catalysts. The results indicated that the porous polymer network with phosphine (PP-P-Pd) possesses higher catalytic activity than phosphine oxide (PP-PO-Pd). This higher activity is contributed to the incorporation of Pd nanoparticles with P(III) in PP-P network and indicates that

triphenylphosphine improves the catalytic activity of the catalyst, whereas in (PP-PO-Pd), Pd nanoparticles were incorporated on PP-PO with a higher oxidation state of the P atom (P(V)). The catalyst was retrieved by filtration and the recyclability performance of the PP-P-Pd proved that after five consecutive runs the palladium content is almost constant.
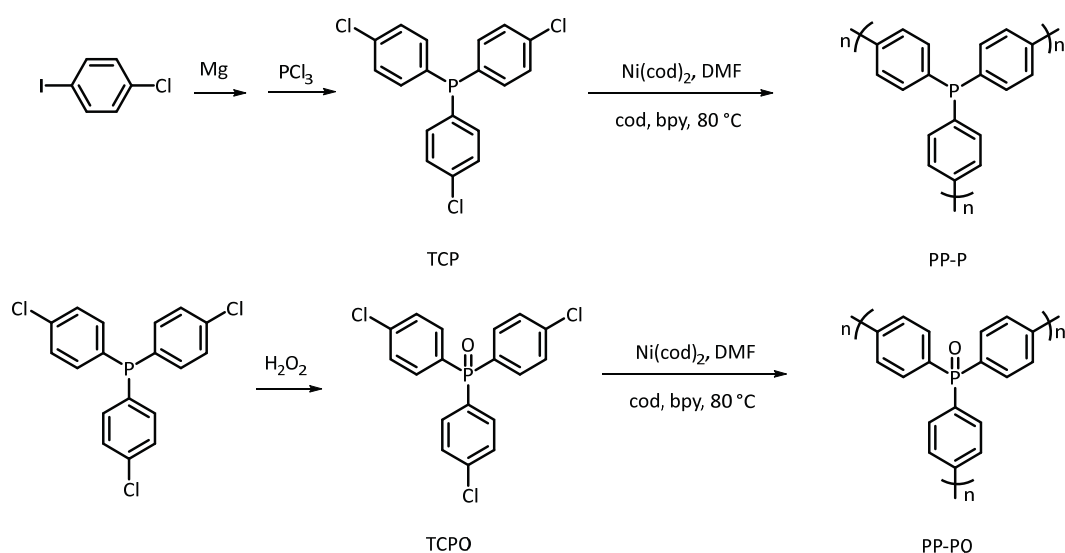
Scheme 27. Synthesis of microporous polymers. TCP: tris(4-chlorophenyl)phosphine, TCPO: tris(4-chlorophenyl)phosphine oxide, cod: 1,5-cyclooctadiene, bpy: 2,2'-bipyridine.

The catalyst also showed good results even with fluoro-derivatives with a strong C-F bond. Notable, triphenylphosphine incorporated with Pd nanoparticles has a significant effect on the catalytic ability and stability of Pd.

Despite triphenylphosphine-palladium complexes were known as excellent catalysts for cross-coupling reactions, there is still a lack of cost-effect and recycling processes to produce desired catalysts at an industrial scale, which in fact limits their practical applications. The advantages of the triphenylphosphine monomer in catalysis applications motivated us to develop the catalyst with an easy recycling strategy based on this monomer. Hence, the Pd@TPP@Co/C **29** were synthesized and used in the Suzuki-Miyaura cross-coupling reaction of deactivated aryl chlorides.

3.2. Results and discussion

We applied cobalt carbon nanobeads as they showed great results in our previous work [9]. Notably, the developed support possesses this potential to use as a recyclable catalyst in the Suzuki-Miyaura cross-coupling reaction.

The synthesis was accomplished within three steps. First, the microporous polymer triphenylphosphine (TPP) **27** was synthesized from tris(4-chlorophenyl)phosphine **26** through the Yamamoto reaction procedure. The electroactive microporous polymer triphenylphosphine **27** was obtained in off-white color (Scheme 28).

26   **27**
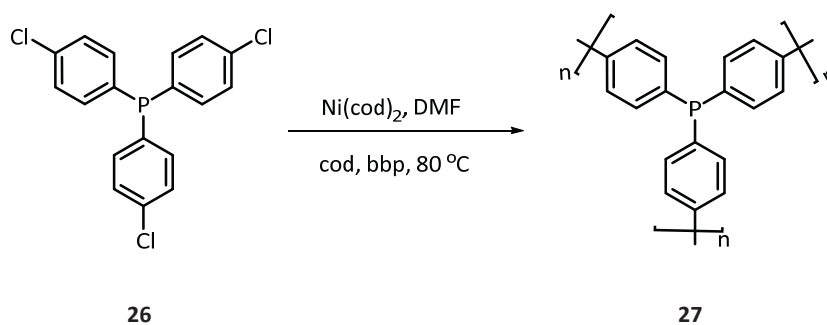
Scheme 28. Polymerization of tris (4-chlorophenyl) phosphine.

Yamamoto reaction is one of the coupling reactions which is mostly applied in develop of conjugated microporous polymer (CMPs) [122]. Hence, the surface area and pore size can be controlled. Afterward, based on the previous investigation [9], Co/C nanobeads were covalently functionalized *via* diazonium chemistry by dispersing them with *p*-toluidine and hydrochloric acid as catalys in water. Subsequently, pre-cooled solution sodium nitrite was added to the mixture in order to produce an aryl radical. Then, aryl radical grafted covalently to the graphene layer of the cobalt nanobeads to obtain Co/C NPs **13a** with carbon loading of 0.04 mmol/g**.**

In the next step, microporous polymer triphenylphosphine **27** were exposed to toluene Co/C NPs **13a** with formaldehyde dimethyl acetal (FDA), anhydrous iron (III) chloride, 1,2-dichloroethane to stabilize polymer on the support (Scheme 29). After 24 hours TPP@Co/C **28** was synthesized with a high carbon loading of 2.5 mmol/g.
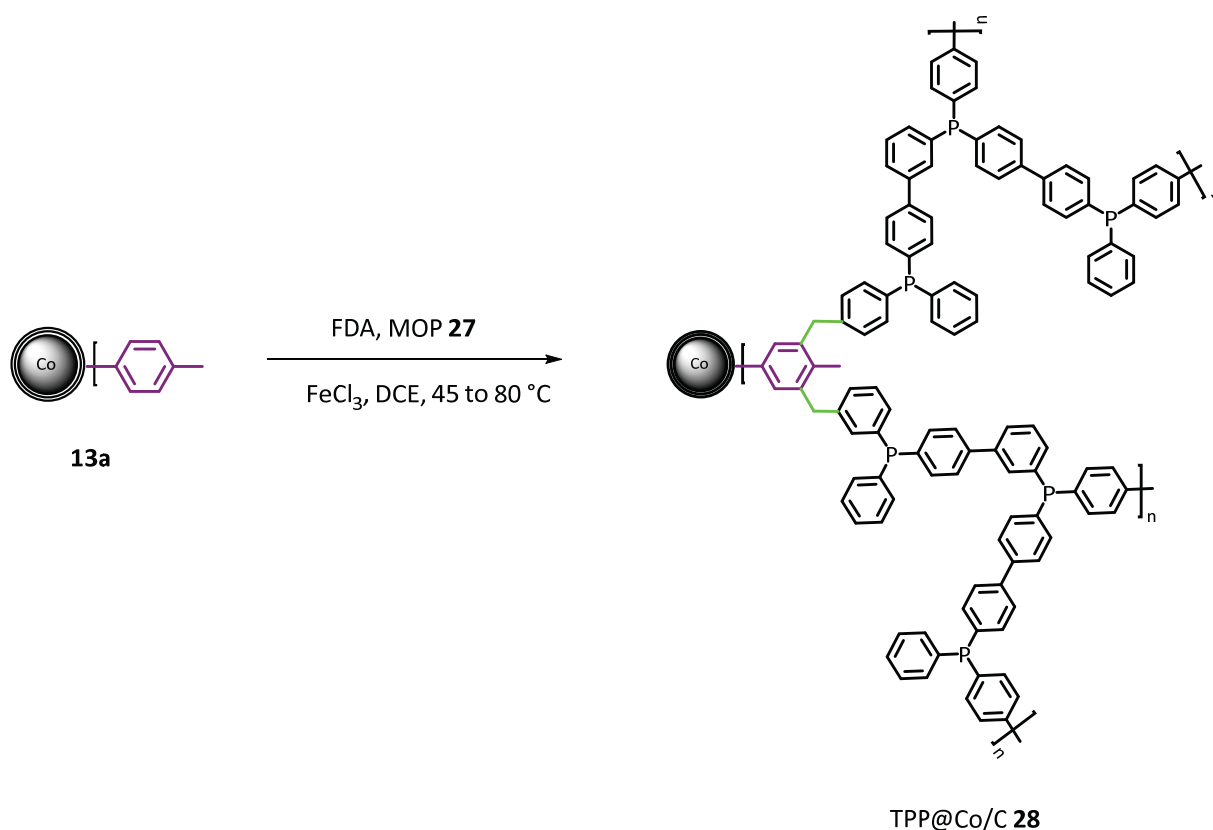
TPP@Co/C **28**

Scheme 29. Immobilization of polymer **27** on the CO/C NPs **13a**.

In order to investigate the reactivity of the catalyst, two kinds of Pd precursors, Pd(0) and Pd(II) were immobilized into TPP@Co/C **28** (Table 20).

Pd(0)@TPP@Co/C **29** was obtained adapting the method of Reiser et al. [2] by using Pd(0) nanoparticles precursor $Pd_2(dba)_3$.$CHCl_3$, dry toluene as solvent, and microwave irradiation condition to embed nanoparticles to polymeric network. The resulting catalyst was recovered *via* magnetic decantation and washed with diethyl ether and dichloromethane. The catalyst was obtained in 82 mg yield (Scheme 30).

Pd(II) species was incorporated into TPP@Co/C **28** through conventional heating at 60 °C in acetonitrile as solvent for 24 hours. Pd(II)@TPP@Co/C **29** were separated from the solution *via* magnetic decantation and washed with diethyl ether and dichloromethane. Pd(II)@TPP@Co/C **29** was produced in 80 mg yield (Scheme 30).
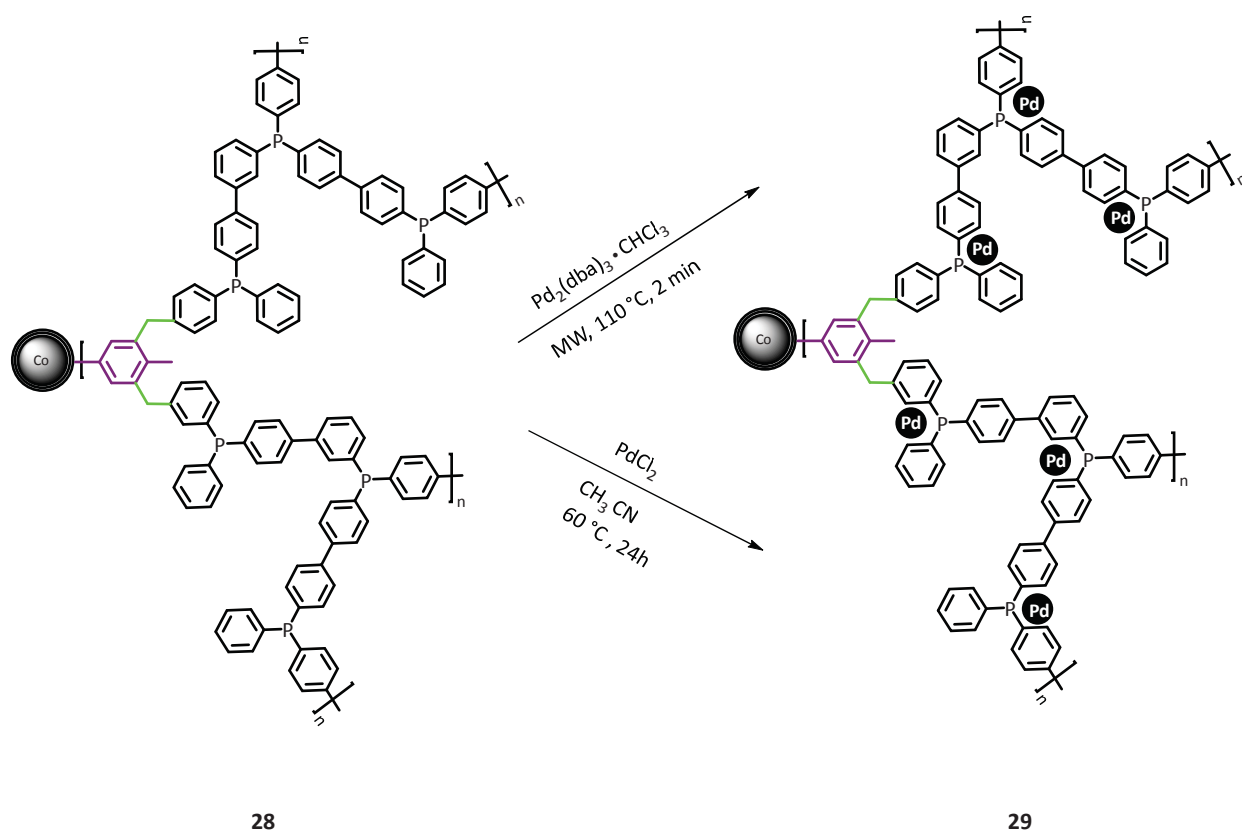
Scheme 30. Synthesis of Pd@TPP@Co/C **29**.

The catalysts were obtained with Pd loading of 1.3 wt% and 3.5 wt% for Pd(0) nanoparticles and Pd(II) clusters, respectively. The resulting Pd incorporation of two catalysts was shown that Pd(0) nanoparticles could disperse in the network more efficiently than Pd(II) clusters (Table 20).

Table 20. Two different palladium precursors were incorporated into TPP@Co/C **28.**

Entry	Pd procedure	Pd (mg)	TPP@Co/C 28 (mg)	mmol/g[a]	Pd [a] (wt%)	Incorporation[a] %
1	Pd$_2$(dba)$_3$.CHCl$_3$	10	100	0.12	1.3	94
2	PdCl$_2$	10	100	0.34	3.5	60

[a] Determined by ICP-OES.

Benchmarking the catalytic activity of Pd(II) and Pd(0)@TPP@Co/C **29** was performed by Suzuki- Miyaura cross-coupling of aryl chlorides (Scheme 31).

72

Deactivated aryl chlorides possessing electron-donating and electron-withdrawing groups reacted with phenylboronic acid and potassium phosphate as base in the presence of 0.5 mol % of Pd(II) and Pd(0)@TPP-MOPs@Co/C in a mixture of water/ethanol (5:5) at 60°C. Both catalysts, Pd(II) and Pd(0)@TPP@Co/C as shown in table 21 indicated promising results in the coupling reaction. In the case of strong electron-donating and withdrawing substituents, the coupling reactions were carried out rapidly and efficiently to afford the desired biaryls in high yields. The product was extracted with water and acetone and the catalyst was retrieved by an external magnet easily. Noteworthy is that the catalysts could promote the coupling of aryl chlorides bearing a free ligand group.

The recyclability of the catalysts was investigated through sequential couplings of 4-chloronitrobenzene according to the general procedure G (GP-G, Experimental Part). Unfortunately, the reactivity of both catalysts was dropped after the first run. The products were measured by ICP- OES in order to find Pd leaching but recycling results showed quite low leaching in both solutions (Table 22). For further investigation, FTIR measurement was performed. The polymerization process was also monitored by FTIR measurement. Accordingly, the disappearance of the C–Cl 700 cm^{-1} vibrations of the starting material indicated the success of phenyl–phenyl coupling. The peak at 1180 cm^{-1} was attributed to P=O stretching vibration which indicates that polymer and starting material are partially oxidized which is inevitable, after Pd incorporation this peak was disappeared. The synthesized polymer has been exposed to air for 24 hours and more phosphorus (P=O) was identified at 1180 cm^{-1} (Figure 24).

R: NO$_2$, CHO, OMe, Me
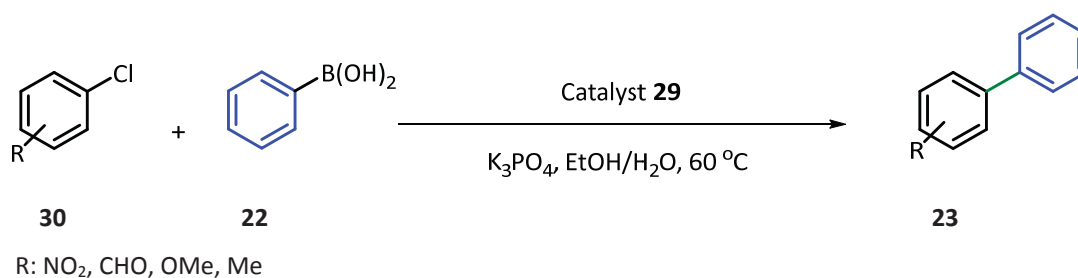
Scheme 31. Suzuki-Miyaura cross-coupling of aryl chlorides **30**.

Table 21. Suzuki-Miyaura cross-coupling of aryl chlorides **30** with Pd(II) and Pd(0)@TPP@Co/C **29** in water and ethanol and determination of their activities towards electron-donating and withdrawing groups[a).

Entry	Substrate	Time (h)	Yield%[b)
1	**30a** (NO$_2$, Cl)	2	Pd (0): 90 % Pd (II): 92%
2	**30b** (CHO, Cl)	3	Pd (0): 75% Pd (II): 80%
3	**30c** (OMe, Cl)	2	Pd (0): 85% Pd (II): 88%
4	**30d** (Cl)	3	Pd (0): trace Pd (II): trace

[a) Reactions carried out with aryl chlorides **30** (0.5 mmol), phenylboronic acid (0.75 mmol), K$_3$PO$_4$ (1.25 mmol) in water (5mL), ethanol (5 mL), 0.5 mol% Pd(0)@TPP@Co/C and Pd(II)@TPP@Co/C with 1.3 wt % and 3.5 wt% Pd loadings, respectively, under N$_2$ atmosphere. [b) Isolated yield, entries 1 and 2 were investigated by GC/MS.
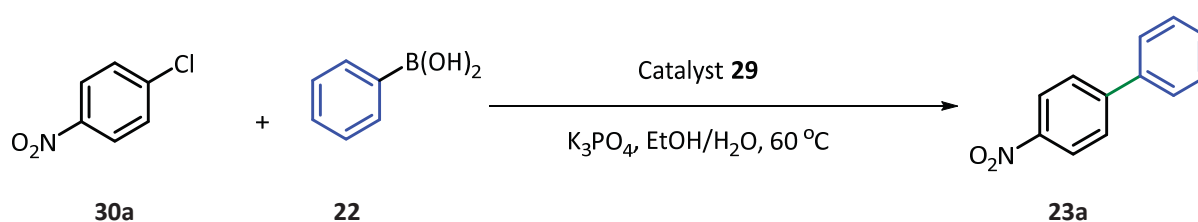
Scheme 32. Consecutive Suzuki-Miyaura cross-coupling of 4-chloronitrobenzene **30a**.

Table 22. Consecutive Suzuki-Miyauracross-coupling of 4-chloronitrobenzene **30a** with Pd(II), Pd(0)@TPP@Co/C, and determination of their leaching.[a]

Run	Time (h)	T (°C)	Yield% (Cat. Pd (0))	Leaching (ppm)[b] Pd	CO	Yield% (Cat. Pd (II))	Leaching (ppm)[b] Pd	CO
1	1	60	90	15	26	92	3	2
2	3	60-100	trace	3	25	trace	5	5

[a] 4-chloronitrobenzen **30a** (1 mmol), phenylboronic acid (1.5mmol), K_3PO_4 (2.5 mmol) were used for recyclability test in water (7 mL), ethanol (7 mL), 0.5 mol% Pd(0) and Pd(II) with 1.3wt% and 3.5wt% Pd loadings, respectively, under N_2 atmosphere. After each run, the leaching was determined. [b] Leaching was determined by ICP-OES. Calculated in µg per g of product.

The retrieved catalysts were used for the consecutive runs. In order to obtain the desired product, the second run was kept either for more time or high temperature but no progress was observed for both catalysts. Notably, comparing Pd and CO leaching in both catalysts indicated that metal contamination in both catalysts was very low. Likewise, Pd leaching in Pd (II) cluster solution was found to be extremely low as well. On average, low palladium contamination of about 4 ppm in the products of Pd(II) cluster was detected, while in Pd(0) products 9 ppm was measured. Thus, the inactivity of the catalysts after the first run cannot be attributed to Pd-leaching.
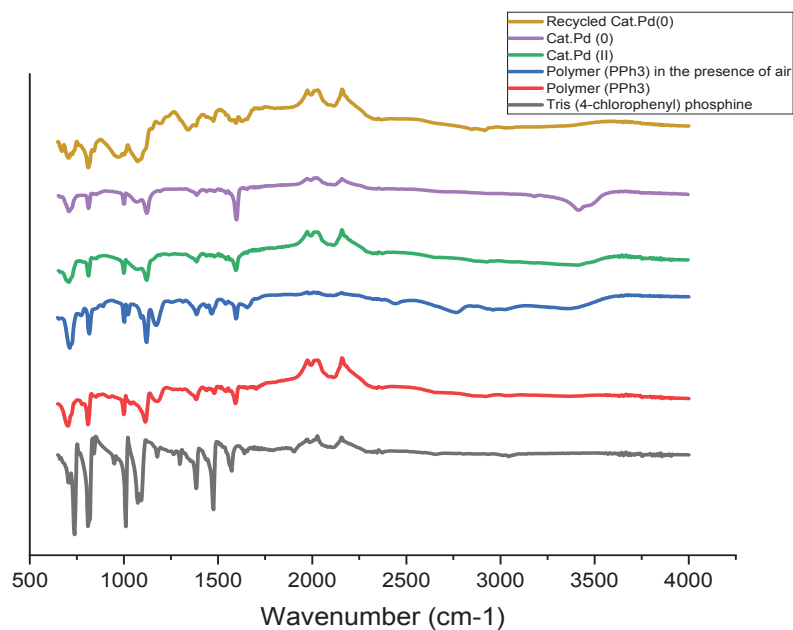
Figure 24. FTIR spectra.

Figure 25. Color of solutions after the first run (left) and after the second run (right).

During the recyclability process, a color change was observed in the second run. As shown in Figure 25, at the end of the first run the color solution is brown, while at the end of the second run the color turns green.

X-ray photoelectron spectral (XPS) survey spectra of the catalysts were investigated for confirming the oxidation state of the Pd nanoparticles.The XPS spectra of Pd3d at 335.66 eV and 340.92 eV is attributed to metallic Pd(0) and the second set of peaks at 337.79 eV and 343.05 eV assigned to Pd(II) in the recycled Pd(0)@TPP@Co/C. The ratio of Pd(0)/Pd(II) was obtained to be 76:24 in the recycled Pd(0)@TPP@Co/C. Two oxidation states of Pd in the recycled Pd(II)@TPP@Co/C were determined to be Pd(II) and Pd(IV) at 335.42 eV, 340.68 eV, 337.64 eV, and 342.90 eV, respectively and the ratio of 80:20 was observed for Pd(II)/Pd(IV) (see Experimental Part). Comparing the XPS spectra of the fresh Pd(II)@TPP@Co/C with its recycled catalyst shows a slight decrease in the Pd(II)/Pd(IV) ratio from 100:00 to 80:20. Hence, it is proven that the catalytically active Pd species still exist in the catalyst.

3.3. Conclusion

The microporous polymer triphenylphosphine@Co/C (TPP@Co/C) was successfully synthesized with the homocoupling of tris (4-chlorophenyl) phosphine through Yamamoto reaction procedure and grafted onto a well-dispersed platform (toluene Co/C NPs) *via* formaldehyde dimethyl acetal (FDA) as a low-cost and commercially available external cross-linker. The catalytic activity of two Pd precursors, Pd(II) and Pd(0)@TPP@Co/C were studied in the Suzuki-Miyaura cross-coupling reaction of deactivated aryl chlorides with phenylboronic acid and potassium phosphate as base in a mixture of water/ethanol (5:5) as solvent at 60°C under N_2 atmosphere. Catalysts showed excellent results for all substituted groups except the low electron-donating group at the first run. The catalyst activity in both catalysts dropped after the first run. The possibility of Pd leaching was rejected based on ICP-OES. XPS analysis also indicated the catalytically active Pd species in the recycled catalysts. A possible explanation for this inactivity could be attributed to the agglomeration of Pd nanoparticles. Unfortunately, TEM images of our catalysts have not been received, otherwise, we could have investigated our catalysts and presented a more confident reason for this defect.

C. Summary

In this thesis, the importance of various polymer networks as an efficient platform for hydrogenation, selective hydrogenation, and Suzuki-Miyaura cross-coupling reactions has been shown. The developed polymers were introduced to magnetic Co/C nanobeads followed by the immobilization of metal nanoparticles.

The first chapter is dedicated to the evaluation of various polymers as an aromatic building block to anchor palladium nanoparticles on the platform of Co/C nanobeads. The aim of this work was to circumvent the leaching of Pd and Co with an efficient microporous polymer matrix. Different polymeric networks were applied by an external cross-linker and their catalytic activity was evaluated in the hydrogenation reaction. Among developed networks, 2,2'-biphenol monomer **h** exhibited minimum leaching of palladium and cobalt nanoparticles. This capability is derived from the presence of hydroxyl groups which can stabilize Pd nanoparticles into the microporous network efficiently. For further investigation, the new hybrid material was applied in the hydrogenation and Suzuki-Miyaura cross-coupling reactions which showed good catalyst activity and low leaching. The developed polymer 2,2'-biphenol **14h** was also used as a scavenger for toxic heavy metal ions such as lead, mercury, copper, and chromium ions, in our group.
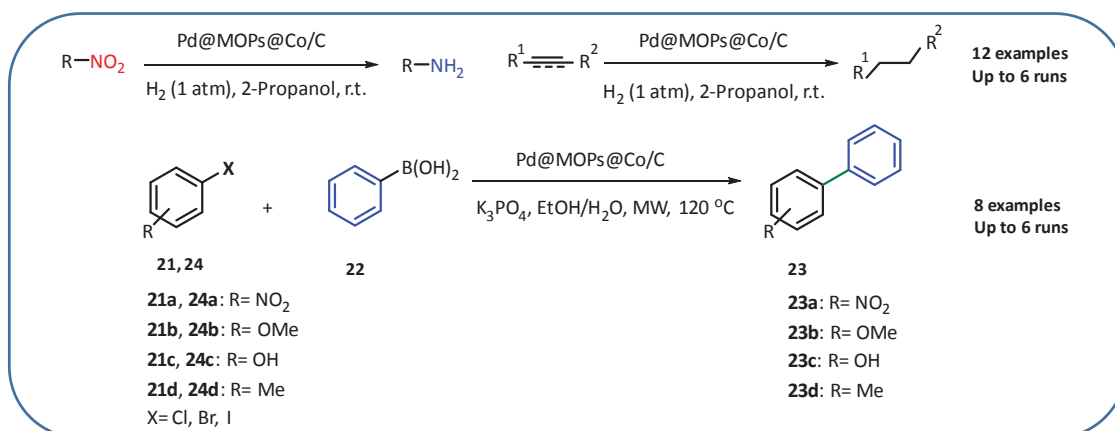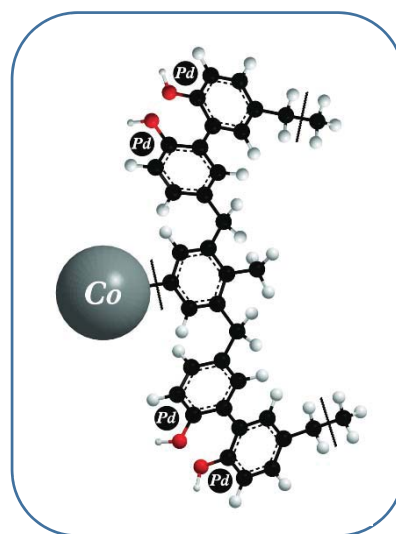
Scheme 33. Hydrogenation and Suzuki-Miyaura cross-coupling reactions.

The second chapter details the synthesis of the bimetallic Zn-Pd catalysts for selective hydrogenation reactions. $Zn_Y@Pd$ @MOPs@Co/C was synthesized with respect to the fact that the addition of a second metal to Pd nanoparticles can suppress further hydrogenation through its geometric and/or electronic effects. To this aim, doping of the Pd@MOP@Co/C with various levels of Zn was performed. The Pd nanoparticles were first immobilized on the polymer 2,2'-biphenol **14h**, followed by incorporation of Zn. Phenyl acetylene was chosen as a model reaction. Further, the selectivity and activity of the developed catalyst were tested for the hydrogenation of diphenyl acetylene as well. Unfortunately, the experimental results obtained using different catalysts with varying Zn:Pd molar ratios did not show selectivity.
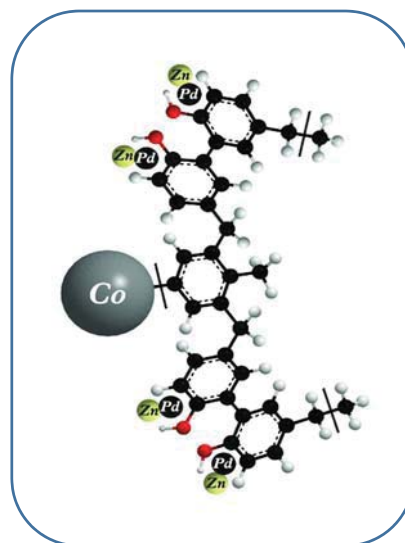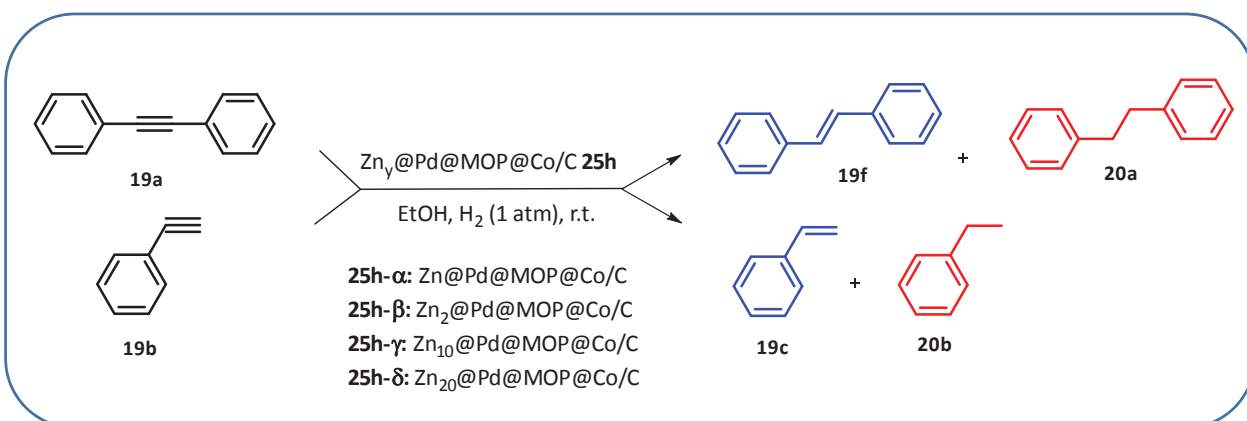
Scheme 34. Selective hydrogenation.

In the third chapter, the efficacy of a triphenylphosphine-functionalized microporous organic polymer as a matrix for a heterogeneous palladium catalyst for the Suzuki-Miyaura cross-coupling reaction of deactivated aryl chlorides is evaluated. The polymeric network was developed by homocoupling of triphenylphosphine through the Yamamoto reaction route (Scheme 35). Palladium nanoparticles were immobilized on the triphenylphosphine-functionalized microporous organic polymer. Different Pd precursors such as $PdCl_2$, $Pd_2dba_3 \cdot CHCl_3$ were incorporated into the MOP with conventional heating and microwave irradiation, respectively. Promising results were obtained for both catalysts at the first run, either for electron-donating or electron-withdrawing groups. In other words, this can be inferred that either electron-withdrawing or electron-donating of aryl chlorides have no influence on the developed catalysts. Unfortunately, the catalytic activity was dropped after the first run.
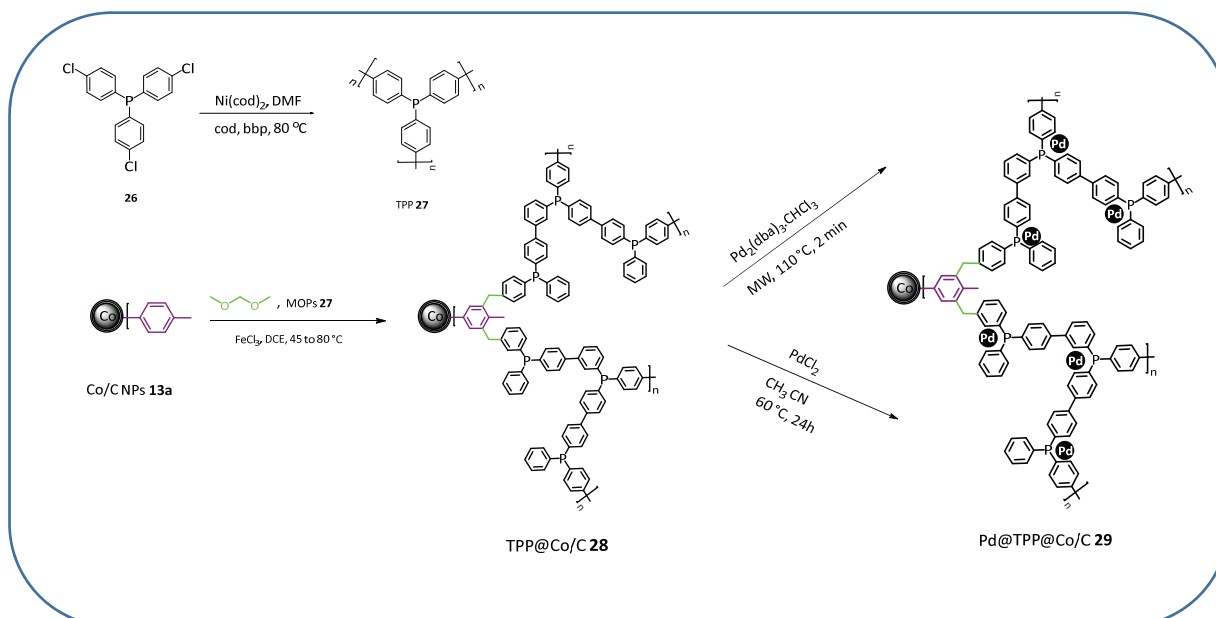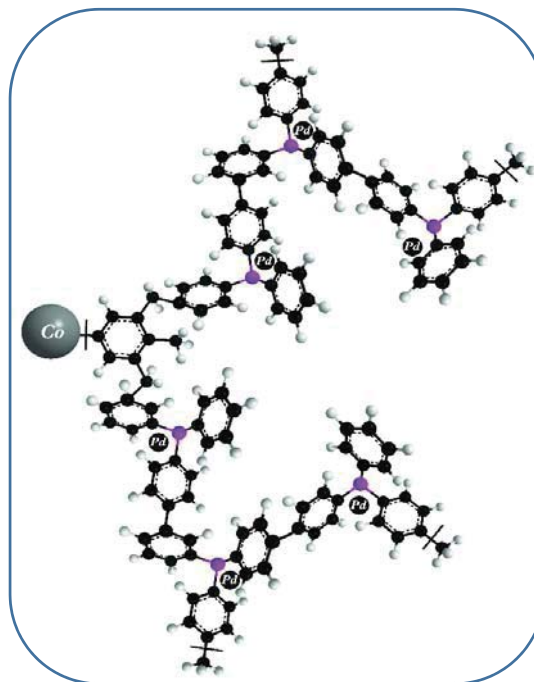
Scheme 35. Synthesis of Pd@TPP@Co/C 29.
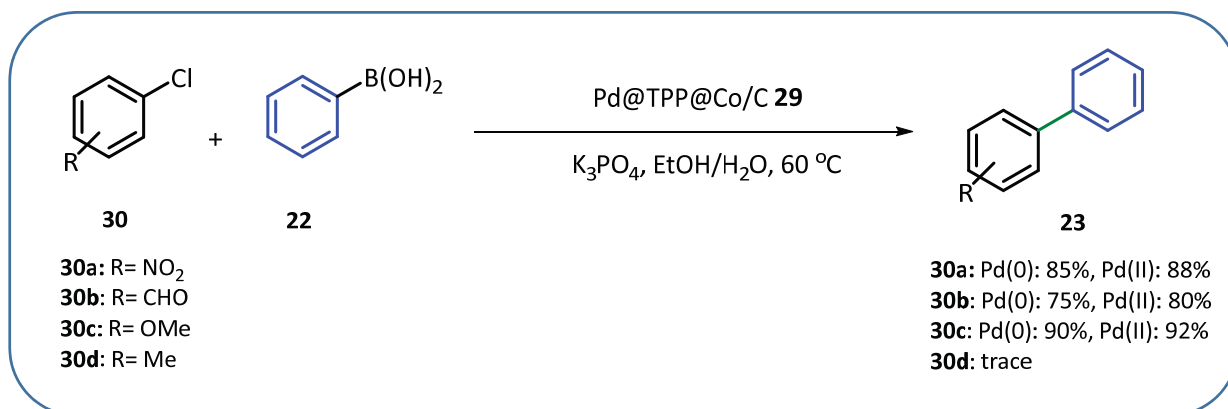
Scheme 36. Suzuki-Miyaura cross-coupling of aryl chlorides.
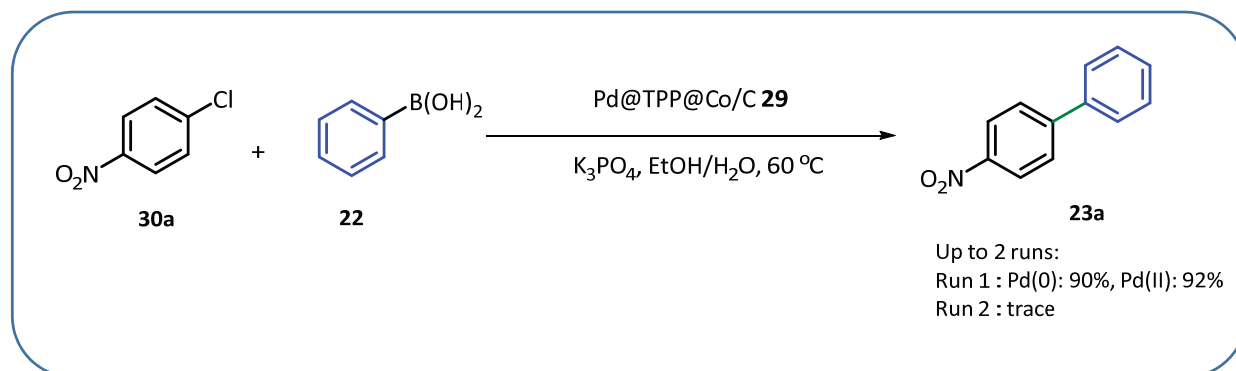
Scheme 37. Recycling of Pd@TPP@Co/C **29.**

D. Zusammenfassung

Die vorliegende Arbeit behandelt die Bedeutung verschiedener Polymernetzwerke als effiziente Plattform für Hydrogenierungen und Suzuki-Miyaura-Kreuzkupplungsreaktionen. Die hierfür entwickelten Polymere wurden auf magnetische Co/C Nanobeads aufgetragen und dienten zur Immobilisierung von Metall-Nanopartikeln.

Das erste Kapitel widmet sich der Evaluierung verschiedener Polymere als aromatischen Baustein zur Verankerung von Palladium-Nanopartikeln auf der Plattform von Co/C-Nanobeads. Ziel dieser Arbeit war es, das Auslaugen von Pd und Co mittels einer effizienten mikroporösen Polymermatrix zu verhindern. Verschiedene polymere Netzwerke wurden durch einen externen Vernetzer aufgebracht und ihre katalytische Aktivität in der Hydrierungsreaktion evaluiert. Unter den entwickelten Netzwerken zeigte 2,2'-Biphenol-Monomer **h** eine minimale Auswaschung von Palladium- und Cobalt-Nanopartikeln. Diese Fähigkeit wurde von der Anwesenheit von Hydroxylgruppen abgeleitet, die Pd-Nanopartikel effizient in dem mikroporösen Netzwerk stabilisieren können. Für weitere Untersuchungen wurde das neue Hybridmaterial in Hydrierungs- und Suzuki-Miyaura-Kreuzkupplungsreaktionen eingesetzt, die eine gute Katalysatoraktivität und eine geringe Auswaschung zeigten. Das entwickelte Polymer 2,2'-Biphenol **14h** wurde in unserer Gruppe auch als Scavenger für toxische Schwermetallionen wie Blei-, Quecksilber-, Kupfer- und Chromionen eingesetzt.
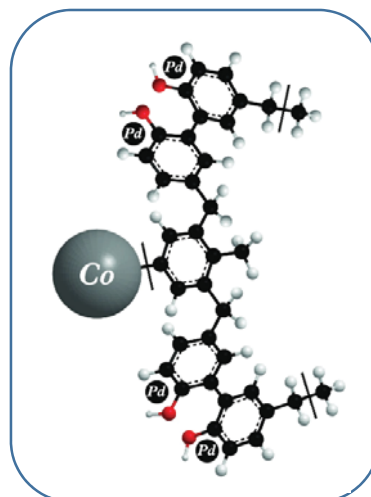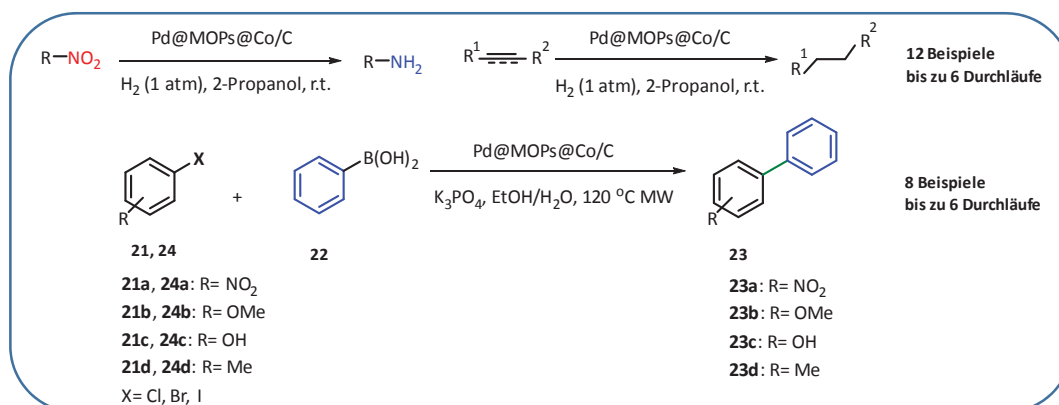
Scheme 33. Hydrogenierungs- und Suzuki-Miyaura-Kreuzkupplungsreaktionen.

Das zweite Kapitel beschreibt die Synthese der bimetallischen Zn-Pd-Katalysatoren für selektive Hydrierungsreaktionen. Zn_y@Pd@MOPs@Co/C wurde im Hinblick darauf synthetisiert, dass die Zugabe eines zweiten Metalls zu den Pd-Nanopartikeln eine weitere Hydrierung durch ihre geometrischen und/oder elektronischen Effekte unterdrücken kann. Zu diesem Zweck wurde eine Dotierung der Pd@MOPs@Co/C mit verschiedenen Gehalten an Zn durchgeführt. Die Pd-Nanopartikel wurden zuerst auf Polymer 2,2'-Biphenol **14h** immobilisiert, gefolgt vom Einbau von Zn. Als Modelsubstrat wurde Phenylacetylen
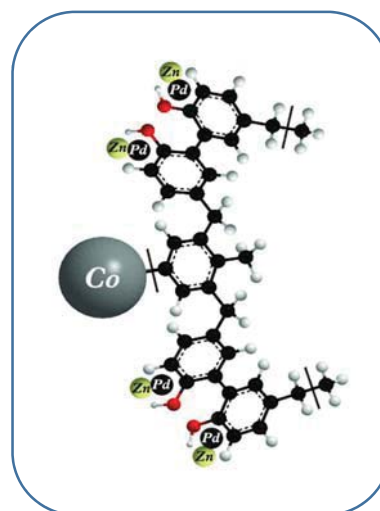
gewählt. Weiterhin wurden die Selektivität und Aktivität des entwickelten Katalysators auch anhand der Hydrierung von Diphenylacetylen getestet. Leider zeigten die experimentellen Ergebnisse, die unter Verwendung verschiedener Katalysatoren mit unterschiedlichen Zn:Pd-Molverhältnissen erhalten wurden, keine Selektivität.
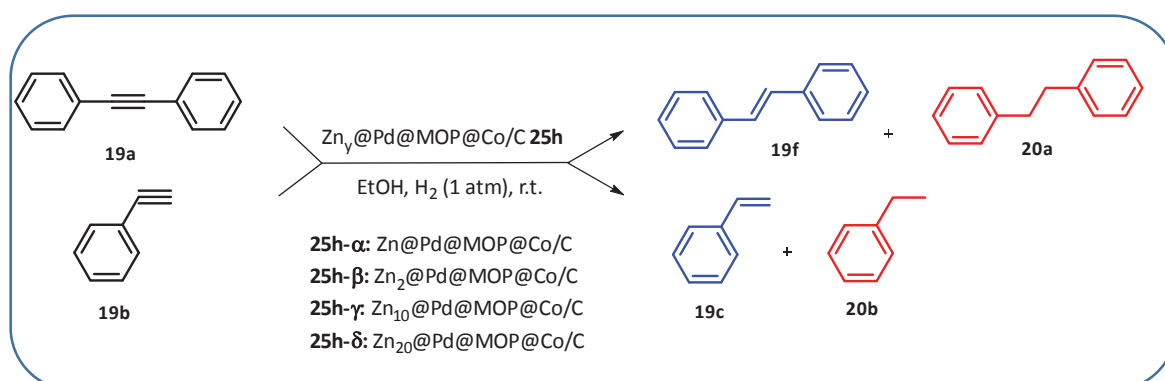
Scheme 34. Selektive Hydrogenierung.

Im dritten Kapitel wurde die Wirksamkeit eines Triphenylphosphan-funktionalisierten mikroporösen organischen Polymers als Matrix für einen heterogenen Palladiumkatalysator für Suzuki-Kreuzkupplungen von deaktivierten Arylchloriden untersucht. Das polymere Netzwerk wurde durch Homokupplung von Triphenylphosphin über den Yamamoto-Reaktionsweg entwickelt (Schema 35). Palladium-Nanopartikel wurden auf dem Triphenylphosphin-funktionalisierten mikroporösen organischen Polymer immobilisiert. Verschiedene Pd-Vorstufen
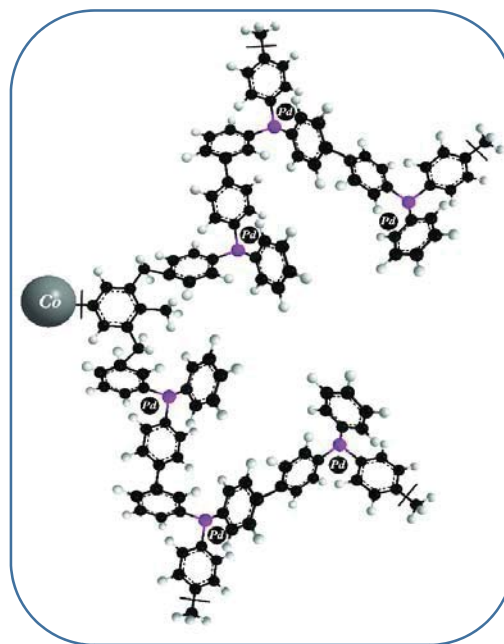
wie PdCl$_2$ oder Pd$_2$dba$_3$·CHCl$_3$ wurden in die MOP durch konventionelles Heizen bzw. Mikrowellenbestrahlung eingebaut. Für beide Katalysatoren wurden im ersten Lauf vielversprechende Ergebnisse für elektronenschiebende oder elektronenziehende Gruppen erzielt. Mit anderen Worten kann daraus geschlussfolgert werden, dass weder Elektronenentzug noch Elektronenzugabe von Arylchloriden einen Einfluss auf die entwickelten Katalysatoren haben. Leider ließ die katalytische Aktivität nach dem ersten Durchlauf nach.
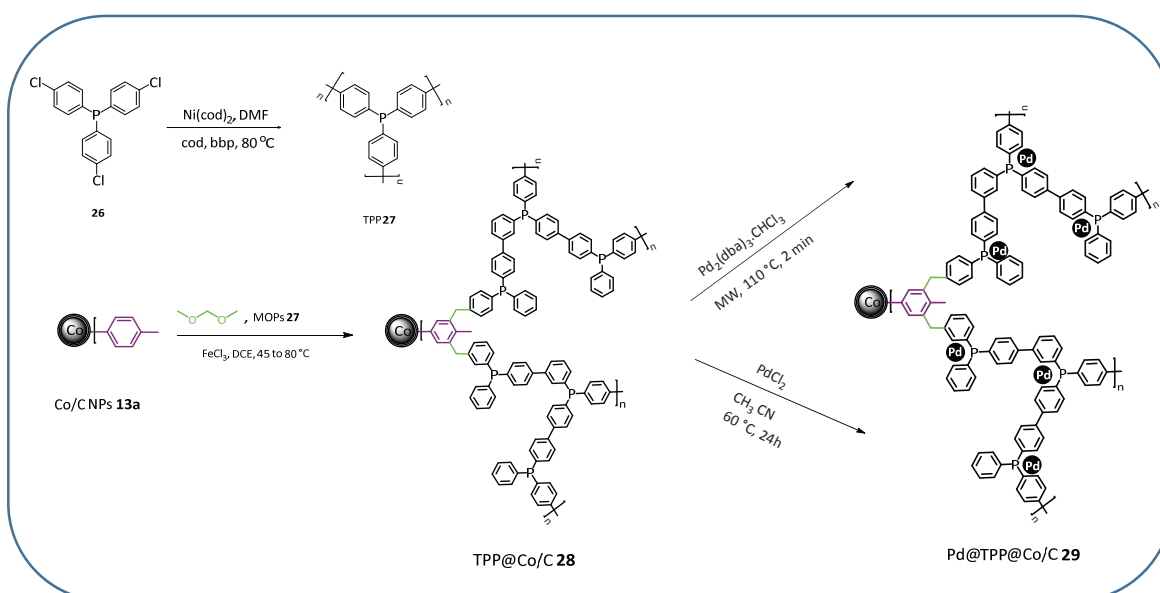
Scheme 35. Synthese von Pd@TPP@Co/C **29**.
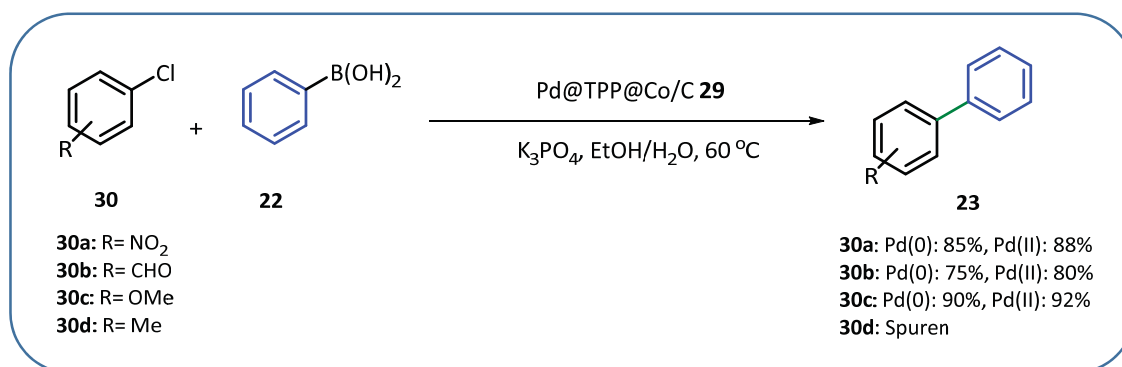
Scheme 36. Suzuki—Miyaura-Kreuzkupplung von Arylchloriden.

30a: R= NO$_2$
30b: R= CHO
30c: R= OMe
30d: R= Me

30a: Pd(0): 85%, Pd(II): 88%
30b: Pd(0): 75%, Pd(II): 80%
30c: Pd(0): 90%, Pd(II): 92%
30d: Spuren

bis zu 2 Durchläufe:
Durchlauf 1 **:** Pd(0): 90%, Pd(II): 92%
Durchlauf 2 **:** Spuren
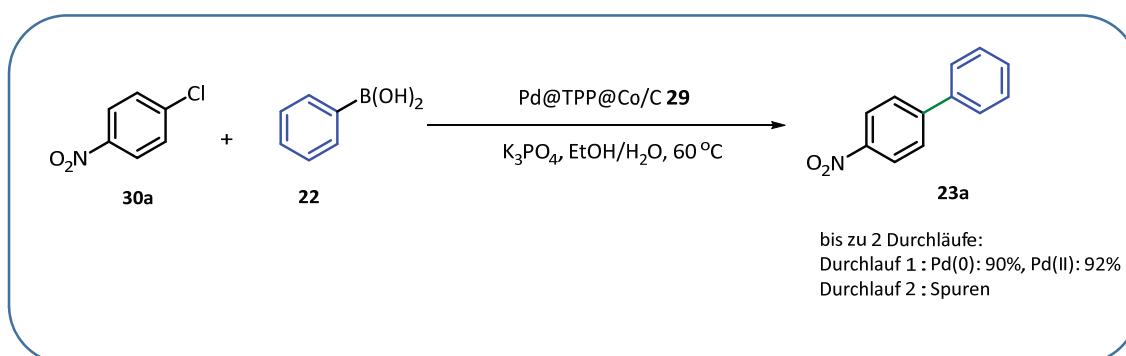
Scheme 37. Recycling von Pd@TPP@Co/C **29**.

E. Experimental Part

1. General information

Chemicals and solvents

All commercially available chemicals were purchased in high quality and used without further purification. For column chromatography, hexanes (60/40) and ethyl acetate were freshly distilled before usage.

CO/C NPs (20.5 m^2/g, particle size ≈ 25 nm) were obtained from Prof. W. J. Stark from the ETH Zurich, Switzerland. Initially, they were washed according to the general procedure. NPs were dispersed by the aid of an ultrasound bath (Sonorex RK 255 H-R, Bandelin) and recovered with the help of a commercially available neodymium based magnet (15 x 30 mm).

Elemental microanalysis (EA)

Elemental microanalysis (EA) was performed by the Micro Analytical Laboratory of the University of Regensburg using a Vario MICRO cube.

Infrared spectroscopy (IR)

Infrared spectra were recorded on an Agilent Cary 630 FT-IR spectrometer. The wavenumber is reported as cm^{-1}.

Inductively coupled plasma-optical emission spectrometry (ICP-OES)

Samples for the inductively coupled plasma optical emission spectrometry (ICP-OES) were measured with a Spectro Analytical Instruments ICP Modula EOP in an acidic medium (32% *aqua regia*, v/v) after prior standardization and calibration. Palladium was determined at λ = 340 nm, cobalt at λ = 229 nm, iron at λ = 239 nm and Zinc at λ = 350 nm.

Gas chromatography (GC)

Gas chromatography (GC) was performed on a Fisons Instruments GC8000 equipped with a capillary column (30 m x 250 μm x 0.25 μm) and flame ionization detector (temperature: 300°C detector, 250°C injector). Gas chromatography coupled with mass spectrometry (GC-MS) was carried out on a Shimadzu GCMS-QCM-QP2010 SE equipped with a quadrupole mass analyzer.

Transmission electron microscopy (TEM)

Transmission electron microscopy (TEM) was carried out on a FEI TecnaiF30 using standard TEM plates (carbon film on 400 mesh grids copper) with 3.05 mm diameter at the Department of Physics of the Italian Institute of Technology, *Genoa*.

High-resolution transmission electron microscopy (HRTEM)

HRTEM analysis the sample was dispersed in ethanol with the aid of an ultrasonic bath for 5 min and a drop of the solution was placed on a copper grid with holey carbon film. These measurements were performed at RCPTM, Palacky University, Czech Republic.

X-ray photoelectron spectroscopy (XPS)

X-ray photoelectron was perfprmed on a Perkin-Elmer Phisical Electronics PHI700 ESCA System at the Department of Physics of University of Regensburg and on a PHI 5000 VersaProbe II XPS system (Physical Electronics) with monochromatic Al-Kα source (15Kv, 50W) and photon energy of 1486.7 eV at thr Palacky University, Czech Republic. Dual beam charge compensation was used for all XPS measurements. All the spectra were measured in the vacuum of 1.3 x 10-7 Pa and at the room temperature of 21 °C. The analyzed area of sample was spot of 100 µm in diameter. The survey spectra were measured with pass energy of 187.850 eV and electronvolt step of 0.8 eV while for the high resolution spectra was used pass energy of 23.500 eV and electronvolt step of 0.2 eV. The spectra were evaluated with the MultiPak (Ulvac - PHI, Inc.) software. The binding energy (BE) values was referenced to the carbon peak C 1s at 284.80 eV.

Thin layer chromatography (TLC)

Thin layer chromatography was performed on silica gel coated aluminium plates (Merck silica gel 60 F254,0.2 mm layer thickness) and Macherey-Nagel ALUGRAM® Xtra SIL G/UV254).

Column chromatography

 (Flash-) Column chromatography was performed using Merck Gerduran 60 (0.063–0.200 mm).

^{1}H NMR and ^{13}C NMR

^{1}H NMR spectra were recorded on a BRUKER Avance III 400 "Nanobay" (400 MHz) spectrometer. The spectra were recorded in CDCl3. ^{1}H NMR splitting patterns are designated as singlet (s), doublet (d), triplet (t), quartet (q), quintet (quint) or doublet of doublets (dd). Splitting patterns

that could not be interpreted are designated as multiplet (m). ^{13}C NMR spectra were recorded on a BRUKER Avance III 400 "Nanobay "(101 MHz) spectrometer.

Nitrogen sorption

Nitrogen sorption measurements were conducted at 77 K using an Autosorb iQ instrument at the Italian Institute of Technology, *Genoa*. The sample was degassed at 200 °C for 3 h under vacuum prior to measurement.

Thermo-gravimetric analysis (TGA)

Thermo-gravimetric was carried out from 30°C to 1000°C at a heating rate of 10 °C/min by the institute of Physical and Theoretical Chemistry of the university of Regensburg (Perkin-Elmer TGA7).

General sample preparation for ICP-OES

5.00 mg catalyst was heated at 100 °C in 1.6 mL *aqua regia* for 10 minutes. After magnetic decantation, the particles were collected and the solution was transferred to a 10 mL volumetric flask. The particles were heated again in order to solve all Pd of nanoparticles, then both solutions were combined and filled up with millipore H_2O to 10 mL (32% *aqua regia* solution). The solution was filtered through a syringe filter (hydrophilic PTFE 0.2 μm).

General sample preparation for leaching experiments for ICP-OES

After the end of the reaction and washing the solutions were added in a round bottom flask, filtered through a syringe filter (hydrophobic PTFE 0.2 μm), then the solvent was evaporated and the precipitate was washed with 2.4 mL HCl$_{conc}$., and 0.8 mL HNO$_{3\ conc}$. (32% *aqua regia* solution) and heated at 100 °C for 10 minutes. The mixture was filled up with millipore water to a 10 mL volumetric flask (filtering through a syringe filter (hydrophilic PTFE 0.2 μm).

2. Microporous Organic Polymer (MOP) Encapsulated with Palladium Nanoparticles and Co/C Nanobeads for Hydrogenation and C-C Coupling Reactions

2.1. Synthesis of catalyst and starting materials

General washing pristine Co/C nanoparticles (11)
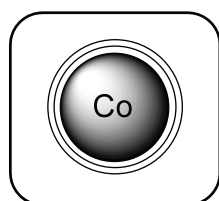
Co/C NPs **11**

Initially, the received carbon-coated cobalt nanoparticles (Co/C) **11** were washed for 24 h in a HCl$_{conc.}$ /H$_2$O $_{millipore}$ mixture (1:1). Afterward, the washed particles were collected by an external magnet and washed again with millipore water until all acid residuals were removed. Finally, the particles were washed with acetone (3x) and diethyl ether (2x) and dried at 50 °C under vacuum. EA (%): 4.50 C, traces H, 0 N.

General procedure A: Synthesis of Co/C NPs (13) (GP-A)
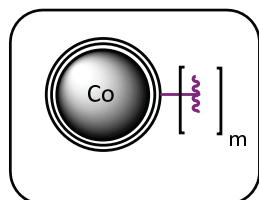
Co/C NPs **13**

Co/C NPs **11** (1000 mg, Elemental microanalysis [%]: 4.5 C, traces H, 0 N), monomer **a/ c** (1.5 mmol, 1.0 equiv.), concentrated HCl (0.6 mL) and H$_2$O$_{millipore}$ (25 mL) were introduced to a round bottom flask by using ultrasonic bath. To the reaction mixture was added pre-cooled solution sodium nitrite (158 mg, 2.3 mmol, 1.5 equiv.) in 12 mL H$_2$O$_{millipore}$ at 0 °C gently, then it was stirred in an ice batch and sonicated for 30 min. After magnetic decantation, the particles were washed with NaOH (1 M, 3x), water (3x), acetone (6x), and dried under vacuum to obtain Co/C NPs **13**.
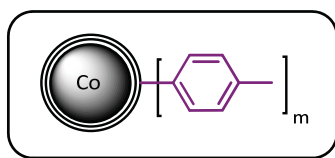
Co/C NPs **13a**

13a was prepared according to the general procedure A on a smaller scale (500 mg of **11**), 81 mg
p-toluidine. Yield: 499 mg **13a**, EA (%): 5.62 C, 0.1H, 0 N; Loading (based on carbon): 0.1 mmol/g.
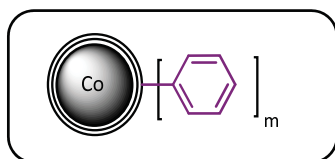
Co/C NPs **13b**

13b was prepared according to the general procedure A on a smaller scale (500 mg of **11**), 70 mg
aniline. Yield: 482 mg **13b**, EA (%): 4.83 C, 0.1H, 0 N; Loading (based on carbon): 0.04 mmol/g.
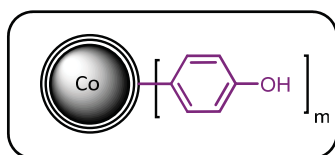
Co/C NPs **13c**

13c was prepared according to the general procedure A on a smaller scale (500 mg of **11**), 60 mg
p-aminophenol, Yield: 390 mg **13c**, EA (%): 5.07 C, 0.08H, 0 N; Loading (based on carbon): 0.08
mmol/g.

General procedure B: Synthesis of MOP@Co/C (14) (GP-B)
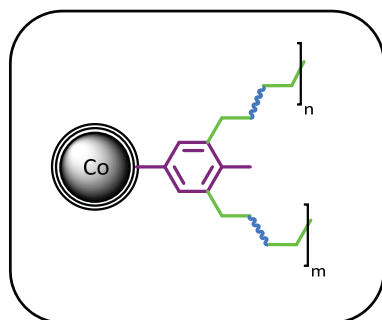
MOP@Co/C **14(d-l)**

500 mg (0.028 mmol ,1 equiv.) functionalized Co/C NPs **13a**, formaldehyde dimethyl acetal (555 µL, 476 mg, 6.25 mmol, 2.5 equiv.), monomer **d-l** (2.50 mmol, 1 equiv.), anhydrous iron(III)chloride (1.01 g, 6.25 mmol, 2.5 equiv.) and 1,2-dichloroethane (45 mL) were introduced to a pressure tube. The resulting mixture was stirred at room temperature and heated for five hours at 45 °C and then 19 hours at 80 °C to produce the microporous network **14**. The particles were washed with ethanol several times and dried *in vacuo* at 60 °C.

2,2'-biphenol: 465 mg;

2,2'-biphenol@Co/C **14h-β**: EA (%) 41.67 C, 2.95 H, 0 N; yield: 916 mg (88%)

Toluene: 230 mg;

toluene@Co/C **14g-γ**: EA (%) 29.72 C, 2.12 H, 0 N; yield: 686 mg (85%)

Synthesis of 14d-β, 14f-β, 14g-β, 14i-β, 14j-β, 14k-β, and 14l-β with 2.5 equiv. FDA (molar ratio respect to the monomer)

The polymers were synthesized according to the general procedure B in smaller scale: functionalized Co/C NPs **13a** (100 mg), monomer (0.50 mmol, 1.0 equiv.), formaldehyde dimethyl acetal (111 µL, 95 g 1.25 mmol, 2.5 equiv.), anhydrous iron(III) chloride (0.20 g, 1.25 mmol, 2.5 equiv.), and 1,2 dichloroethane (9 mL).

1,4-diaminobenzene: 54 mg;

1,4-diaminobenzene@Co/C **14d-β**: yield: 130 mg; EA (%):25.10 C, 2.38 H, 5. 21 N.

1,1'biphenyl: 77 mg;

1,1'biphenyl@Co/C **14e-β**: yield: 158 mg; EA (%):43.24 C, 2.50 H, 0 N.

2,3-naphthalenediol: 80 mg;

2,3-naphthalenediol@Co/C **14f-β**: yield: 134 mg; EA (%): 33.71 C, 2.53 H, 0 N.

Benzene: 39 mg;

Benzene@Co/C **14i-β**: yield: 125mg; EA (%):27. 27.42 C, 1.5 H, 0 N.

Mesitylene: 60 mg;

Mesitylene@Co/C **14j-β**: yield: 109 mg; EA (%): 13.23C, 0.76 H, 0 N.

Pyrrole: 34 mg;

Pyrrole@Co/C **14k-β**: yield: 108 mg; EA (%): 12.31 C, 0.85 H 1.4 N.

1,3,5 triphenylbenzene: 153 mg;

1,3,5 triphenylbenzene@Co/C **14l-β**: yield: 152 mg; EA (%): 44.77 C, 3.24 H, 0 N.

Synthesis of 14d-γ, 14e-γ, 14h-γ, and 14f-γ with 3 equiv. FDA (molar ratio respect to the monomer)

14d-γ, **14e-γ**, **14h-γ, and 14f-γ** were synthesized according to the general procedure B with 3 equiv. FDA in smaller scale: **13a** (100 mg), monomer (0.50 mmol, 1.0 equiv.), formaldehyde dimethyl acetal (0.13 mL, 110 mg 1.5 mmol, 3.0 equiv.), anhydrous iron (III) chloride (240 mg, 1.5 mmol, 3.0 equiv.), and 1,2-dichloroethane (9 mL).

14d-γ: yield: 110 mg; EA (%): 25.14 C, 2.58 H, 5. 91 N.

14e-γ: yield:160 mg; EA (%): 44.28 C, 2.70 H, 0 N.

14h-γ: yield:170 mg; EA (%): 38.29 C, 3.11 H, 0 N.

14f-γ: yield: 130mg; EA (%): 34.58 C, 2.71 H, 0 N.

General procedure C: Synthesis of Pd@MOP@Co/C (15) (GP-C)
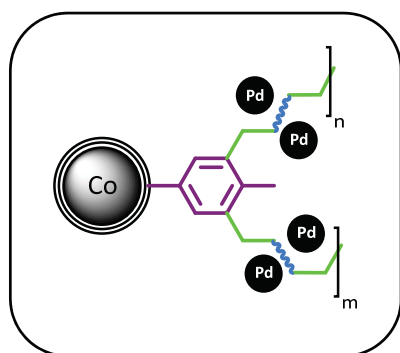
Pd@MOP@Co/C **15**

500 mg of MOP@Co/C **14**, $Pd_2(dba)_3CHCl_3$ (52 mg, 50 µmol), and dry toluene (15 mL) were introduced to microwave vial under nitrogen. The particles were sonicated for 10 min and then heated in a focused microwave oven to 110 °C for 2 min. The magnetic catalyst was retrieved by using an external magnet and washed with CH_2Cl_2, then dried *in vacuo* at 60 °C to obtain Pd@MOP@Co/C **15**.

Catalysts **15h-β** and **15g-γ** were synthesized on large scale from **14h-β** and **14g-γ** according to the general procedure **C**:

15h-β: EA (%): 37.07 C, 2.57 H, 0 N; loading (Pd): 0.19 mmol/g, 2 wt% (97% Pd incorporation) yield: 530 mg.

15g-γ: EA (%): 25.23 C, 1.75 H, 0 N; loading (Pd): 1.9 wt%, 0.18 mmol/g (89% Pd incorporation).

Catalysts **15d-γ, 15e-γ, 15f-γ, 15h-γ** were also synthesized in 100 mg scale according to the general procedure **C**, $Pd_2dba_3·CHCl_3$ (2.0 mg, 1.9 µmol), and dry toluene (8 mL).

15d-γ: EA (%): 22.71 C, 2.03 H, 5.60 N; Loading (Pd): 0.02 mmol/g, 0.26 wt% (64% Pd incorporation); yield (g): 0.081.

15e-γ: EA (%): 42.97 C, 2.50 H, 0 N; Loading (Pd):0.03 mmol/g, 0.28 wt% (70% Pd incorporation); yield (g): 0.093.

15f-γ: EA (%): 30.84 C, 2.31 H, 0 N; Loading (Pd): 0.04 mmol/g, 0.38 wt% (93% Pd incorporation); yield (g): 0.075.

15h-γ: **EA (%):** 36.94 C, 2.81 H, 0 N; Loading (Pd): 0.04 mmol/g, 0.38 wt% (95% Pd incorporation); yield (g): 0.094.

2.2. Catalysis

General procedure D: Representative procedure for the hydrogenation using Pd@2,2'-biphenol@Co/C 15h-β (GP-D)

To a Schlenk flask catalyst **15h-β** (5.3 mg, 1.0 µmol, 0.2 mol%), substrate (0.50 mmol, 1.0 equiv.) and 2-propanol (10 mL) were introduced. Dodecane was used as an internal standard (125 µL, 94 mg, 0.55 mmol). The slurry was stirred for 10 minutes then the tube was evaporated and flushed with H_2 several times followed by vigorous stirring under 1 atm H_2 (balloon). The reaction progress was monitored by GC analysis. Then nanoparticles were retrieved by an external magnet and the resulting solution was filtered by a syringe filter (hydrophobic PTFE 0.2 µm) before injection to GC.

Hydrogenation of 4-nitrophenol

Hydrogenation of 4-nitrophenol was performed according to the general procedure in 1 mol% of catalyst **15h-β** (26 mg, 5 µmol, 1 mol%), 0.5 mmol substrate (1.0 equiv.) was added to a Schlenk flask, 2-propanol (10 mL). Subsequently, the mixture was stirred at room temperature until good dispersion was achieved. Before starting the reaction, the flask was evaporated and flushed with H_2 several times followed by vigorous stirring under 1 atm H_2 at 50 °C.

General procedure E: Representative procedure for the catalyst recyclability of the hydrogenation reaction (GP-E)

For recycling experiments, catalyst **15h-β** (10 mg, 1.96 µmol, 0.2 mol%), diphenylacetylene (180 mg, 1.0 mmol, 1.0 equiv) was hydrogenated in 20 mL 2-propanol according to the general procedure. The catalyst was isolated from the reaction mixture after full conversion by an external magnet and washed with 2-propanol (3x), dichloromethane (3x). Subsequently, the catalyst was dried under vacuum and reused in the next run directly. The reaction progress was monitored by GC. After six runs, (9 mg, 1.76 µmol) catalyst **15h-β** was retrieved (90% of the original catalyst).

2.3. GC data

General GC conditions for hydrogenation reactions
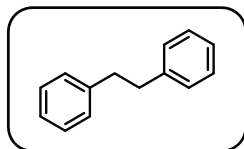
1,2-Diphenylethane (17a): 3 min at 140 °C, 16 °C/min to 300 °C; retention time: dodecane (3.18 min), 1,2-diphenylethane (6.23 min), 1,2-diphenylethyne (7.91 min).

1,2-Diphenylethane (17f): 3 min at 140 °C, 16 °C/min to 300 °C; retention time: dodecane (3.23 min), 1,2-diphenylethane (6.23 min), (*E*)-1,2-diphenylethene (7.5 min).
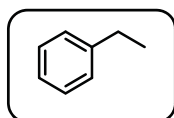
Ethylbenzene (17b): 1 min at 50 °C, 1 °C/min to 60 °C (0 min), 20 °C/min to 250 °C: dodecane (15.82 min), ethylbenzene (5.75 min), ethynylbenzene (6.19 min).

Ethylbenzene (17c): 1 min at 50 °C, 1 °C/min to 60 °C (0 min), 20 °C/min to 250 °C; retention time: dodecane (15.82 min), ethylbenzene (5.01 min), styrene (6.3 min).
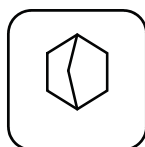
bicyclo [2.2.1] heptane (17d): 3 min at 60 °C, 30 °C/min to 300 °C; Retention time: Norbornene (2.53 min), bicyclo[2.2.1]heptane (2.83 min), dodecane (7.19 min).
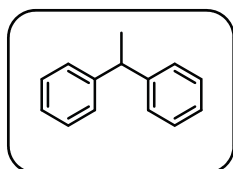
Ethane-1,1-diyldibenzene (17e): 3 min at 140 °C, 16 °C/min to 300 °C; retention time: dodecane (3.23 min), ethane-1,1-diyldibenzene (5.95 min), ethane-1,1-diyldibenzene (6.17 min).
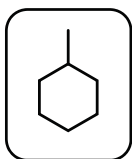
Methylcyclohexane (17g): 3 min at 50 °C, 10 °C/min to 200 °C; retention time:

methylcyclohexane (2.71 min), 1-methylcyclohex-1-ene (3.38 min), dodecane (11.54 min).
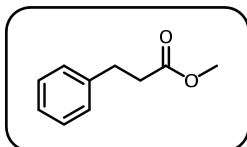
Methyl 3-phenylpropanoate (17h): 3 min at 100 °C, 20 °C/min to 300 °C; retention time:

dodecane (5.70 min), methyl 3-phenylpropanoate (6.15 min), methyl cinnamate (7.15 min).
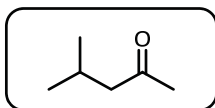
4-Methylpentan-2-one (17i): 3 min at 50 °C, 10 °C/min to 75 °C (0 min), 20 °C/min to 200 °C;

retention time: dodecane (9.87 min), 4-methylpent-3-en-2-one (2.78 min), 4-methylpentan-2-

one (3.70 min).
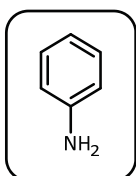
Aniline (17j): 3 min at 50 °C, 10 °C/min to 200 °C; retention time: ethylbenzene (5.00 min),

aniline (7.05 min), nitrobenzene (9.04 min).
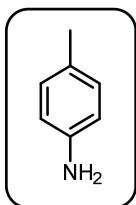
4-Aminotoluene(17k): 3min at 50 °C, 10 °C/min to 200 °C; Retention time: 4-Aminotoluene

(6.80 min), 4-nitrotoluene (8.69 min), dodecane (8.89 min).

2.4. Miscellaneous

N$_2$ sorption

A

B
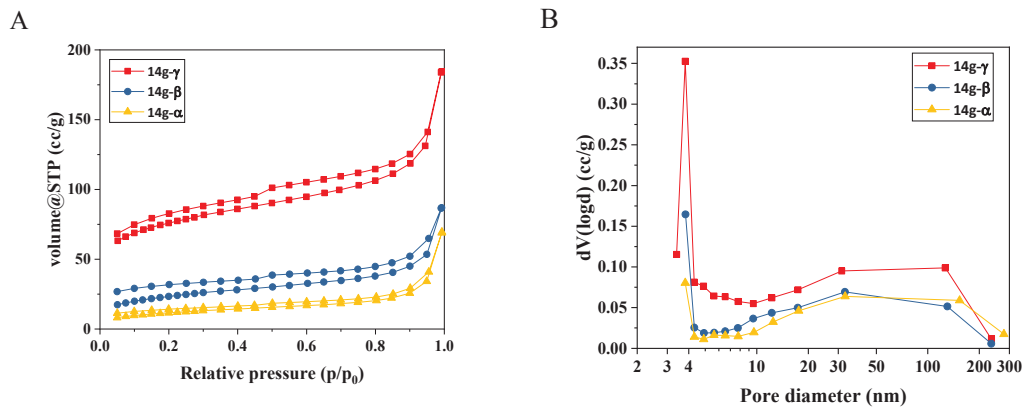
Figure 25. A) N$_2$ sorption data of **14g-α** to **14g-γ.** Brunauer-Emmett-Teller (BET) method, B) Barrett-Joyner--Halenda (BJH) method.

A

B
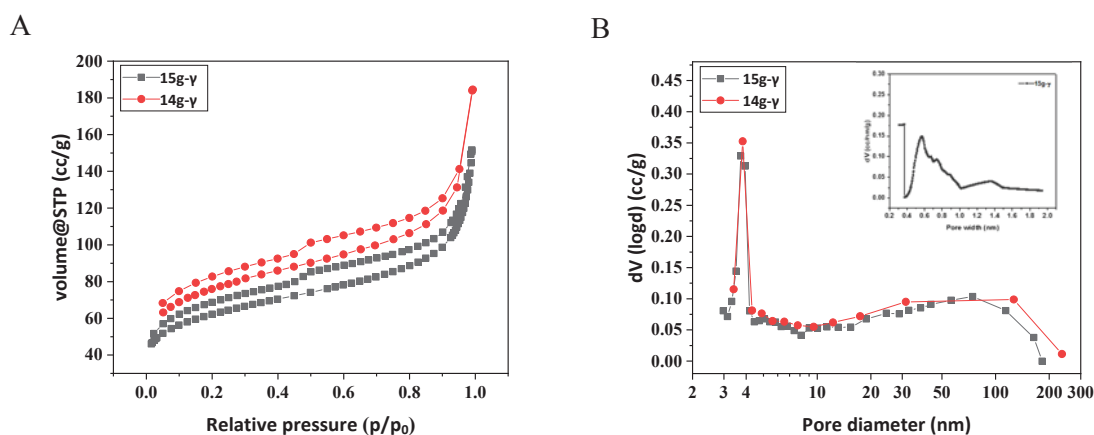
Figure 26. A) N$_2$ adsorption-desorption isotherms of **14g-γ** (red) and **15g-γ** (grey). B) Logarithmic presentation of the pore size distribution calculated by the Barrett-Joyner-Halenda (BJH) method for **14g-γ** (red) and **15g-γ** (grey). Inset: Size distribution of the micropores of **15g-γ** obtained by Horvath-Kawazoe (HK) method.

XPS measurements
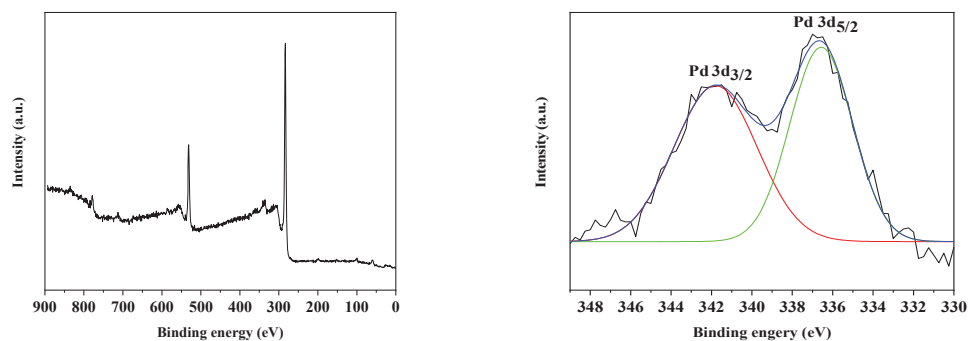
Figure 27. The valence state of Pd in the catalyst **15h-β** with 2 wt % Pd. The peak binding energies of 336.0 eV (Pd 3d$_{5/2}$) and 335.2 eV (Pd 3d$_{3/2}$) confirming the present of Pd (0) in the catalysts.
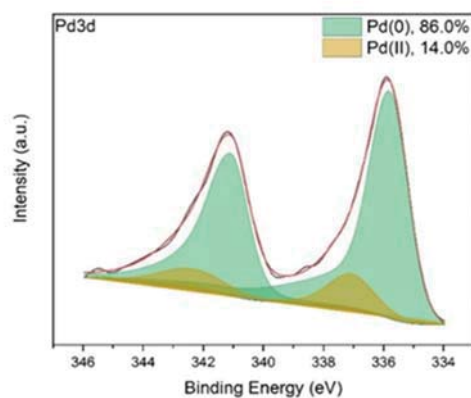
Figure 28. Pd3d of the **15h-β** with 2 wt% Pd after pre-treatment with hydrogen at atmospheric pressure before measurement.
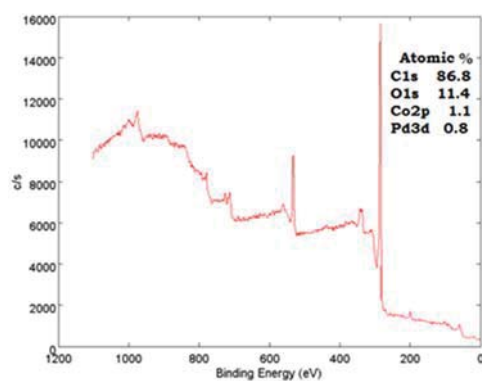
Figure 29. XPS survey spectrum of the catalyst **15g-γ** (1.9 wt %).
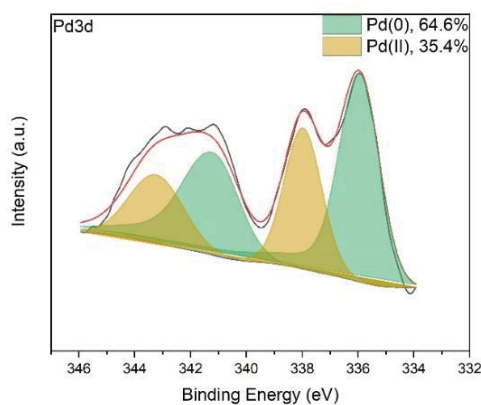
Figure 30. Pd3d of the **15g-γ** with 1.9 wt % Pd after pre-treatment with hydrogen at atmospheric pressure before measurement.
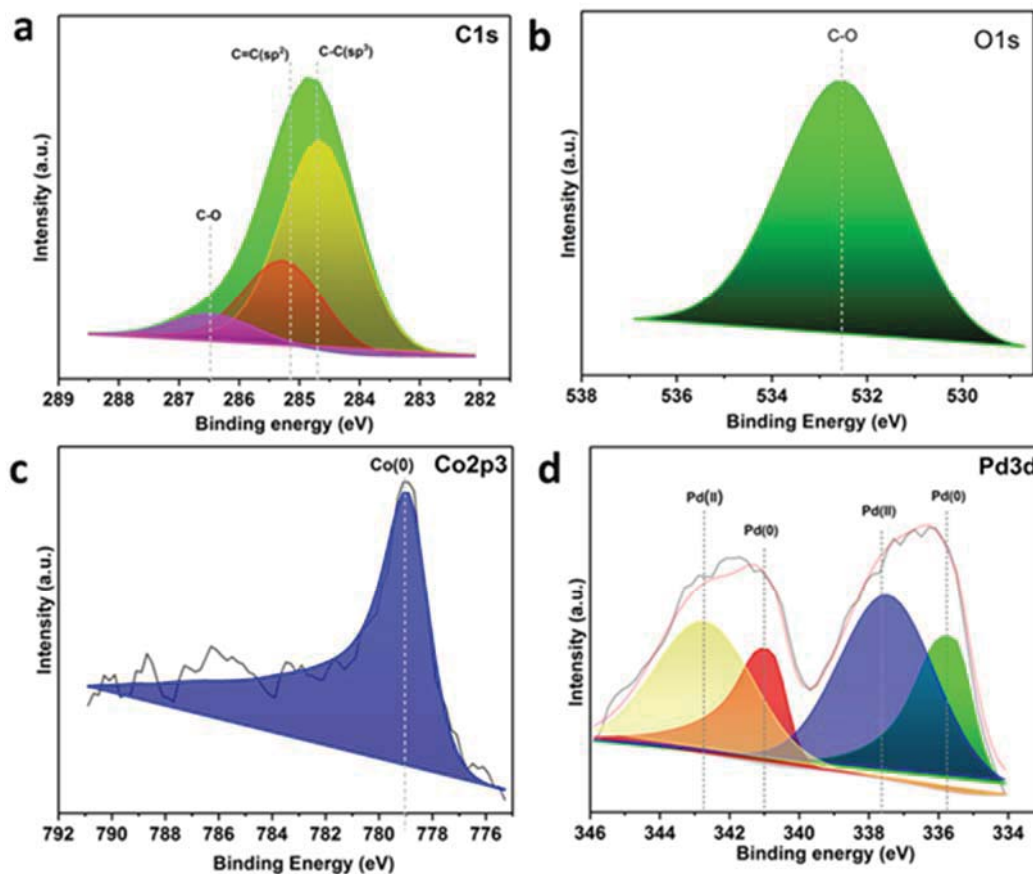
Figure 31. XPS spectra of **15g-γ** with 1.9 wt % Pd. Ratio of Pd(0)/Pd(II) = 36:64
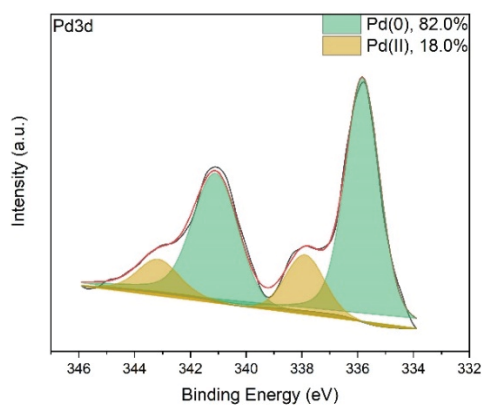
Figure 32. XPS spectra of **15g-γ** (1.9 wt % recycled after six runs).

TEM images and Pd nanoparticles size distributions
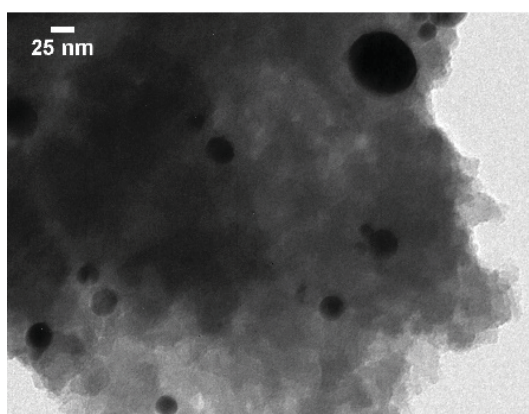
Figure 33. 14g-γ with 0.2 wt % Pd.
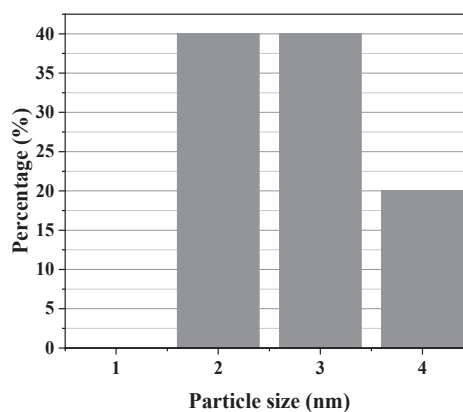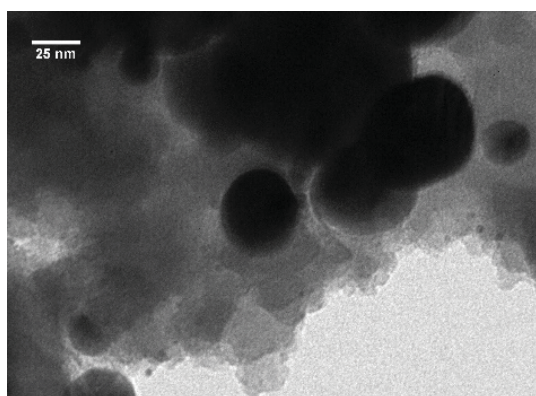
Figure 34. 14g-γ with 0.4 wt % Pd.
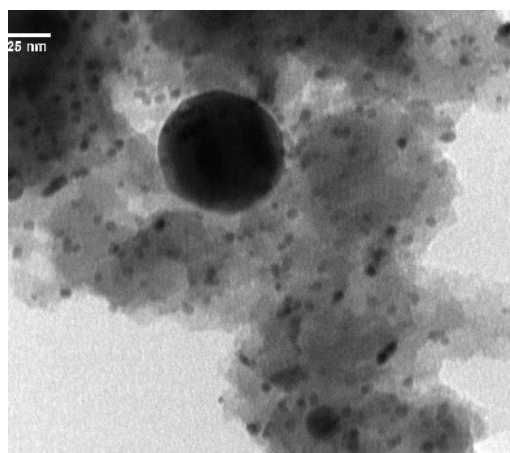
Figure 35. 14g-γ with 1.0 wt % Pd.
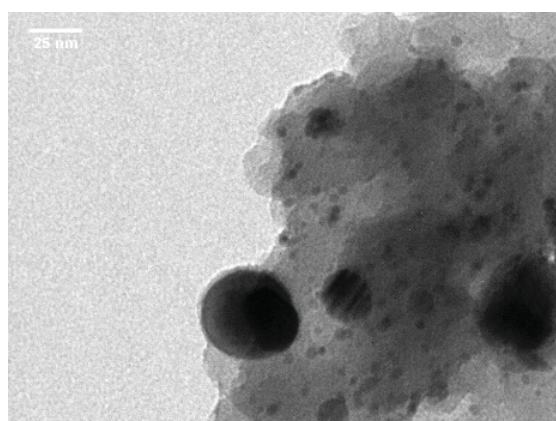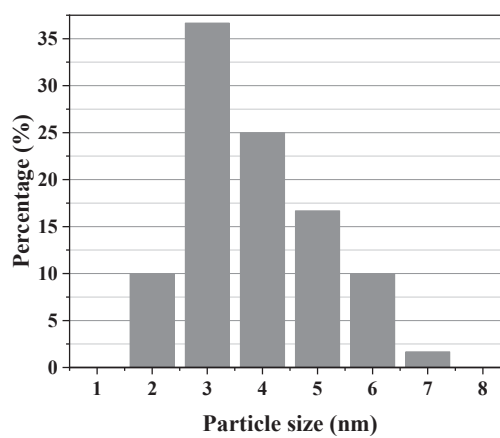
Figure 36. 14g-γ with 1.7 wt % Pd.
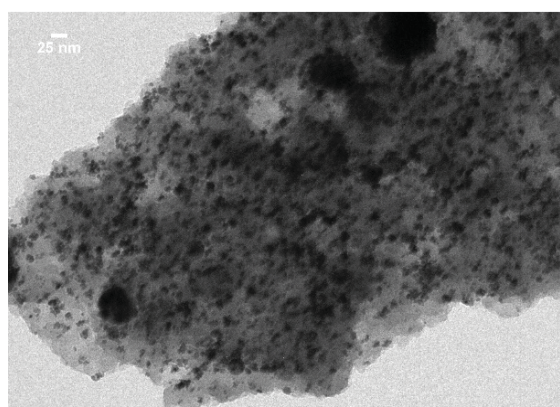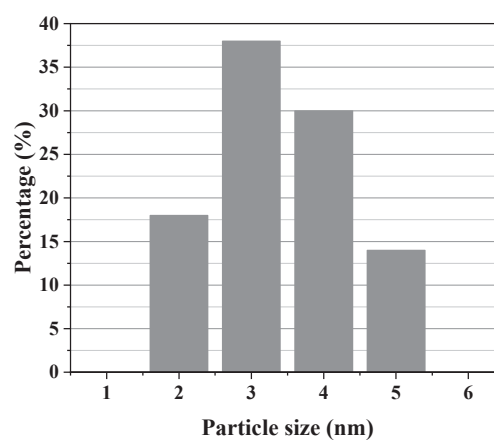
Figure 37. 14g-γ with 3.9 wt % Pd.
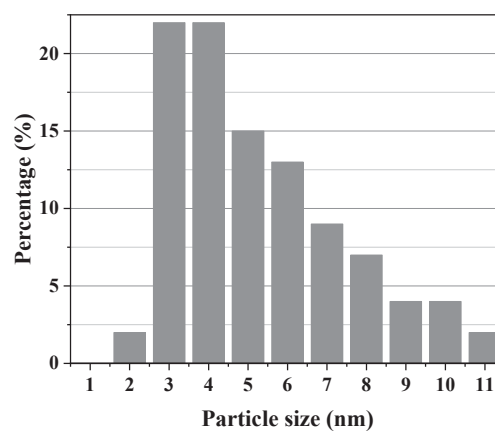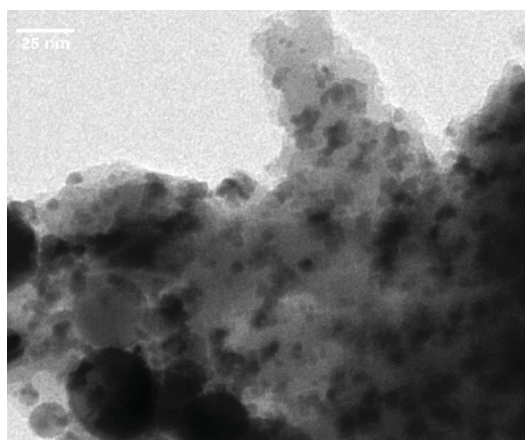
Figure 38. 14g-γ with 14 wt % Pd.
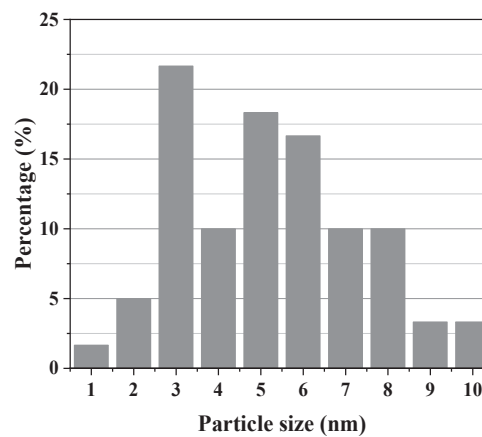
HRTEM
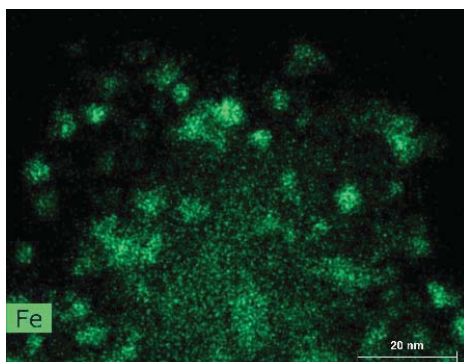
Figure 39. **HAADF images and EDS chemical mapping of** 15g-γ **(1.9 wt %) showing elemental mapping of Fe.**
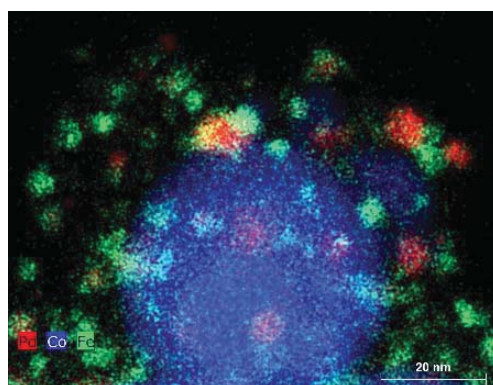
Figure 40. HAADF images and EDS chemical mapping of **15g-γ** (1.9 wt %) showing elemental mapping of Pd-Co-Fe together.

2.5. Suzuki-Miyaura cross-coupling reaction

2.5.1. Catalysis

General procedure F: Representative procedure for the Suzuki cross-coupling reaction (GP-F)

To a microwave vial catalyst **15h-β** (5.3 mg, 1.0 µmol, 0.2 mol%), ary halide (0.50 mmol, 1.0 equiv.) phenylbronoic acid (0.75mmol, 0.091 g), potassium phosphate (1.25 mmol,0.26 g) were introduced in 7 ml water and 7 ml ethanol. The suspension was sonicated for 10 min and then heated in a microwave oven to 120 °C. For workup, after allowing the reaction mixture to cool down, the contents poured into a reparatory funnel. Water (20 mL) and ethyl acetate (20 mL) were added and the organic material extracted and removed. After further extraction of the aqueous layer with ethyl acetate and washing with dichloromethane, combining the organic washings and drying them over MgSO$_4$, the solvent was removed *in vacuo* and leaving the crude product. Products were purified and isolated by chromatography using hexane/ethyl acetate as eluent.

General procedure G: Representative procedure for the catalyst recyclability of Suzuki cross-coupling reaction (GP-G)

4-idoanisol and 4-bromoanisol were chosen for recycling experiments as model substrates. Catalyst **15h-β** (26 mg, 5 µmol, 0.5 mol%), 4-idoanisol (0.23 g, 1.0 mmol, 1.0 equiv.) were used in 20 mL water and 20 mL ethanol. The catalyst was isolated from the reaction mixture after each reaction time by an external magnet and washed with dichloromethane. Subsequently, dried under vacuum and reused in the next run directly. The reaction progress was monitored by TLC. After six runs, (13 mg, 2.5 µmol) catalyst **15h-β** was retrieved (56% of the original catalyst). In the case of 4-bromoanisol, (0.12 g, 1.0 mmol, 1.0 equiv.) substrate was used for recycling with (26 mg, 5 µmol, 0.5 mol%) catalyst **15h-β**. At the end of the sixth run, (11 mg, 2.2 µmol) catalyst **15h-β** was regained (47% of the original catalyst).

3. Bimetallic Zn@Pd@MOP@Co/C Catalyst for Selective Hydrogenation

3.1. Synthesis of catalyst and starting materials

General procedures A, B, C for the synthesis of 15h-β

| Co/C NPs **11** | Co/C NPs **13a** | 2,2'-biphenol@Co/C **14h** | Pd@2,2'-biphenol@Co/C **15h** |
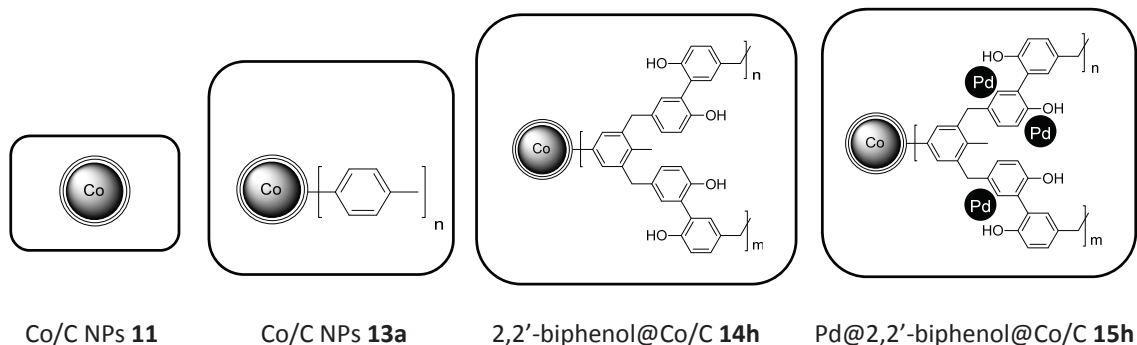
2,2'-Biphenol@Co/C **14h** was synthesized according to the general procedures A, B, C in the first chapter. 250 mg (0.014 mmol ,1 equiv.) functionalized Co/C NPs **13a**, formaldehyde dimethyl acetal (277 µL, 238 mg, 6.25 mmol, 2.5 equiv.), 2,2'-biphenol (232 mg, 1.25 mmol, 1 equiv.), anhydrous iron (III) chloride (500 mg, 3.12 mmol, 2.5 equiv.), and 1,2-dichloroethane (25 mL) were introduced to a pressure tube. The resulting mixture was stirred at room temperature and heated for five hours at 45 °C and then 19 hours at 80 °C to produce the microporous network. The particles were washed with ethanol several times to obtain clear solution and dried *in vacuo* at 60 °C. 2,2'-biphenol@Co/C **14h:** yield: 430 mg (84%); EA (%) 40.37 C, 2.71 H, 0 N.

300 mg of 2,2'-biphenol@Co/C **14h**, $Pd_2(dba)_3CHCl_3$ (6.0 mg, 5.7 µmol), and dry toluene (15 mL) were introduced to microwave vial under nitrogen. The particles were sonicated for 10 min and then heated in a focused microwave oven to 110 °C for 2 min. The magnetic catalyst was retrieved by using an external magnet and washed with CH_2Cl_2, then dried *in vacuo* at 60 °C to obtain Pd@MOP@Co/C **15h**. EA (%): 38.11 C, 2.93 H, 0 N; Loading (Pd): 0.03 mmol/g, 0.31 wt% (78% Pd incorporation) yield: 308 mg.

General procedure H: Synthesis of Zn@Pd@MOP@Co/C (GP-H)
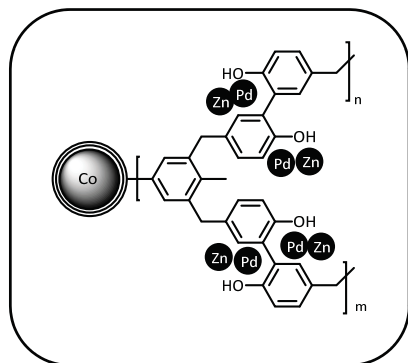
Zn$_y$@Pd @MOPs@Co/C **25h (α- δ)**

In the mixture of water-methanol (1:1), hydrazine monohydrate solution along with NaBH$_4$ were added to 70 mg **15h** to bring the PH of the mixture to 9, allowed to proceed under ultrasonic condition for 2h. Subsequently, Zn(NO$_3$)$_2$.6H$_2$O were treated by the mixture under nitrogen and allowed to stirred for 24 h at 60 °C to produce catalyst **25h**. Then, the catalysts were separated magnetically, washed with water and acetone several times, dried for 5h *in vacuo* at 60 °C. To produce catalysts **25h-α, 25h-β**, **25h-γ**, and **25h-δ**, (2.0 mg, 0.006 mmol), (3.5 mg, 0.01 mmol), (17 mg, 0.06 mmol) and (35 mg, 0.1 mmol) Zn(NO$_3$)$_2$.6H$_2$O were added to 70 mg **12h-β**. Thus, catalysts with various Zn:Pd molar ratios were synthesized in 70 mg scale. For Zn$_y$@Pd@MOPs@Co/C (**25h-α-25h- δ),** $_y$= 1, 2, 10, 20 represents molar ratio of Zn to Pd. The Pd loading for all the catalysts was considered 0.3 wt%.

Zn@Pd@MOP@Co/C **25h-α**: Loading (Zn): 0.02 mmol/g, 0.2 wt% (14% Zn incorporation), Loading (Pd): 0.03 mmol/g, 0.3 wt% (79% Pd incorporation); yield (g): 0.063.

Zn$_2$@Pd@MOP@Co/C **25h-β**: Loading (Zn): 0.04 mmol/g, 0.5 wt% (20% Zn incorporation), Loading (Pd): 0.03 mmol/g, 0.28 wt% (74% Pd incorporation); yield (g): 0.061.

Zn$_{10}$@Pd@MOP@Co/C **25h-γ**: Loading (Zn): 0.20 mmol/g, 1.7 wt% (32% Zn incorporation), Loading (Pd): 0.03 mmol/g, 0.28 wt% (72% Pd incorporation); yield (g): 0.060.

Zn$_{20}$@Pd@MOP@Co/C **25h-δ**: Loading (Zn): 0.23 mmol/g, 2.2 wt% (39% Zn incorporation), Loading (Pd): 0.03 mmol/g, 0.3 wt% (78% Pd incorporation); yield (g): 0.063.

Pd@MOP@Co/C **15h-β**: Loading (Pd): 0.038 mmol/g, 0.4 wt% (82% Pd incorporation); yield (g): 0.073.

3.2. Catalysis

General procedure I: Selective hydrogenation (GP-I)

To a Schlenk flask Zn_y@Pd@MOPs@Co/C **25h** (0.5 mol%), substrate (0.50 mmol, 1.0 equiv.) and 2-propanol (10 mL) were introduced. Dodecane was used as an internal standard (125 µL, 94 mg, 0.55 mmol). The slurry was stirred for 10 minutes then the tube was evaporated and flushed with H_2 several times followed by vigorous stirring under 1 atm H_2 (balloon). The reaction progress was monitored by GC analysis. Then nanoparticles were retrieved by an external magnet and the resulting solution was filtered by a syringe filter (hydrophobic PTFE 0.2 µm) before injection to GC.

General sample preparation for ICP-OES

5.00 mg catalyst was heated at 120 °C in 1.6 mL *aqua regia* for 20 minutes. After magnetic decantation, the particles were collected and the solution was transferred to a 10 mL volumetric flask. The particles were heated again in order to solve all Zn and Pd, then both solutions were combined and filled up with millipore H_2O to 50 mL (32% *aqua regia* solution). The solution was filtered through a syringe filter (hydrophilic PTFE 0.2 µm).

General sample preparation for leaching experiments for ICP-OES

In the end, after washing, the solutions were added in a round bottom flask, filtered through a syringe filter (hydrophobic PTFE 0.2 µm), then the solvent was evaporated and the precipitate was washed with 2.4 mL $HCl_{conc.}$, and 0.8 mL HNO_3 conc. (32% *aqua regia* solution) and heated at 120 °C for 20 minutes. The mixture was filled up with millipore water to a 50 mL volumetric flask (filtering through a syringe filter (hydrophilic PTFE 0.2 µm).

4. Palladium Nanoparticles Supported on Electroactive Microporous Organic Polymer Based on Triphenylphosphine (TPP)

4.1. Synthesis of catalyst and starting materials

General procedure J: Synthesis of polymer (TPP) (27) (GP-J)
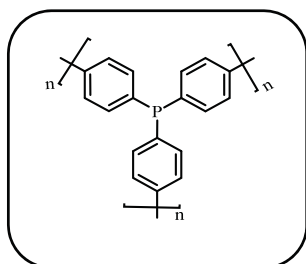
TPP **27**

To a solution of 1,5 cyclooctane (0.5 mL ,4.18 mmol) and 2.2 bipyridyl (0.64 mL,4mmol), 1 g Ni(cod)$_2$ (4mmol) was added in 50mL anhydrous DMF this step was done in glove box system. Subsequently, the mixture was heated to 80 °C for 1 h. Tris (4-chlorophenyl) phosphine **26** (0.38 g, 0.78 mmol) was then added to the mixture and was kept at this temperature under stirring for 10 hours. After cooling the mixture, HCl (2.5M, 10ml) was added to the solution. Then the solid was filtered and the residue was washed with water (2x), ethanol(5x), chloroform(3x), acetone(4x). The polymer was dried under vacuum at 120 °C to obtain 0.6 g microporous polymer (TPP) **27**. EA (%): 53.13 C, 6.61 H, 0 N.

General procedure K: Synthesis of TPP@Co/C (28) (GP-K)
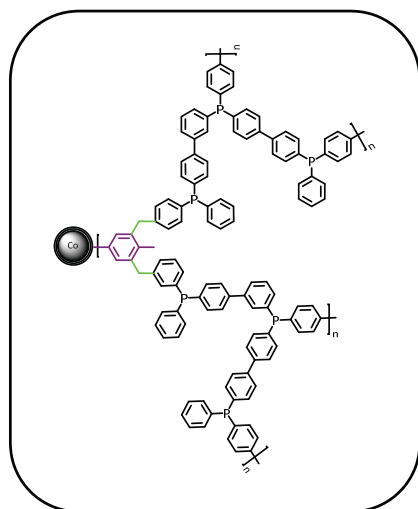
TPP@Co/C **28**

To a Schlenk flask 100 mg (1 mmol ,1 equiv.) triphenylphosphine polymer, toluene functionalized Co/C NPs **13a** (100 mg), formaldehyde dimethyl acetal (100 µL, 90 mg, 1.2 mmol, 2.5 equiv.), anhydrous iron (III) chloride (0.2 g, 1.2 mmol, 2.5 equiv.) and 1,2-dichloroethane (20 mL) were introduced. Then the mixture was stirred at room temperature and heated for five hours at 45 °C to form the network then the mixture was kept at 80 °C for 19 hours. After allowing to cool the particles were washed with ethanol, toluene, diethylether several times and dried *in vacuo* at 80 °C to obtain (260 mg) TPP@Co/C **28**. EA (%): 31.12 C, 2.28 H, 0 N; Loading (based on carbon): 1.2 mmol/g.

General procedure L: Synthesis of Pd(II)@TPP@Co/C (29) (GP-L)
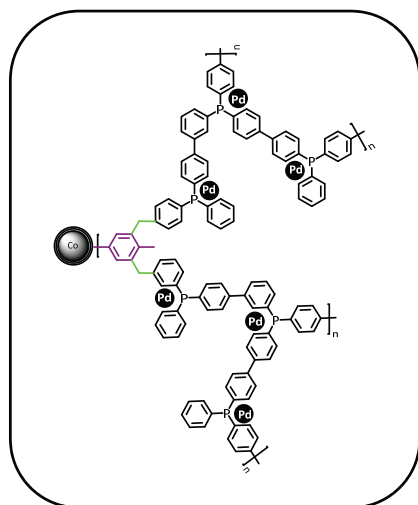
Pd(II)@TPP@Co/C **29**

TPP@Co/C **28** 100 mg, PdCl$_2$ (10 mg, 56 µmol) and acetonitrile (10 mL) were introduced to a Schlenk flask. The particles were sonicated for 10 minutes and then heated to 60 °C for 24 hours. The magnetic catalyst was retrieved by using an external magnet and washed with toluene and dichloromethane, then dried under vacuum at 70 °C to obtain Pd(II)@TPP@Co/C. Yield: 80 mg: EA (%): 30.67 C, 1.89 H, 0 N; loading (Pd): 3.5 wt %, 0.34 mmol/g (60% Pd incorporation).

General procedure M: Synthesis of Pd(0)@TPP@Co/C (29) (GP-M)

Pd$_2$(dba)$_3$CHCl$_3$ (10 mg, 9.6 µmol) was added to a suspension of TPP@Co/C **28** (100 mg) and dry toluene (15 mL) to microwave vial under nitrogen. The particles were sonicated for 10 minutes and then heated in a focused microwave oven to 110 °C for 2 minutes. After retrieving the magnetic catalyst by an external magnet, the catalyst was washed with diethyl ether and dichloromethane. Subsequently, Pd(0)@TPP@Co/C was dried under vacuum at 70 °C. Yield: 82 mg: EA (%): 30.54 C, 1.80 H, 0 N; loading (Pd): 1.3 wt %, 0.12 mmol/g (94 % Pd incorporation).

4.2. Catalysis

General procedure N: Suzuki cross-coupling reaction

To a Schlenk flask Pd(0)@TPP@Co/C or Pd(II)@TPP@Co/C catalyst (0.5 mol%), aryl chloride (0.50 mmol, 1.0 equiv.) phenylbronoic acid (0.75 mmol, 0.091 g), potassium phosphate (1.25 mmol, 0.26 g) were introduced in 5 ml water and 5 ml ethanol. The mixture was sonicated for 10 minutes and then heated to 80 °C. The product was extracted with diethylether and ethyl acetate. The catalyst was washed with water and acetone and retrieved by an external magnet. The organic solution was dried over $MgSO_4$ and was removed *in vacuo*. Products were purified and isolated by chromatography using hexane/ethyl acetate as eluent.

4.3. XPS measurements
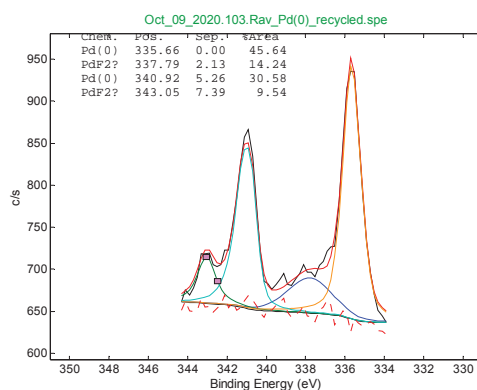
Figure 41. XPS spectra of Pd 3d of the recycled Pd(0)@TPP@Co/C with 1.3 wt % Pd.
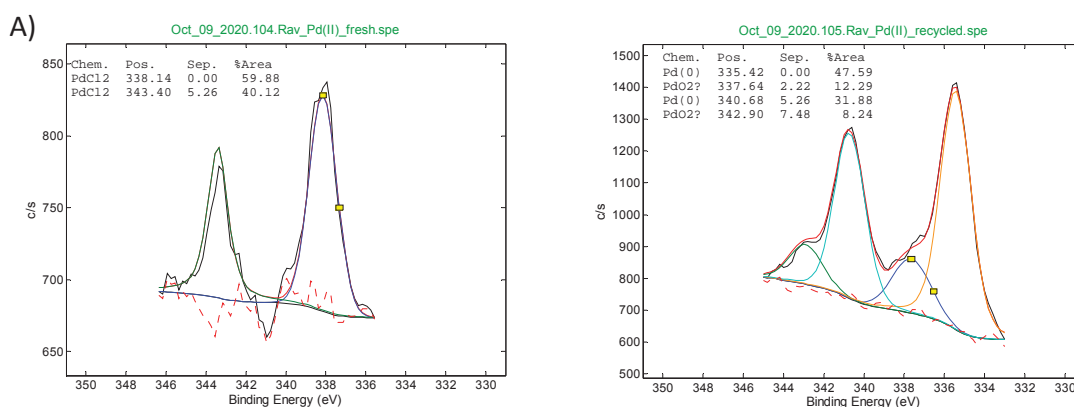
Figure 42. XPS spectra of Pd 3d of the Pd(II)@TPP@Co/C with 3.5 wt % Pd. A) freshly prepared and B) after recycling step.

F. References

[1]   F. P. Blondet, T. Vincent , E. Guibal, *Int. J. Biol*. *Macromol*. **2008**, 43, 69-78.

[2]   Q. Kainz, R. Linhardt, R. Grass, G. Vilé, J. Pérez-Ramírez, W. Stark, O. Reiser, *Adv. Funct. Mater*. **2014**, 24, 2020-2027.

[3]   L. Li, Ch. Zhou, H. Zhao, R. Wang, *Nano Res*. **2015**, 8, 709-721.

[4]   T. Ishida, Y. Onuma, K. Kinjo, A. Hamasaki, H. Ohashi, T. Honma, T. Akita, T. Yokoyama, M. Tokunaga, M.Haruta, *Tetrahedron*. **2014**,70, 6150–6155.

[5]   R. Linhardt, Q. M. Kainz, R. N. Grass, W. J. Starkb , O. Reiser, *RSC Adv.* **2014**, 4, 8541.

[6]   B.Li, R. Gong, W. Wang, X. Huang, W. Zhang, H. Li,C. Hu, B. Tan, *Macromolecules* **2011**, *44*, 2410–2414.

[7]   R. N.Grass, E. K. Athanassiou, W. J. Stark, Angew. Chem. Int. Ed. **2007**, 46, 4909–4912.

[8]   S. Ranjbar, Dissertation, Universitat Rovira I Virgili (ICIQ), Tarragona; Universität Regensburg, Regensburg, 2016

[9]   L. Stadler, M. Homafar, A. Hartl, Sh. Najafishirtari, M. Colombo, R. Zboril, M. Petr, M. B. Gawande, J. Zhi, O. Reiser, *ACS Sus. Chem. Eng*. **2019**, 7, 2388-2399.

[10]   L. Li, H, Zhao, J. Wang, R. Wang, *ACS Nano*. **2014**, *8*, 5352–5364.

[11]   K. S. W. Sing, *Pure Appl. Chem.* **1985**, 57.

[12]   M. P. Tsyurupa, V.A. Davankov, *React. Funct. Polym.* **2006**, 66.

[13]   J. Weber, J. Schmidt, A.Thomas, W. Böhlmann, *Langmuir*. **2010**, *26*, 15650–15656.

[14]   B. Li, Z. Guan, W. Wang, X. Yang, J. Hu,B. Tan, T.Li, *Adv. Mater.* **2012**, *24*.

[15]   R. Dawson,T. Ratvijitvech, M. Corker, A. Laybourn, Y. Z Khimyak, A.I. Cooper, D.J. Adams, *Polym. Chem*. **2012**, 3, 2034–2038.

[16]   M. Cano, A. Benito, A. W. K Maser. E.P. Urriolabeitia, *Carbon*. **2011**, 49, 652–658.

[17]   C. E. Garrett, K. Prasad, *Adv. Synth. Catal*. **2004**, 346, 889-900.

[18]   R. Li, P. Zhang, Y. Huang, P.Zhang, H. Zhong , Q. Chen, *J. Mater. Chem*. **2012**, 22, 22750.

[19]   N. Miyaura, A. Suzuki, *Chem.Rev*. **1995**, 95, 2457-2483.

[20]   A. Schätz, T. Long, R. N. Grass, W. J. Stark, P. Hanson, O.Reiser, *Adv. Funct. Mater*. **2010**, 20, 4323-4328.

[21]   S. Schlick, E. Borte, K. Dyrek, Acta Polymer. **1996**, 47, 1-15.

[22]   S. Ogasawara, S. Kato, *J. AM. CHEM. SOC*. **2010**, 132, 4608-4613.

[23]   A. Zapf, M. Beller, *Chem. Commun*. **2005**, 431-440.

[24]   W. A. Herrmann, *Angew. Chem. Int. Ed*. **2002**, 41, 1290-1309.

[25]   S. A. Patil, Ch. M. Weng, P.Ch. Huang, F. E. Hong, *Tetrahedron*. **2009**, 65, 2889-2897.

[26]   M. Ohff, A. Ohff, D. Milstein, *Chem. Commun*. **1999**, 357–358.

[27]   L. Botella, C.Nàjera, *Angew. Chem. Int. Ed*. **2002**, 41.

[28]   G. A. Grasa, A. C. Hillier, S. P. Nolan, *Org. Lett*. **2001**, 3, 1077-1080.

[29]   X. Le, Zh. Dong, Zh. Jin, Q. Wang , J. Ma, *Catal. Commun*. **2014**, 53, 47–52.

[30]   R. Martin, S. L. Buchwald, *ACCOUNTS OF CHEMICAL RESEARCH.* **2008**,41, 1461-1473.

[31]   A. A. Tukov, A. T. Normand, M.S. Nechaev, *R. Soc.Chem*. **2009**, 7015-7028.

[32]   W. A. Herrmann, M. Elison, J. Fischer, C. Köcher, G. R. J. Artus, *Angew. Chem. Int. Ed. Engl.* **1995**, 34.

[33]   V. Lavallo, Y. Canac, C. Präsang, B. Donnadieu, G. Bertrand, *Angew. Chem. Int. Ed.* **2005**, 44, 5705-5709.

[34]   X. Le, Z.h. Dong, Y. Liu, Zh. Jin, Th. D. Huy, M. Leb, J. Ma, *J. Mater. Chem. A*. **2014**, 2, 19696-19706.

[35]   R. K. Arvela, N. E. Leadbeater, *Org.Lett*. **2005**, 7, 2101-2104.

[36]   G. Marck, A. Villiger, R. Buchecker, F. Hoffmann, *Tetrahedron Lett.* **1994**, 35, 3277-3280.

[37]   L.Stadler, Magnetic carbon-carbon cobalt nanoparticles as a versatile platform for polymer-design, scavenging and catalysis. Doctoral dissertation, university of Regensburg. **2020**.

[38]   A. Alshammari, V. Narayana Kalevaru, A. Martin, *Catalyst*. **2016**, 6, 97.

[39]   M. Sankar, N. Dimitratos, P. J. Miedziak, P. P. Wells, Ch. J. Kiely, G. J. Hutchings, *Chem. Soc. Rev*. **2012**, 14, 8099-8139.

[40]   R. F.Tylecote. History of Metallurgy, 2nd ed. Maney Publishing for the Institute of Materials, London. **1992**

[41]   J. H. Sinfelt, Bimetallic catalysts: Discoveries, concepts, and applications,

        Wiley, New York. **1983**.

[42]   R. Ferrando, J. Jellinek, R.L. Johnston, *Chem. Rev*. **2008**, 108, 845-910.

[43]   P. Lisowski, J. C. Colmenares, D. Lomot, O. Chernyayeva, D. Lisovytskiy, *J. Mol. Catal*. *A Chem*. **2016**, 411, 247-256.

[44]   T. Yuan, D. Liu, Y. Pan, X. Pu, Y. Xia, J. Wang, W. Xiong, *Catalysis Letters*. **2019**, 149, 851-859.

[45]   A. A. Shesterkina, L. M. Kustov, A. A. Strekalovaa, V. B. Kazansky, *RSC*. **2012**. 1-3.

[46]   O. Skoplyak, M. A. Barteau, J. G. Chen, *ChemSusChem*. **2008**, 1, 524–526.

[47]   W. Bonrath, M. Eggersdorfer, T. Netscher, *Catal. Today*. **2007**, 121, 45-57.

[48]   H. Bönnemann, R. M. Richards, *Eur. J. Inorg. Chem*. **2001**, 2455-2480.

[49]   C. Burda, X. Chen, R. Narayanan, M. A. El-Sayed, *Chem.Rev*. **2005**, 105, 1025-1102.

[50]   C. N. R. Rao, G. U. Kulkarni, P. J. Thomas and P. P. Edwards, *Chem. Soc. Rev*. **2000**, 29, 27-35.

[51]   X. Liu, D. Wang, Y.Li. *Nano Today*. **2012**, 7, 448-466.

[52]   H. Zhang, T.Watanabe, M. Okumura, M.Haruta, N. Toshima. *Nat. Mater*. **2012**, 11, 49-52.

[53]   P. Bhol, M. B. Bhavya, S. Swain, M. Saxena, A. K. Samal. *Front.Chem*. **2020**, 8.

[54]   L. Wang, Y. Nemoto, Y. Yamauchi. *J. Am. Chem*. *Soc*. **2011**, 133, 9674.

[55]   Q. Zhang, W. Wang, J. Goebl, Y. Yin, *Nano Today*. **2009**, 4, 494.

[56]   X. Yu, D. Wang, Q. Peng, Y. Li, *Chem. Commun*. **2011**, 47, 8094.

[57]   X. Liu, X. Li, D. Wang, R. Yu, Y. Cui, Q. Peng, Y. Li, *Chem. Commun*. **2012**, 48, 1683.

[58]   L. Yang, C. Hu, J. Wang, Z. Yang, Y. Guo, Z. Bai, K. Wang, *Chem. Commun*. **2011**, 47, 8581.

[59]   C. Thede, U. Wiedwald, M. Bartsch, L. Kienle, S. Barcikowski, *Sci. Rep*. **2016**, 6, 23352.

[60]   Y. G. Sun, Y. N. Xia, *Science*. **2002**, 298, 2176.

[61]   C. M. Cobley, M. Rycenga, F. Zhou, Z. Y. Li, Y. N. Xia, *Angew. Chem., Int. Ed*. **2009**, 48, 4824.

[62]   U. Sanyal, D.T. Davis and B. R. Jagirdar, *Dalton Trans.*, **2013**, 42, 7147–7157.

[63]   M. Pileni, *Langmuir*. **1997**, 13, 3266-3276.

[64]   X. Fu, Y. Wang, N. Wu, L. Gui, Y. Tang. *Langmuir.* **2002**, 18, 4619-4624.

[65]   A. Sárkány, A. H. Weiss, L. Gucz, *J. Catal*. **1986**, 98, 550.

[66]   S. K. Kim, Ch. Kim, J. H. Lee, J. Kim, H. Lee, S. H. Moon, *J. Catal*. **2013**, 306, 146–154.

[67]   S. De, J. Zhang, R. Luqueb, N. Yana. *Rsc.Org*. **2013**, 1-3.

[68]   M. Raney, *Journal*. **1927**.

[69]   D. Wang, P. Zhao, Y. Li. *Sci. Rep*. **2011**, 37.

[70]   L. Chen, H. Guo, T. Fujita, A. Hirata, W. Zhang, A. Inoue, M. *Chen, Adv. Funct. Mater*. **2011**, 21, 4364-4370.

[71]   G. Sharma, D. Kumar, A. Kumar, A. H. Al-Muhtaseb, D. Pathania, M. Naushad, G.T. Mola. *Mater. Sci. Eng*. *C.* **2017**, 71, 1216–1230.

[72]   L. Zhang, A. M. Karim, M. H. Engelhard, Zh. Wei, D. L. King, Y. Wang, *Catalysis*. **2012**, 287 37-43.

[73]   L. Yang, X. Chen, Zh. Zhou, R. Zhang, L. Li, Zh. Cheng, X. Fang, *ChemistrySelect*. **2016**, 1, 5599 – 5606.

[74]   Z. Wang, L. Yanga, R. Zhang, L. Lic, Zh. Cheng, Zh. Zhou, *Catal Today*. **2016**, 264, 37-43.

[75]   Q. Zhang, J. Li, X. Liu, Q. Zhu, *Appl. Catal. A Gen*. **2000**, 197, 221-228.

[76]   Y. Zhang, W. Diao, J.R. Monnier, C.T. Williams, *Catal. Sci. Technol*. **2015**, 5,4123-4132.

[77]   J.H. Kang, E.W. Shin,W.J. Kim, J.D. Park, S.H. Moon, *J. Catal*. **2002**, 208, 310-320.

[78]   M. W. Tew, H. Emerich, J. A. van Bokhoven, J. Phys. Chem. C. **2011**, 115, 8457-8465.

[79]   W. N. A. W. Khalit, T. Sh. Marliza, N. Asikin-Mijan, *RCS Adv*. **2020**, 10, 37218-37232.

[80]   T. Yuan, D. Liu, Yue Pan, X. Pu, Y. Xia, J. Wang, W. Xiong, *Catalysis Letters*. **2019**, 149, 851-859.

[81]   I. S. Mashkovsky, G.N. Baeva, A. Yu. Stakheev, M. N. Vargaftik, N. Yu. Kozitsynab, I. I. Moiseev, *Mendeleev Commun*. **2014**, 24, 355–357.

[82]   C. E. Gigola, H. R. Aduriz, P. Bodnariuk, *Appl. Catal*. **1986** , 27, 133-144.

[83]   A. Borodzin´ski and A. Cybulski, *Appl. Catal*. **2000**, 198, 51.

[84]   C. Lederhos, C. Betti, D. Liprandi, E. Cagnola, M. Quiroga, New Advances in Hydrogenation *Processes* - Fundamentals and Applications. **2017**.

[85]   L. Hongyi, M. Yubo, *PROG REACT KINET MEC*. **2020**, 45, 1-17.

[86]   M. Sankar, N. Dimitratos, P.J. Miedziak, P. P. Wells, Ch. J. Kielye, G.J. Hutchings. *Chem. Soc. Rev*. **2012**, 41, 8099–8139.

[87]   M. Mosińska, M. I. Szynkowska-Jóźwik,P. Mierczyński, *Materials*. **2020**, 13, 5601.

[88]   Y. F. Han, J. H. Wang, D. Kumar, Z. Yan, D. W. Goodman, *J. Catal.* **2005**, 232, 467.

[89]   G. Sharma, A. Kumar, Sh. Sharma, M. Naushad, R. P. Dwivedi, Z. A. ALOthman, G.T. Mola, *J. King Saud Univ. Sci.* **2019**, 31, 257-269.

[90]   E. K. Fodjo, K. M. Gabriel, B. Y. Serge, D. Li, C. Kong, A. Trokourey, *Chem.Cent. J.* **2017**, 12.

[91]   P. R. Ellis, Ch. M. Brown, P. T. Bishop, D. Ievlev, J. Yin, K. Cooke, R. E. Palmer, *Catal. Struct. React*. **2018**, 4, 1-8.

[92]   P. M. Uberman, N. J. S. Costa, K. Philippot, R. C. Carmona , A. A. Dos Santosd, L. M. Rossi, *Green Chem*. **2014**, 16, 4566–4574.

[93]   M.G. Musolino, L.A. Scarpino, F, Mauriello, R. Pietropaolo, *ChemSusChem*. **2011**, 4, 1143–1150.

[94]   D. Loua, H. Wangb, S. Liub, L. Lia, W. Zhaob, X. Chenb, J. Wanga, X. Lib, P. Wua, J. Yangb, *Catalysis Communications*. **2018**, 109, 28–32.

[95]   X. Jiang, N. Koizumi, X. Guo, C. Song, *Applied Catalysis B: Environmental*. **2015,** 170–171, 173-185.

[96]   R. Hou, W. Yu, M. D. Porosoff, J. G. Chen, T. Wang, *Journal of Catalysis*. **2014**, 316, 1–10.

[97]   Z. Tian, C. Dong , D. Li, G.H. Wang, *Materials Today Chemistry*. **2021**, 20, 100467.

[98]   T. Conant, A. M. Karim, V. Lebarbier, Y. Wang, F. Girgsdies, R. Schlögl, A. Datye, *Journal of Catalysis*. **2008**, 257, 64-70.

[99]   J. D. Waele, V. V. Galvita, H. Poelman, C. Detavernierb, J. W. Thybaut. *Catal. Sci. Technol*. **2017**,7, 3715–3727

[100]   S. Gupta, T. Suvra Khan, B. Saha, M. Ali Haider, *Ind. Eng. Chem. Res*. **2019**, 58, 16153–16163.

[101]   L. Bollmann , J. L. Ratts , A. M. Joshi , W. D. Williams , J. Pazminoa, Y. V. Joshi, J.T. Miller , A. J. Kropf , W. N. Delgass , F. H. Ribeiro, *Journal of Catalysis.* **2008**, 257, 43–54.

[102]   N. Iwasa, O. Yamamoto, R. Tamura, M. Nishikubo, N.Takezawa, *Catal. Lett*. **1999**, 62, 179–184.

[103]   A. Zakhtser, A. Naitabdi, R. Benbalagh, F. Rochet, C. Salzemann, C. Petit, S, Giorgio, *ACS Nano*. **2021**, 15, 3, 4018–4033.

[104]   A. Taguchi, F. Schüth, *Microporous Mesoporous Mater*. **2005**, 77, 1-45.

[105]   R. Dawson, E. Stockel, J. R. Holst, D. J. Adams, A. I. Cooper, *Energy Environ. Sci*. **2011**, 4, 4239–4245.

[106]   A. U. Czaja, N. Trukhan, U. Müller, *Chem. Soc. Rev*. **2009**, 38, 1293–1284.

[107]   J. Germain, J. M.J. Fréchet. F. Svec, *small*, **2009**, 10, 1098-1111.

[108]   B. Li, Z. Guan, X. Yang, W. D. Wang, W. Wang, I. Hussain, K. Song, B. Tan, T. Li, *J. Mater. Chem. A.* **2014**, *2*, 11930.

[109]   J. Bi, Y. Dong, D. Meng, D. Zhu, T. Li, *Polymer*. **2019**, 164, 183.

[110]   A.Thomas, *Angew. Chem. Int. Ed*. **2010**, 49, 8328 – 8344.

[111]   Ph. Makowski, A. Thomas, P. Kuhn, F. Goettmann, *Energy Environ. Sci*. **2009**, 2, 480-490.

[112]   L. Wang, R. T. Yang, *Energy Environ. Sci*. **2008**, 1, 268–279.

[113]   Q. Zhang, Y. Yang, S. Zhang, *Chem. Eur. J*. **2013**, 19, 10024-10029.

[114]   Y. Luo, B. Li, W. Wang, K. Wu, B. Tan, *Adv. Mater*. **2012**, 24, 5703-5707.

[115]   J. Germain, F. Svec, J. M. J. Frechet, *Chem. Mater*. **2007**, 17, 4989-4997.

[116]   J. Germain, J. M. J. Frechet and F. Svec, *Chem. Commun*. **2009**, 1526–1528.

[117]   G. Liu, Y. Wang, C. Shen, Z. Jua, D.Yuan, *J. Mater. Chem. A*. **2015**, 3051.

[118]   Y. Lei, L. Wu, X. Zhang, H. Mei, Y. Gu, G. Li, *J. Mol. Catal. A: Chem*. **2015**, 398,164–169.

[119]   S. Fukuzumi, Y.-M. Lee, W. Nam, *ChemCatChem*. **2018**, 10, 1686–1702.

[120]   B. Li, Z. Guan, W. Wang, X. Yang, J. Hu, B. Tan, T. Li, *Adv. Mater.* **2012**, *24,* 3390–3395.

[121]   Z. Jia, K. Wang, B. Tan, Y. Gu, *Adv. Synth. Catal*. **2017**, 359, 78.

[122]   J. Chen, W. Yan, E. J. Townsend, J. Feng, L. Pan, V. D. A. Hernandez, C. F. J. Faul, *Angew. Chem*. **2019**, 131, 11841 –11845.

G. Appendix

1. GC Chromatograms

1,2-diphenylethane (20a)   Ph⌒Ph
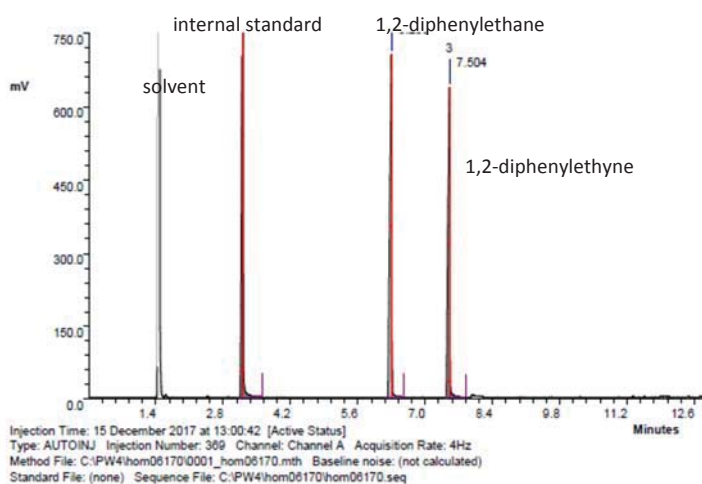
GC chromatogram of the calibration with dodecane as internal standard, 1,2-diphenylethyne as starting material and 1,2-diphenylethane as product.

Ethylbenzene (20b,20c)
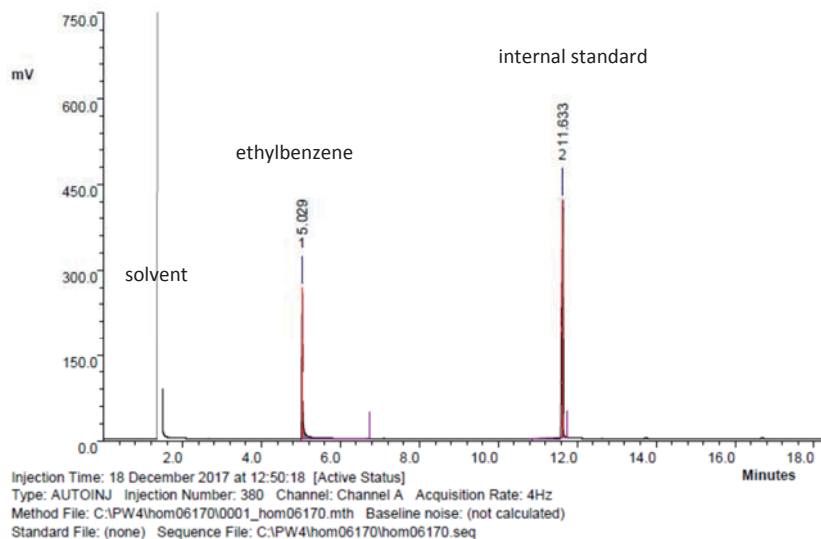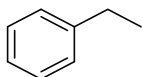

```
Peak   RT        Area    %Ar  Conc.(Ar)       Height  M    Units  Name
  1 5.029      514.517  36.58 Not Calculated  264.813 0
  2 11.633     892.086  63.42 Not Calculated  416.869 1
```
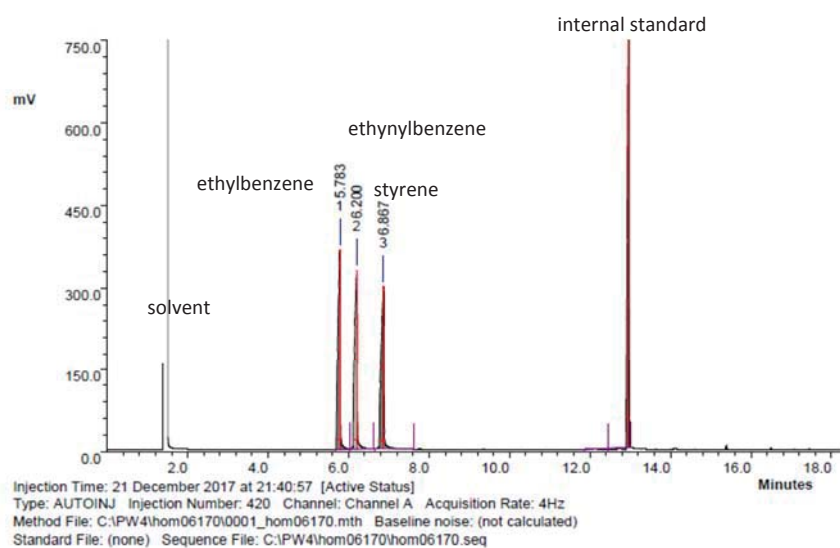


```
Peak   RT         Area     %Ar  Conc.(Ar)       Height   M    Units  Name
  1 5.783      1469.689  21.19 Not Calculated  365.658  0
  2 6.200      1465.570  21.13 Not Calculated  328.100  0
  3 6.867      1500.137  21.63 Not Calculated  298.132  0
  4 12.963     2500.318  36.05 Not Calculated 1084.717  1
```

GC chromatogram of the calibration with dodecane as internal standard, ethynylbenzene as starting material, styrene as intermediate product, and ethylbenzene as product.

119

bicycle [2.2.1] heptane (20d)

internal standard

mV

solvent

bicyclo[2.2.1]heptane

~2.608

Injection Time: 09 January 2018 at 14:43:50 [Active Status]
Type: AUTOINJ Injection Number: 461 Channel: Channel A Acquisition Rate: 4Hz
Method File: C:\PW4\hom06170\0001_hom06170.mth Baseline noise: (not calculated)
Standard File: (none) Sequence File: C:\PW4\hom06170\hom06170.seq
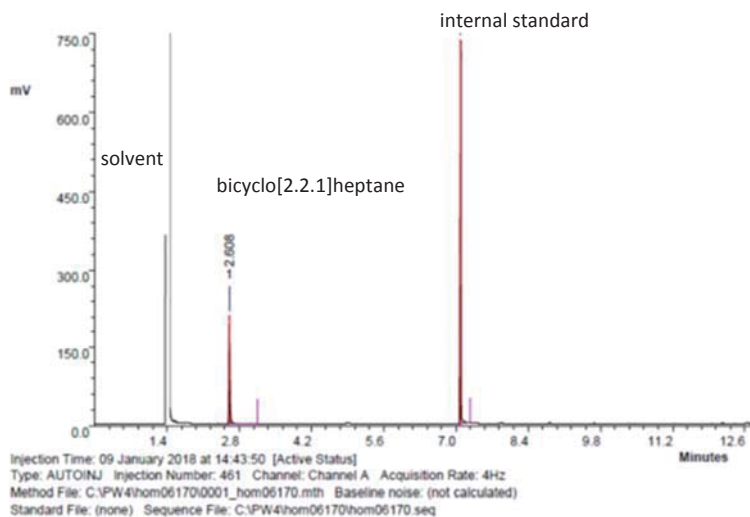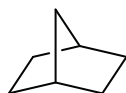
```
Peak   RT      Area     %Ar  Conc.(Ar)       Height   M   Units  Name
  1 2.608   316.999   25.38 Not Calculated   209.673  0
  2 7.087   932.144   74.62 Not Calculated   734.328  1
```


internal standard

mV

bicyclo[2.2.1]heptane

1 2.296
   2.596

solvent

bicyclo[2.2.1]hept-2-ene

Injection Time: 09 January 2018 at 14:21:51 [Active Status]
Type: AUTOINJ Injection Number: 460 Channel: Channel A Acquisition Rate: 4Hz
Method File: C:\PW4\hom06170\0001_hom06170.mth Baseline noise: (not calculated)
Standard File: (none) Sequence File: C:\PW4\hom06170\hom06170.seq
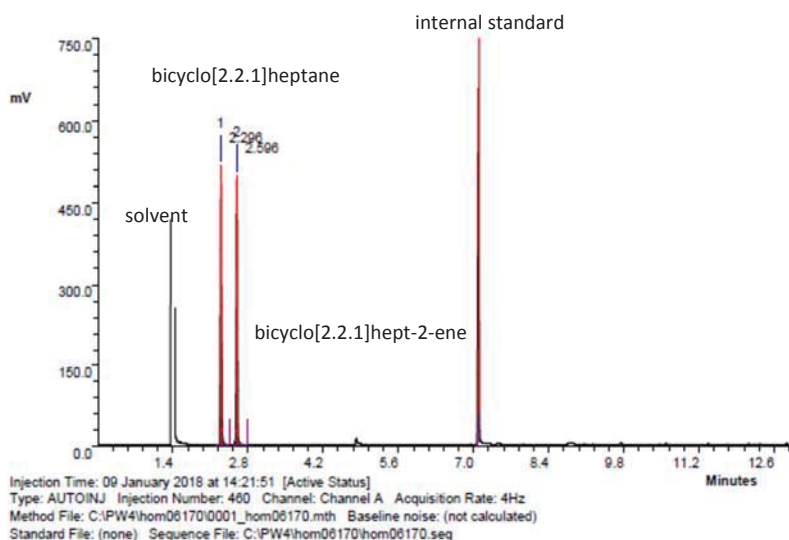
```
Peak   RT       Area      %Ar  Conc.(Ar)       Height   M   Units  Name
  1 2.296    729.227   25.07 Not Calculated   512.987  1
  2 2.596    753.080   25.89 Not Calculated   494.761  1
  3 7.100   1426.253   49.04 Not Calculated   997.641  0
```

GC chromatogram of the calibration with dodecane as internal standard, bicycle [2.2.1] hept-2-ene as starting material and bicycle [2.2.1] heptane as product.

Ethane-1,1-diyldibenzene (20e)

Ph⟍C=CH₂⟋Ph

Injection Time: 22 December 2017 at 13:35:49 [Active Status]
Type: AUTOINJ   Injection Number: 422   Channel: Channel A   Acquisition Rate: 4Hz
Method File: C:\PW4\hom06170\0001_hom06170.mth   Baseline noise: (not calculated)
Standard File: (none)   Sequence File: C:\PW4\hom06170\hom06170.seq
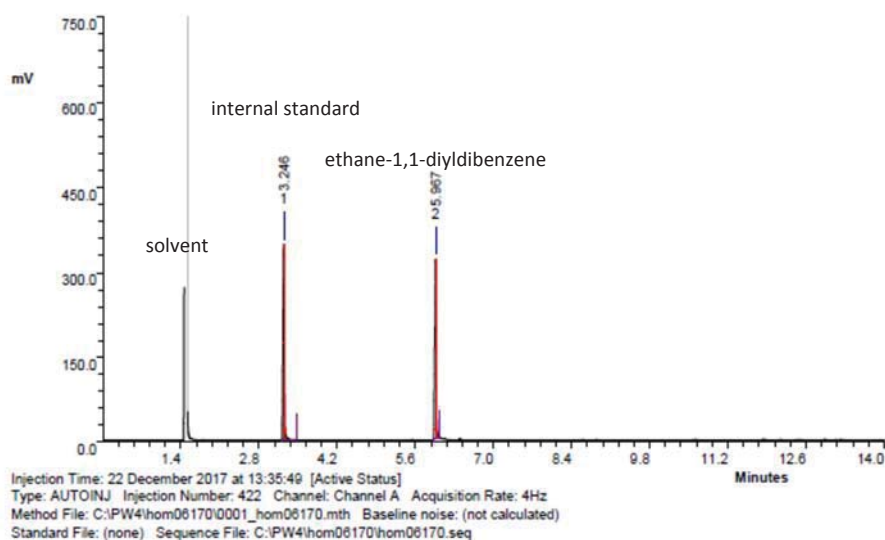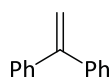
Peak	RT	Area	%Ar	Conc.(Ar)	Height	M	Units	Name
1	3.246	585.490	52.00	Not Calculated	346.050	1		
2	5.967	540.523	48.00	Not Calculated	317.154	1		

Injection Time: 16 January 2018 at 14:11:01 [Active Status]
Type: AUTOINJ   Injection Number: 462   Channel: Channel A   Acquisition Rate: 4Hz
Method File: C:\PW4\hom06170\0001_hom06170.mth   Baseline noise: (not calculated)
Standard File: (none)   Sequence File: C:\PW4\hom06170\hom06170.seq
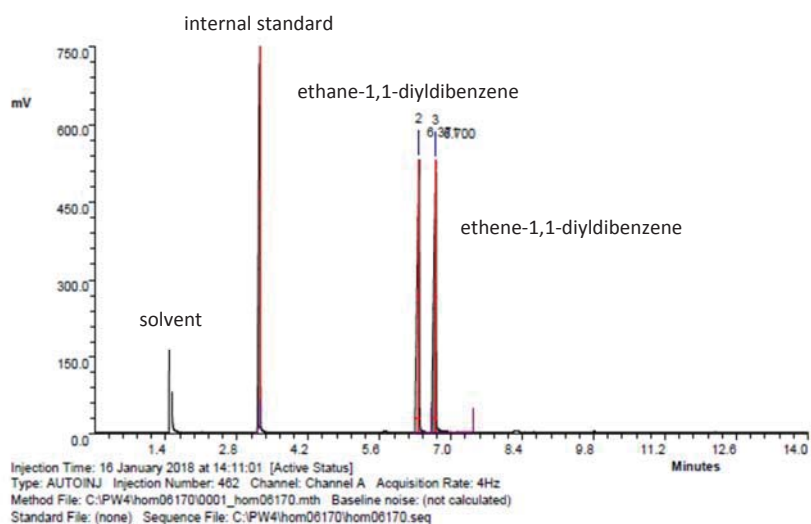
Peak	RT	Area	%Ar	Conc.(Ar)	Height	M	Units	Name
1	3.250	1705.761	33.61	Not Calculated	899.983	0		
2	6.371	1675.394	33.01	Not Calculated	528.209	0		
3	6.700	1693.670	33.37	Not Calculated	526.812	0		

GC chromatogram of the calibration with dodecane as internal standard, ethene-1,1-diyldibenzene as starting material and ethane-1,1-diyldibenzene as product.

1,2-diphenylethane (20f)   Ph⌒Ph
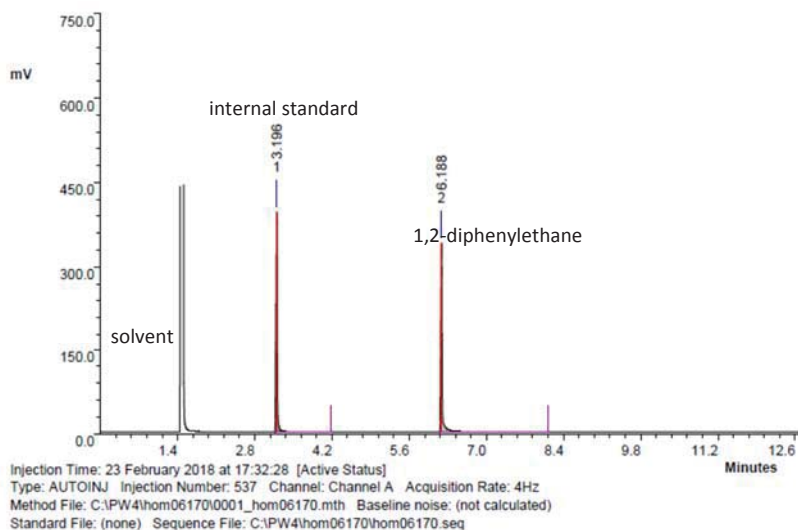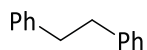
Peak   RT   Area   %Ar Conc.(Ar)   Height M   Units Name
   1 3.196   659.089   49.57 Not Calculated 394.677 0
   2 6.188   670.485   50.43 Not Calculated 339.606 0
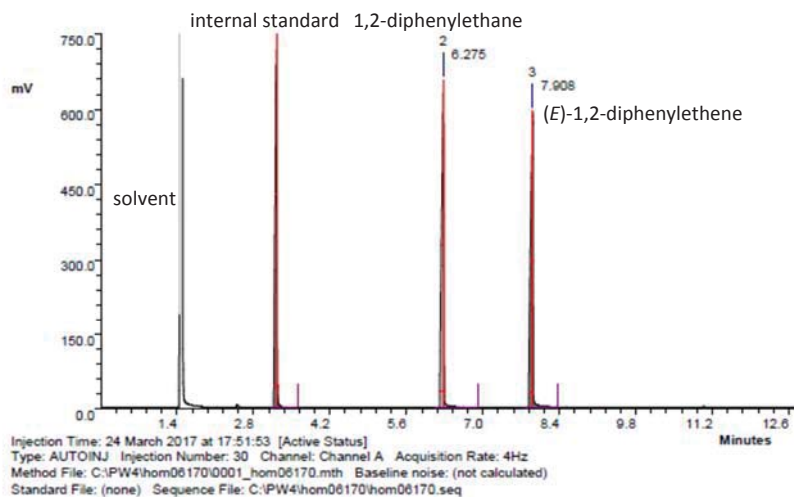
Peak   RT   Area   %Ar Conc.(Ar)   Height M   Units Name
   1 3.225   1781.842   33.04 Not Calculated 857.009 1
   2 6.275   1823.576   33.82 Not Calculated 653.550 1
   3 7.908   1786.799   33.14 Not Calculated 591.387 1

GC chromatogram of the calibration with dodecane as internal standard, (*E*)-1,2-diphenylethene as starting material and ethane- 1,2-diphenylethane as product.

Methylcyclohexane (20g)
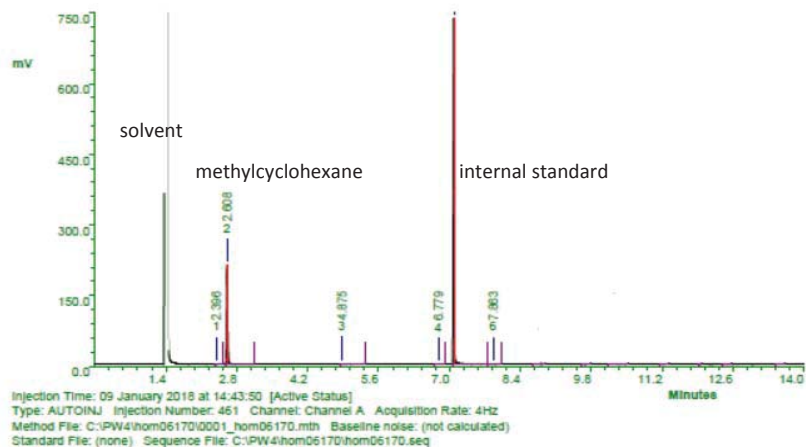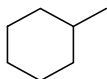
Peak   RT   Area   %Ar   Conc.(Ar)   Height   M   Units Name
1 2.396   0.444   0.03 Not Calculated   0.169   0
2 2.608 316.999   24.34 Not Calculated 209.673   0
3 4.875   10.007   0.77 Not Calculated   1.645   0
4 6.779   1.091   0.08 Not Calculated   0.149   0
5 7.088 958.499   73.60 Not Calculated 734.498   0
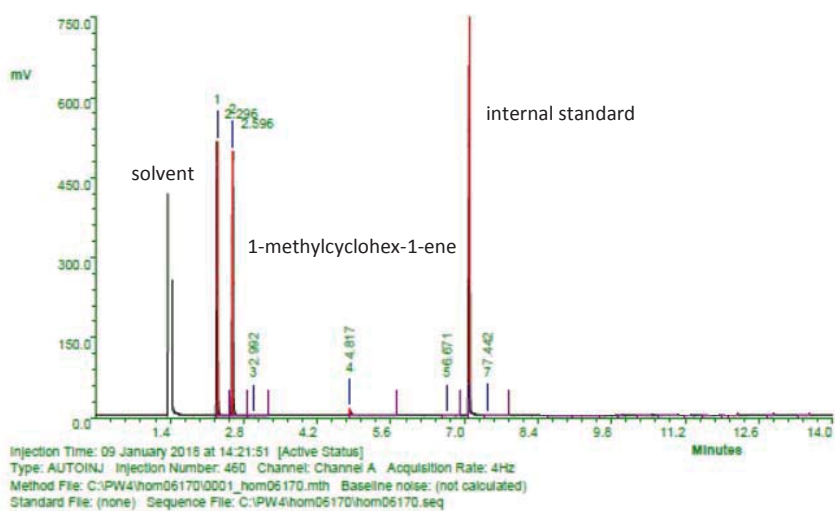
Peak   RT   Area   %Ar   Conc.(Ar)   Height   M   Units Name
1 2.296   730.199   24.36 Not Calculated   513.000   0
2 2.596   754.348   25.17 Not Calculated   494.842   0
3 2.992   1.626   0.05 Not Calculated   0.278   0
4 4.817   30.864   1.03 Not Calculated   11.908   0
5 6.671   1.705   0.06 Not Calculated   0.244   0
6 7.100   1426.253   47.59 Not Calculated   997.641   0
7 7.442   3.962   0.13 Not Calculated   0.377   0

GC chromatogram of the calibration with dodecane as internal standard, 1-methylcyclohex-1-ene as starting material and methylcyclohexane as product.

Methyl 3-phenylpropanoate (20h)
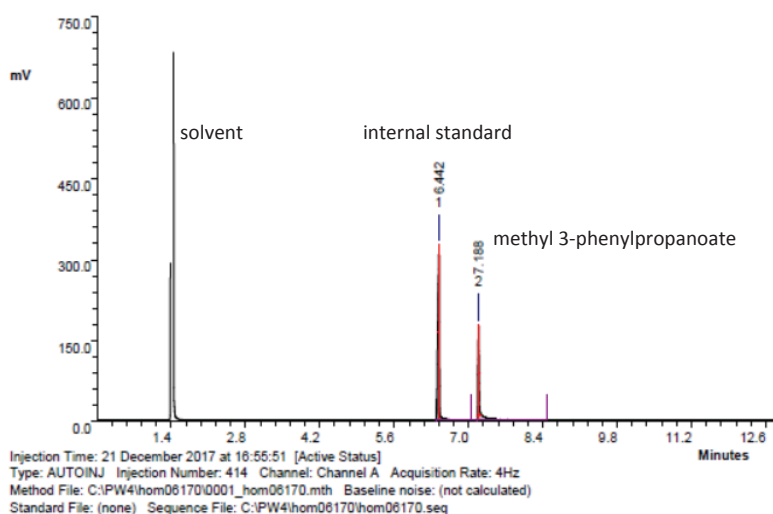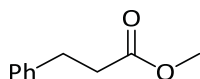

```
Peak    RT       Area      %Ar  Conc.(Ar)       Height   M   Units  Name
  1  6.442    704.087   64.62  Not Calculated   324.025  0
  2  7.188    385.559   35.38  Not Calculated   175.608  0
```
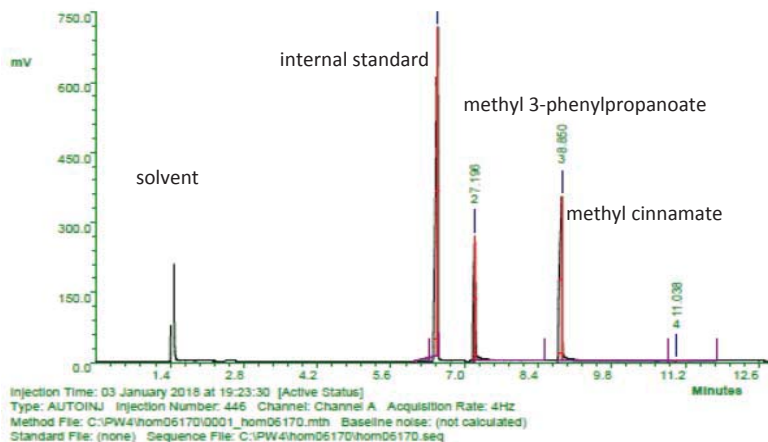


```
Peak    RT        Area      %Ar  Conc.(Ar)       Height   M   Units  Name
  1  6.492    2032.871   49.63  Not Calculated   703.344  0
  2  7.196     717.000   17.51  Not Calculated   267.303  0
  3  8.850    1337.646   32.66  Not Calculated   351.216  0
  4  11.038      6.353    0.16  Not Calculated     0.267  0
```

GC chromatogram of the calibration with dodecane as internal standard, methyl cinnamate as
starting material and methyl 3-phenylpropanoate as product.

4-methylpentan-2-one (20i)

GC chromatogram of the calibration with dodecane as internal standard, 4-methylpent-3-en-2-one as starting material and 4-methylpentan-2-one as product.

aniline (20j)
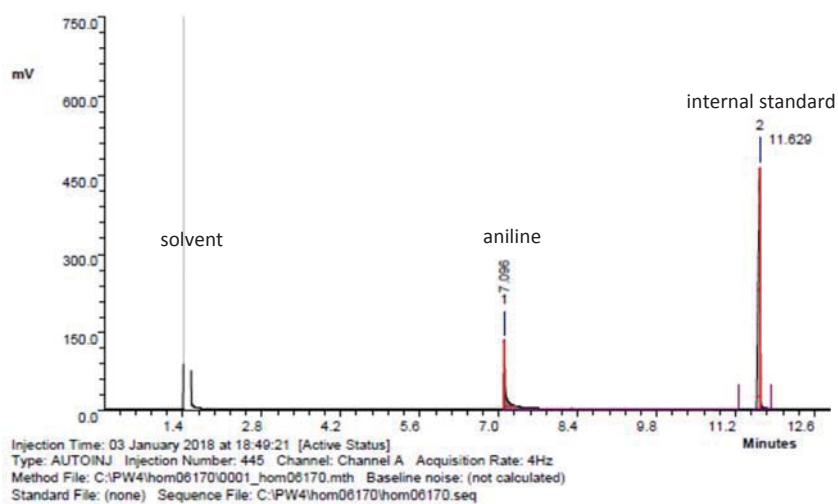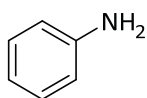
Peak   RT   Area   %Ar Conc.(Ar)   Height M   Units Name
  1 7.096   461.298 29.09 Not Calculated   131.646 1
  2 11.629   1124.729 70.91 Not Calculated   461.089 1
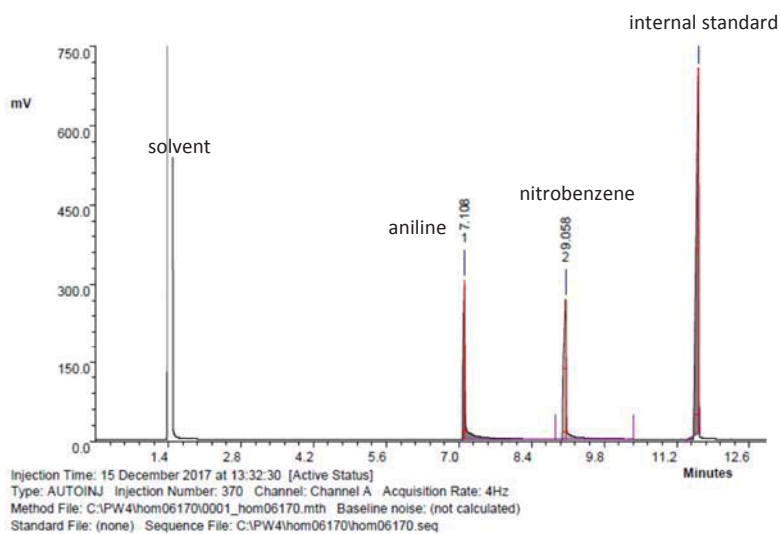
Peak   RT   Area   %Ar Conc.(Ar)   Height M   Units Name
  1 7.108   932.517 21.98 Not Calculated   304.422 0
  2 9.058   997.562 23.52 Not Calculated   267.918 0
  3 11.613   2311.533 54.50 Not Calculated   693.769 0

GC chromatogram of the calibration with ethylbenzene as internal standard, nitrobenzene as starting material and aniline as product.

4-aminotoluene (20k)
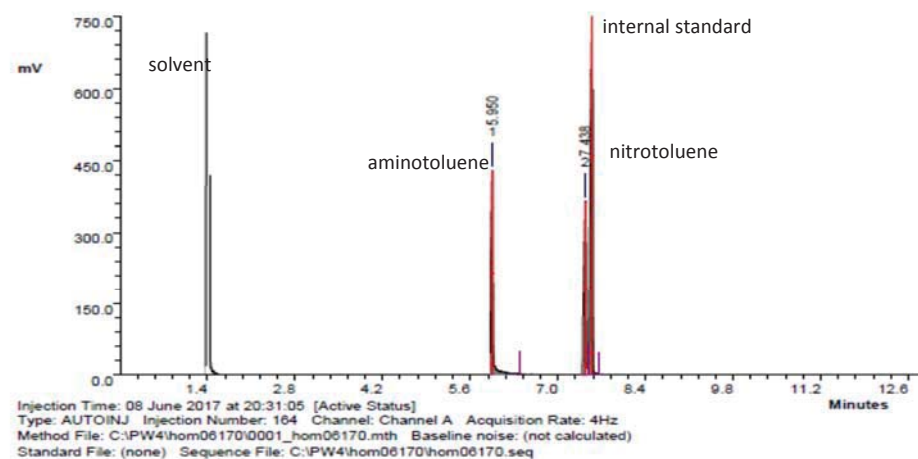
GC chromatogram of the calibration with dodecane as internal standard, 4-nitrotoluene as starting material and 4-aminotoluene as product.

2. NMR spectra

^{1}H-NMR and ^{13}C-NMR (400MHz, MeOD)
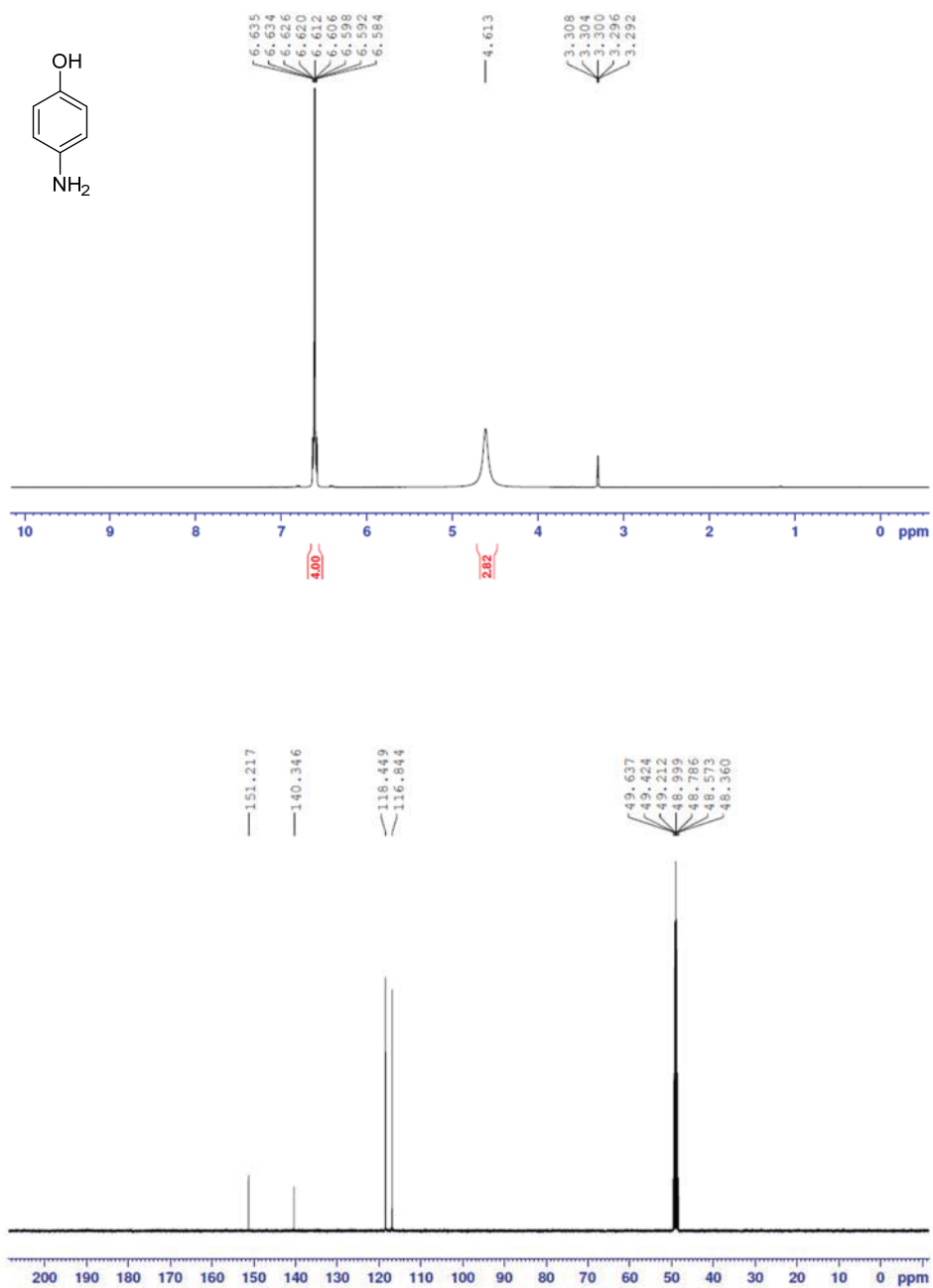
4-Aminophenol (20l)

NMR spectra

^{1}H-NMR and ^{13}C-NMR (400MHz, MeOD)
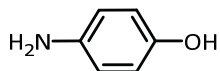
4-Aminophenol (20l): ^{1}H-NMR (400 MHz, MeOD) δ= 6.58-6.63 (m, 4H), 4.6 (s,2H); ^{13}C-NMR (400 MHz, MeOD) δ= 151.2, 140.3, 118.4, 116.8, 48.99.

^{1}H-NMR and ^{13}C-NMR (400 MHz, CDCl$_3$)
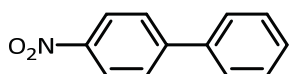
4-Nitrobiphenyl (23a): ^{1}H-NMR (400 MHz, CDCl$_3$) δ= 8.32 (d, J = 8.4 Hz, 2H), 7.76 (d, J = 8.4 Hz, 2H), 7.66 (d, J = 7.5 Hz, 2H), 7.53 (t, J = 7.4 Hz, 2H), 7.46-7.49 (m, 1H); ^{13}C-NMR (400 MHz, CDCl$_3$) δ= 147.6, 147.1, 138.8, 129.2, 129.0, 127.8, 127.4, 124.1.
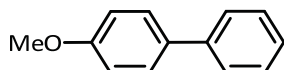
4-Methoxybiphenyl (23b): ^{1}H-NMR (400 MHz, CDCl$_3$) δ= 7.53-7.58 (m, 4H), 7.43 (t, J = 7.7 Hz, 2H), 7.32 (t, J = 7.4 Hz, 1H), 6.99 (d, J = 8.8 Hz, 2H), 3.86 (s, 3H); ^{13}C-NMR (400 MHz, CDCl$_3$) δ= 159.2, 140.9, 133.8, 128.7, 128.2, 126.8, 126.7, 114.2, 48.88.
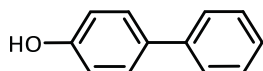
4-Phenylphenol (23c): ^{1}H-NMR (400 MHz, CDCl$_3$) δ= 7.56 (dd, J = 9.0, 1.5 Hz,2H),7.51(dt, J = 9.5, 2.5 Hz, 2H), 7.44(t, J = 7.5 Hz,2H), 7.33(t, J = 7.5 Hz, 1H), 6.93 (dt, J = 9.5, 3.0 Hz, 2H),5.04 (s,1H); ^{13}C-NMR (400 MHz, CDCl$_3$) δ=155.1, 140.2, 130.9, 128.7, 127.7, 126.3, 125.9, 115.7.
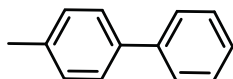
4-Methylbiphenyl (23d): ^{1}H-NMR (400 MHz, CDCl$_3$) δ= 7.64 (d, J = 7.1 Hz, 2H), 7.55 (d, J = 8.1 Hz, 2H), 7.48 (t, J = 7.5 Hz, 2H), 7.37 (t, J = 7.3 Hz, 1H), 7.30 (d, J = 7.9 Hz, 2H), 2.45 (s, 3H));
 ^{13}C-NMR (400 MHz, CDCl$_3$) δ= 141.2, 138.4, 137.0, 129.5, 128.7, 127.2, 127.0, 21.1.
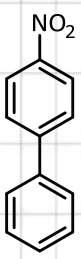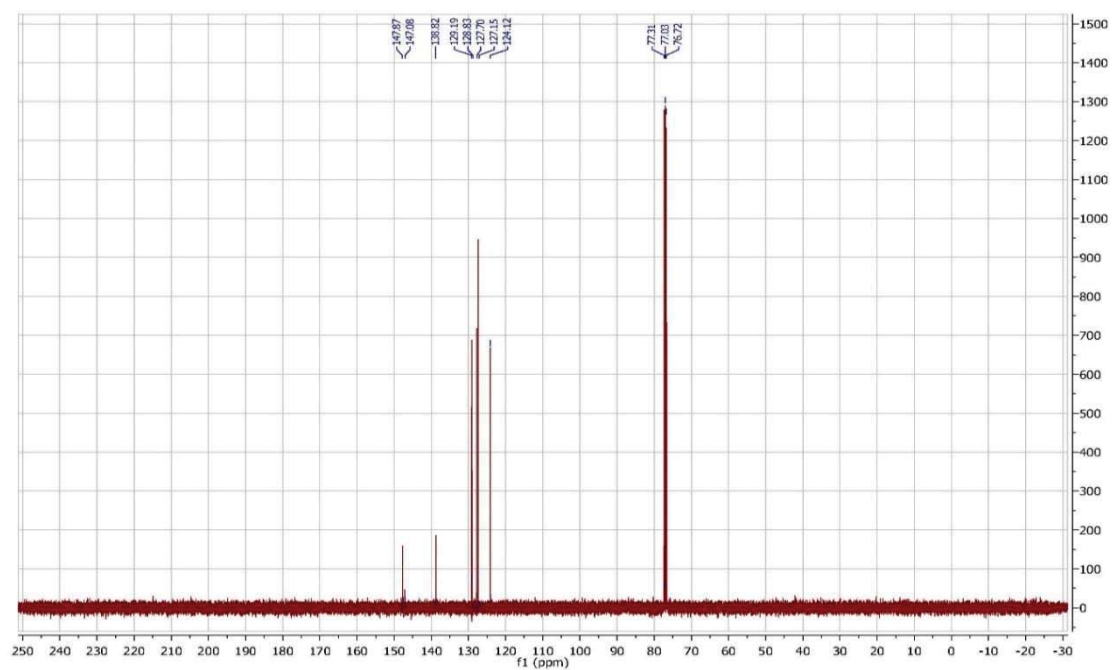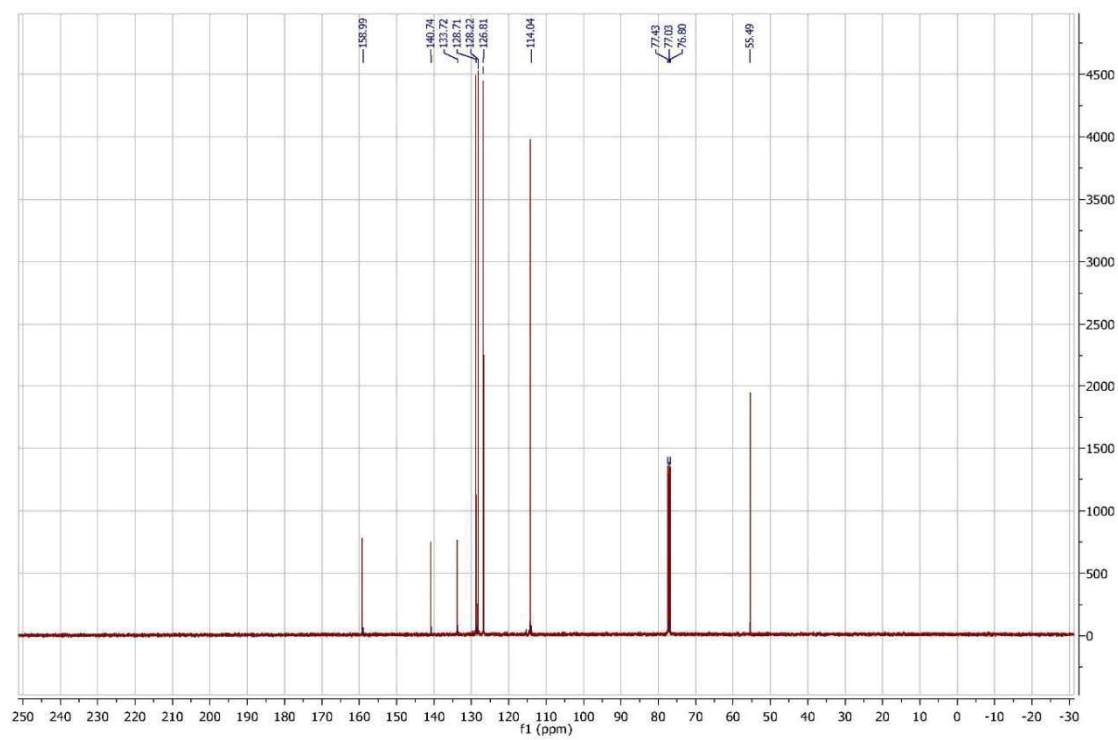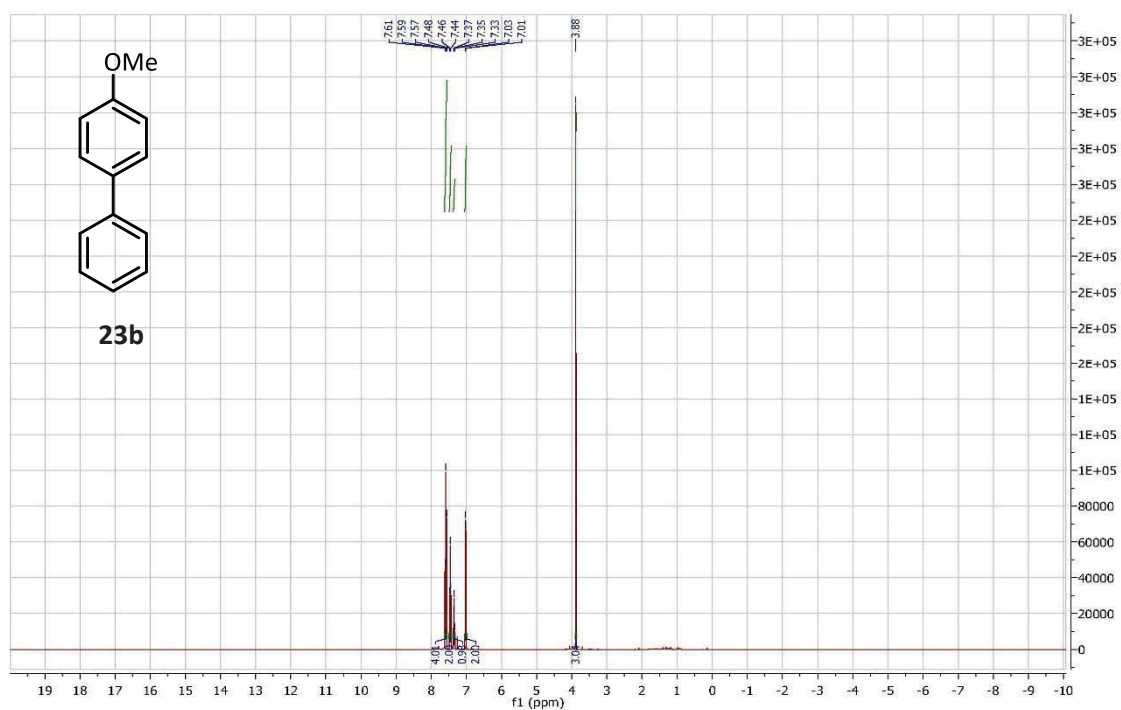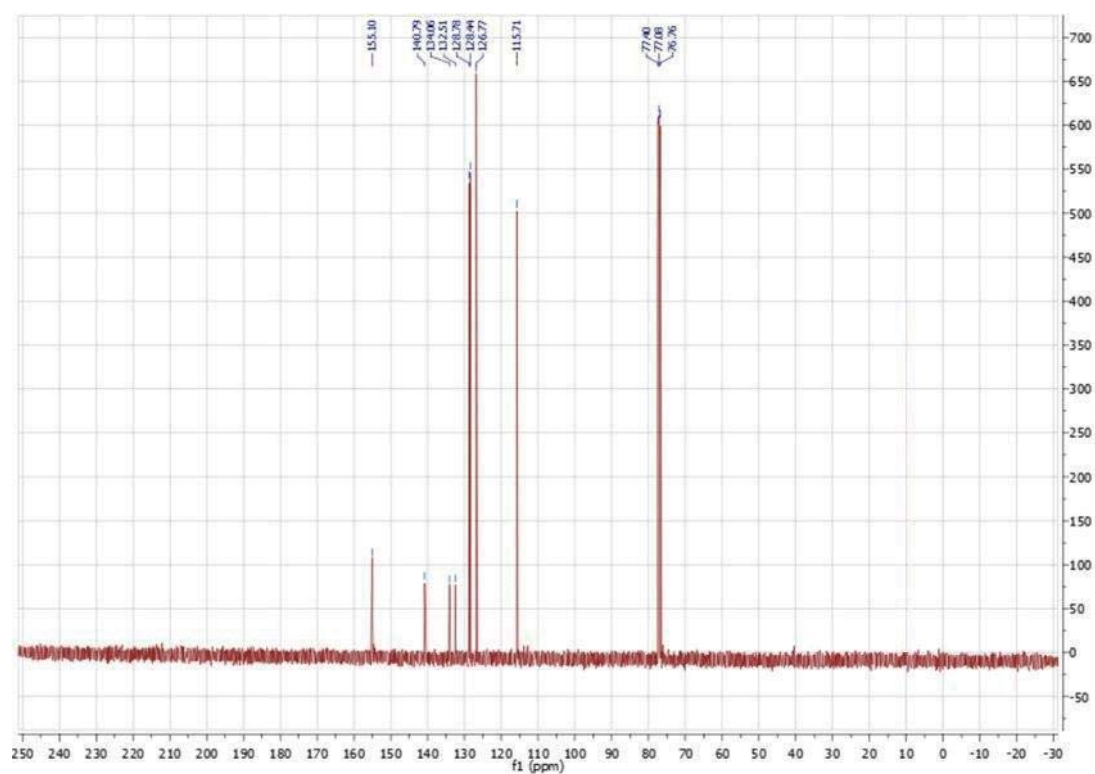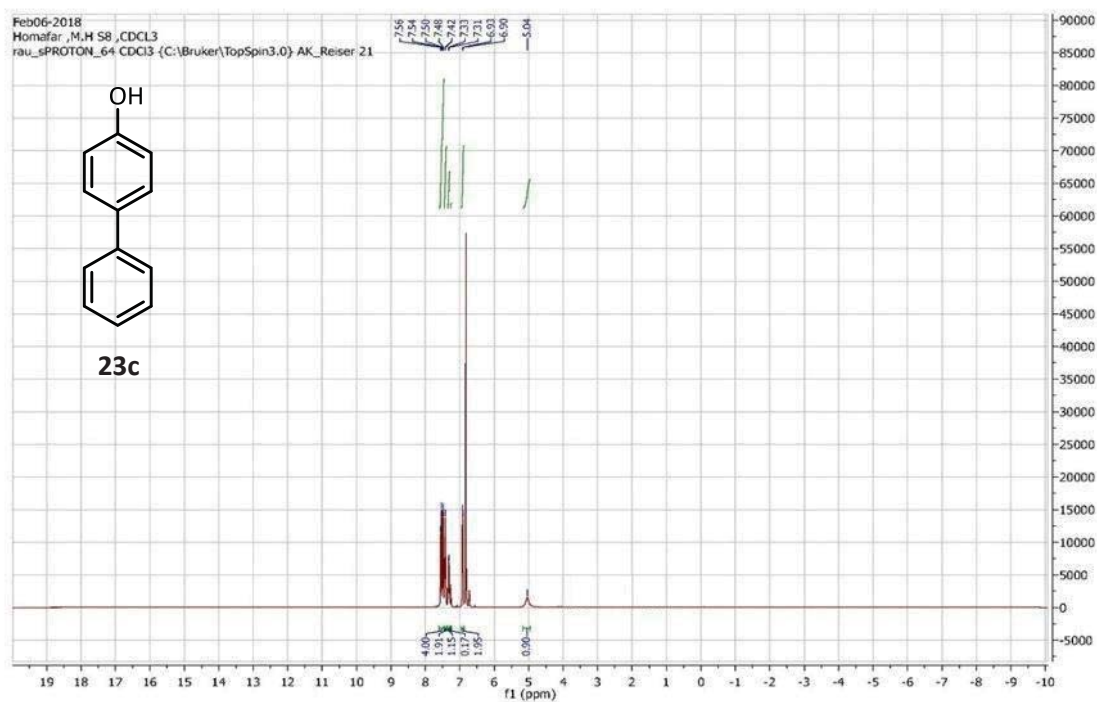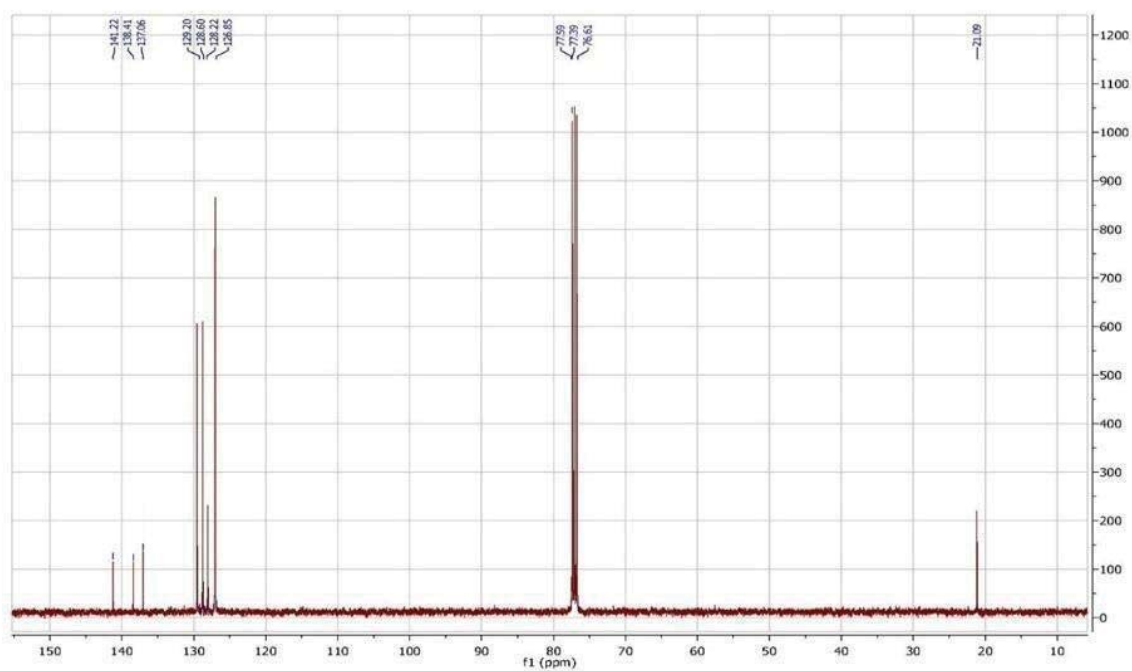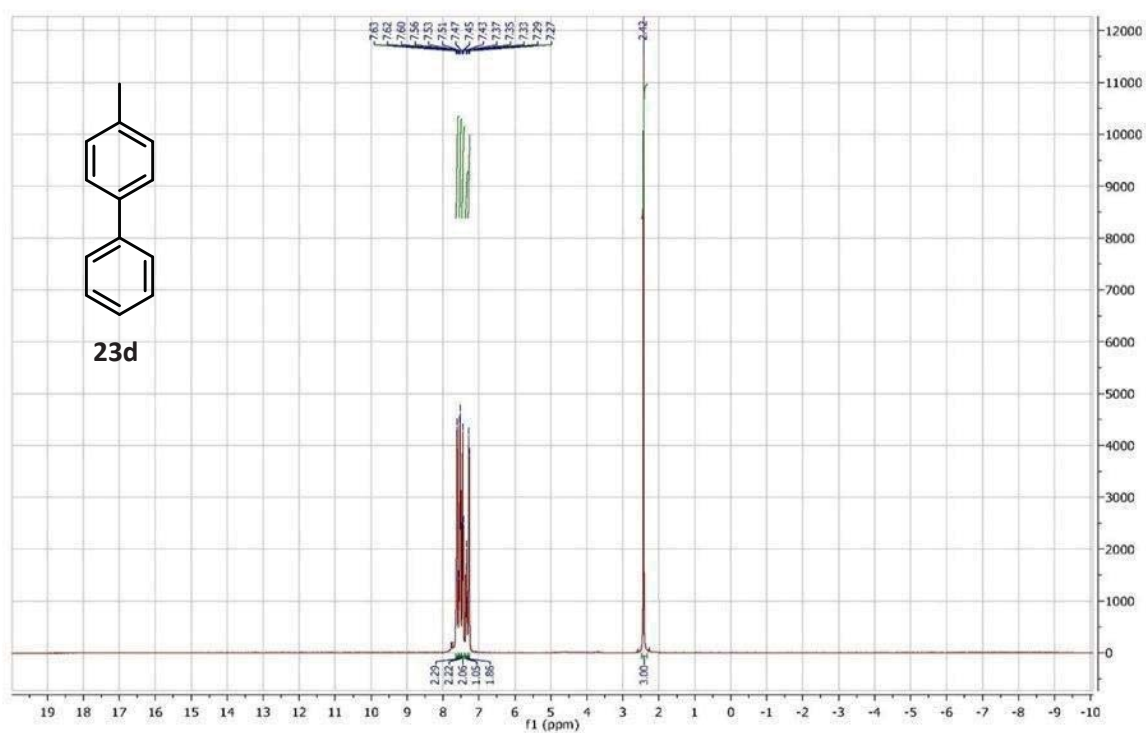
3. Curriculum Vitae

Personal Data:

Name:	Maryam Homafar
Date/Place of Birth:	17.01.1982, Toyserkan, Iran
Nationality:	Iranian
Email:	maryam.homafar1982@gmail.com

Education:

04.2016 – 03.2020   PhD thesis in the research group of *Prof. Dr. O. Reiser* (University of Regensburg, Germany)

09.2008 – 02.2011   Azad University of Karaj, Faculty of Chemistry, Iran

M.Sc. in Organic chemistry

Thesis title: Synthesis of polyhydroquinoline derivatives through the Hanthzsch four component using iron (III) phosphate as a catalyst

09.2001 – 09.2005   Azad University of Karaj, Faculty of Chemistry, Iran

B.Sc. in applied Chemistry

Thesis title: Dairy products manufacturing plan

Working Experiences:

09.2011 – 02.2016   Institute of Standard and Industrial Research of Iran (ISIRI),R&D department, Karaj, Iran

Quality Assurance Assistant

- Identification and characterization of pharmaceutical products.
- Performing internal audit.

- Workshop trainer: Physicochemical tests of oil products, Certified by Chemical Analysis Center.
- Workshop trainer: Instrumental analysis (FT-IR, GC), Certified by Chemical Analysis Center.

01.2010 – 09.2011   Meditechsys Co., Karaj, Iran

<u>Quality Assurance Assistant</u>

- Chemical identification and characterization of medical equipment.

01.2006 – 01. 2010   Yegane sazan Co., Karaj, Iran

<u>Quality control expert</u>
- Synthesis and identification of Pre-drug.

Certificates:

- Practical Regulatory Affairs 2020 - US FDA Medical Devices (udamy, Jan 2021).

- Practical Regulatory Affairs 2020 - European Medical Devices (udamy, Jan 2021).

- Quality Management Systems (udamy, Jan 2021).

- Quality Management for Business Excellence (udamy, Jan 2021).

- National conference on high technologies in chemical industry from Tarbiyat Modares University, Iran (July 2013).

- Scientific writing from Bu-Ali Sina University, Hamedan, Iran (Mar 2011).

- EN ISO 17025 from TÜV – Academy Rhineland, certification No: CTC-B- 09/04 30 (Dec 2009).

- Instrumental analysis (HPLC, GC, IR, UV-VIS) from Sharif Center (S.C.T.A.E) (Aug 2008).

Publications:

L. Stadler, **M. Homafar**, A. Hartl, S. Najafishirtari, M. Colombo, R. Zboril, P. Martin, M. B. Gawande, J. Zhi, O. Reiser, *ACS Sustainable Chem. Eng.* **2019**, *7*, 2388-2399.

''*Recyclable magnetic microporous organic polymer (MOP) encapsulated with palladium nanoparticles and Co/C nanobeads for hydrogenation reactions.*"

M. Homafar, O. Reiser, *Manuscript in preparation*.

''*Noble metal nanoparticles encapsulated in microporous organic polymers and their application in catalysis.*''

F.K. Behbahani, **M. Homafar**, *Metal-Organic, and Nano-Metal Chemistry*, **2012**, 42, 291-295.

''*Synthesis of Polyhydroquinoline Derivatives Through the Hantzsch Four Component Using Iron (III) Phosphate as a Catalyst.*''

Conference:

26th ISHC Congress – Regensburg (Germany), August 03-08, 2017.

"*Different Monomers– Containing Microporous Organic Polymers Encapsulated with Pd Nanoparticles and CO/C nanobeads for Hydrogenation*" (poster presentation).

Technical Skills:

- Experience in chromatography - Instrumental analysis: HPLC, GC.

- Experience in spectroscopy - Instrumental analysis: AAS, ICP-OES, FT-IR, ASTM, UV-VIS.

- Experience in cosmetic and drug chemical analysis.

- Experience in oil products.

- Experience in food, beverages and drinking water chemical analysis.

- Familiar with different techniques for synthesis of catalytic materials.

Professional References:

Prof. Dr. Oliver Reiser

Institut für Organische Chemie

Universität Regensburg, Universitätsstr. 31

93053 Regensburg, Germany

Phone: 0049 941 943 4631

Email: Oliver.Reiser@chemie.uni-regensburg.de

H. Acknowledgment – Danksagung

I. Declaration

Herewith I declare that this present thesis is a presentation of my original work prepared single-handed. Wherever contributions from others are involved, all of them are marked clearly, with reference to the literature, license, and acknowledgment of collaborative research.

Regensburg, 01.August.2022

_____

Maryam Homafar